FCTUC **FACULDADE DE CIÊNCIAS E TECNOLOGIA**
UNIVERSIDADE DE COIMBRA

DEPARTAMENTO DE
ENGENHARIA MECÂNICA

The Flexural Properties of Corrugated Hybrid Composite Plates

Submitted in Partial Fulfilment of the Requirements for the Degree of Master in Mechanical Engineering in the speciality of Production and Project

As Propriedades à Flexão dos Compósitos Híbridos em Placas Enrugadas

Author
Francisco Manuel Gonçalves Mesquita

Advisors
Prof. Stepan V. Lomov
Prof. Ana Paula B. M. Amaro

Jury

President	Professor Doutor **Fernando Jorge Ventura Antunes** Professor Auxiliar da Universidade de Coimbra Professor Doutor **Paulo Nobre Balbis dos Reis** Professor Auxiliar da Universidade da Beira Interior
Advisor	Professor Doutor **Ana Paula Betencourt Martins Amaro** Professor Auxiliar da Universidade de Coimbra

Institutional Collaboration

Katholieke Universiteit Leuven

Coimbra, September, 2016

ACKNOWLEDGEMENTS

The work developed here presented was not possible without the help and collaboration of some people, to whom I cannot leave without my recognition.

To Larissa Gorbatikh, Stepan Lomov and Marina Selezneva, who guided me throughout the course of this work. Thank you for all you support and ideas that helped me achieve my goals and for accepting my application to do the work at KU Leuven.

To Yentl Swolfs, who, even at a distance, always provided with his insights on the contents of this work. His knowledge was also invaluable to the production of this thesis.

To Paulo Reis and Ana Amaro, who suggested my application to KU Leuven and helped me make the arrangements for my mobility period.

To the people from the Composite Materials Group at the Materials Engineering Department of KU Leuven, who accepted me as one of their own and gave their help in everything that was needed for this work, providing with their knowledge and experience.

To my parents, who provided me with the best conditions for getting where I am today. Without them, there would be no superior education, no possibility of moving to Leuven. Without their personal education, I would not be who I am today. For that and all the rest, thank you.

To my brother, who was always an example as an older brother. His experiences were always a reference to me on how to and how not to do everything in life.

To my aunt Maria, who provided me with a stable home in the last part of my Integrated Masters in Mechanical Engineering. Without her efforts to always making me feel at home, my life would be very different.

To the rest of my family, that were always there for me. They are all an inspiration for me.

To my friends Joel, Diogo, Pedro and Patricia, who have been there for me for the last ten years of my life, always prepared for times of fun and also times of seriousness. They are one of the reasons that I am glad I have ever practiced rowing.

To Tomás, who was my working partner during the better part of the Integrated Masters in Mechanical Engineering. His contribution to this work is the same as for every

other work we ever did together. Without the experience of working with him, there would be a lot of things I would not have learned.

To Carlos Lavoura and José Canhola, my mentors in my rowing experience. They were the ones who guided me throughout ten years of rowing, making me a better athlete and a better person. For giving me the will to never give up on my goals and dreams, thank you.

Abstract

The traditional carbon fibre-reinforced composites offer excellent mechanical properties while having a low density, which makes them an ideal solution for the applications where weight is a major concern. The self-reinforced composites (SRC's) consist of polymer fibres reinforcing a matrix made from the same material. In fact, it is by partially melting the fibres that the matrix is created. This type of composites provide a high toughness but lack the high stiffness and strength needed in structural applications.

Hybrid composites are a combination of at least two types of fibres in a matrix. By hybridizing self-reinforced polypropylene (SRPP) with unidirectional (UD) carbon fibre reinforced polypropylene (CFRPP), it is expected to combine properties of both composite types. The goal is to have a stiff and strong composite while maintaining a high toughness.

This thesis aims to understand how the material properties of a hybrid composite influence the flexural properties in a corrugated plate. The flexural properties of hybrid composites have been studied but always in flat surfaces. Also, the low compressive properties of polymer fibres make it difficult to capture the flexural properties.

By using this type of surface, the flexural properties should not be as highly dependent on the position of the carbon fibre (CF) laminae in relation to the neutral plane as they are for flat laminates. Experimental work has been performed to understand the dependence of the flexural properties of hybrid composite materials on the carbon fibre volume fraction (V_f) and position.

The experimental work was supported by a numerical modelling study. This study established preliminary knowledge needed for further developments of the model. In combination with the experimental work, the limitations of the current model are pointed out. The achievement of a more advanced model in the future, that can predict the behaviour of these hybrid composite materials when subjected to bending, is possible.

The main conclusions of this work were that the stiffness of a corrugated hybrid composite plate is not influenced by the position of the UD CFRPP layers. This property only changes with the CF V_f. The maximum flexural load and displacement at this point are also influenced by the CF content and by the thickness of the UD CFRPP layers. The

modelling work confirmed the stiffness behaviour but the model is not able to predict any other property. A large development of the model is still possible to be made.

Resumo

Os tradicionais materiais compósitos reforçados com fibras de carbono oferecem excelentes propriedades mecânicas enquanto mantêm uma baixa densidade, o que faz deles uma solução ideal para aplicações nas quais o peso é um fator a considerar. Os materiais compósitos auto-reforçados consistem em fibras poliméricas que reforçam uma matriz do mesmo material. De fato, é ao fundir parcialmente as fibras que se obtém a matriz. Este tipo de materiais compósitos proporciona uma elevada tenacidade mas não tem a alta rigidez e resistência mecânica necessária em aplicações estruturais.

Os materiais compósitos híbridos resultam da combinação de dois tipos de fibras numa matriz. Ao hibridizar polipropileno auto-reforçado com polipropileno reforçado com fibras de carbono unidirecionais, é esperada a combinação das propriedades dos dois tipos de compósitos. O objetivo é que se tenha um compósito rígido e resistente enquanto se mantém uma alta tenacidade.

Esta dissertação tem como objetivo a compreensão de como as propriedades materiais de um compósito híbrido influenciam as propriedades à flexão numa placa enrugada. As propriedades à flexão de compósitos híbridos já foram estudadas, mas sempre em superfícies planas. Além disso, as fracas propriedades compressivas das fibras poliméricas tornam difícil capturar as propriedades à flexão destas.

Ao usar este tipo de superfície, as propriedades à flexão não deverão ser tão dependentes da posição das camadas de fibras de carbono em relação ao plano neutro como se verifica para laminados. O trabalho experimental foi realizado para entender a dependência das propriedades à flexão de um material compósito híbrido com a variação da fração volúmica e posição das fibras de carbono.

O trabalho experimental foi suportado por um estudo de modelação numérica. Este estudo estabeleceu conhecimentos preliminares necessários para desenvolvimentos futuros do modelo. Em combinação com o trabalho experimental, as limitações do modelo atual são enunciadas. O desenvolvimento de um modelo mais avançado no futuro, que possa

prever o comportamento destes materiais compósitos híbridos quando sujeitos a flexão, é possível.

As principais conclusões deste trabalho são que a rigidez dos compósitos híbridos em placas enrugadas não é influenciada pela posição das camadas de fibras de carbono. Esta propriedade apenas varia com a fração volúmica de fibras de carbono. A carga de flexão máxima e deslocamento também são influenciados pelo conteúdo de fibras de carbono e pela espessura das camadas de fibras de carbono unidirecionais. O trabalho de modelação confirmou o comportamento da rigidez mas o modelo não é capaz de prever as outras propriedades. Ainda é possivel fazer um grande desenvolvimento do modelo.

Palavras-chave: Compósitos Auto-Reforçados, Híbrido, Enrugado, Propriedades à Flexão

Contents

LIST OF FIGURES

LIST OF TABLES

SIMBOLOGY AND ACRONYMS

Simbology

b_1 – Width of the flange

b_2 – Width of the cross section

d – Distance from the centroid of the web to neutral axis of the section

E – Young's Modulus

h_1 – Vertical height of the web

h_2 –Height of the cross section

L – Support span length

P – Applied Force

T_g – Glass transition temperature

T_m – Melting temperature

t_w – Entire thickness of the web

$(t_w)_i$ – Thickness of the ith composite layer in the web

V_f – Volume fraction

z_j – Closest distance from the jth composite layer in the flange to the neutral axis

δ – Mid-Span Displacement

ε – Strain at the outer surface

θ – Angle between the web and the neutral axis

λ – Draw-ratio

σ – Stress at the outer surface

ϕ_0 – Initial cross-sectional area

ϕ_f – Final cross-sectional area

Acronyms

ASTM – American Society for Testing and Materials

CD – Compression Damage

CF – Carbon Fibre

CFRPP – Carbon Fibre Reinforced Polypropylene

CLT – Classical Laminate Theory

FEA – Finite Element Analysis

FRP – Fibre Reinforced Polymer

HE – High Elongation

LE – Low Elongation

PE – Polyethylene

PP – Polypropylene

SRC – Self-Reinforced Composite

SRPP – Self-Reinforced Polypropylene

TD – Tension Damage

UD – Unidirectional

1. INTRODUCTION

A fibre-reinforced composite material is composed of fibres that give stiffness and strength to the composite and a matrix that binds the fibres together. Without the fibres, the matrix would just be a homogenous material belonging to another material class. The fibres, on their own, do not provide the structural integrity. A matrix is needed so that the fibres are able to deform as a whole. This combination usually offers excellent mechanical properties, while maintaining a low density.

The earliest men-made composites were straw and mud to make bricks. Other primary composite materials are recorded in history as, for example, the bows made by the Mongols in the 12th century. Only between 1870 and 1890, with the revolution in the field of chemistry, the first synthetic resins were developed, which could be converted from a liquid to a solid state by polymerization. These early synthetic resins included celluloid, melamine and Bakelite [1].

The incorporation of fibre-reinforced polymers (FRP) into the industrial world happened just after the beginning of the 20th century. The first FRP product was a boat hull manufactured in the mid 1930's using fibreglass fabric and polyester resin. Since then, FRP's have established themselves in industries like aircraft, military, automotive, construction or corrosion-resistant equipment [2].
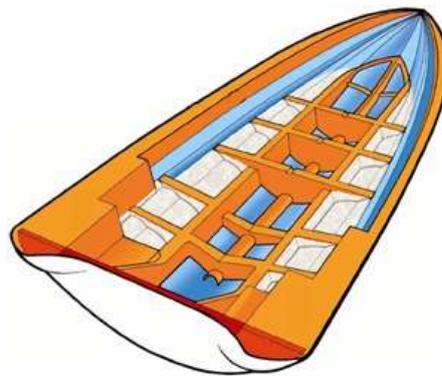
Figure 1.1. A boat made from composite materials (adapted from [3])

The traditional composite materials are made of carbon or glass fibres and a polymeric matrix. Thermoplastics are of great interest as matrix material, given the ability to achieve short production cycles, since no curing is necessary, and also the better

recyclability. Nevertheless, there are some disadvantages in using thermoplastic resins. The high viscosity of these makes impregnation more difficult [4 - 6], requiring expensive equipment to provide high pressures that help impregnation. Also, melting thermoplastics only creates new physical bonds but no chemical bonds. Inherent chemical differences between fibres and matrix also occur using thermoset resins, but are more pronounced for thermoplastics.

To solve the impregnation and interfacial bonding issues in thermoplastic composites, the use of SRC's is a possibility. These consist of polymeric fibres reinforcing a matrix made from the same polymer. In fact, it is by melting the fibres that the matrix is created. By being made of the same material, fibres and matrix are chemically compatible, creating a strong interface that is difficult to break [7, 8]. This kind of composites is also known by their high toughness in relation to the traditional composites [9 - 11]. Currently, SRPP is the most important SRC, commercially speaking [10, 12, 13].

A stiffness-toughness dilemma is introduced. On one hand, the traditional composites have a high stiffness and strength, but a low toughness. On the other hand, SRC's have a high toughness, but a low stiffness and strength. The use of composite materials is therefore limited by this dilemma.

To achieve a better balance between stiffness, strength, toughness and interfacial bonding, hybrid composites have been created. These consist of at least two types of fibres reinforcing a matrix. By hybridization of a SRC with carbon fibres, the best properties from both fibre types can be achieved, breaking the barriers of the stiffness-toughness dilemma.

One key parameter to understand how the failure of hybrid composites occurs is the volume fraction of the brittle fibres. The sudden loss of load carrying capability of the hybrid composites is more accentuated when the volume fraction of the brittle fibres is higher. By exploring the flexural properties of hybrid composites, the position of the brittle and ductile fibres in relation to the neutral plane is also a factor due to the stress variability through the thickness when subjected to bending. Therefore, the key parameters are CF fibre volume fraction and position in relation to the neutral plane.

When a laminate is bent, the middle layers are always subjected to less elongation, since the neutral plane coincides with the middle of the laminate. Having a hybrid composite, if the CF are placed next to the neutral plane, their contribution to the stiffness and strength of the composite is reduced. The use of corrugated surfaces is a good solution,

as the neutral plane only coincides with the cross section in certain locations. The majority of the cross section is either under tension or compression, escaping to the possibility that the middle layers do not contribute to the load carrying.
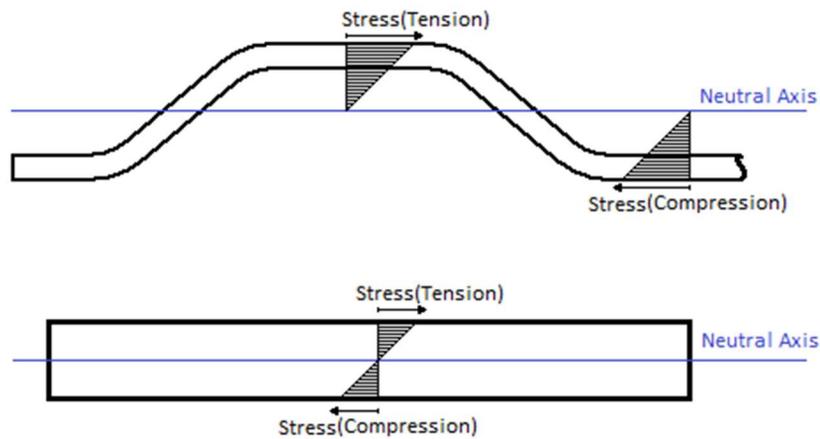
Figure 1.2. Stress Distribution on a corrugated and on a flat surface.

An understanding of how the material properties of a hybrid composite influence the flexural properties of a corrugated plate is developed in this thesis. An experimental work, supported by numerical modelling is explored, in order to determine how the flexural properties are influenced by the CF volume fraction and position.

2. STATE OF THE ART REVIEW

It is important to understand what self-reinforced composites are and how they are produced, since one of the composite materials studied belongs to this class. Then, the field of hybrid composites is explored and in it, an important concept: the hybrid effect.

After the materials sections are understood, the focus will go to the flexural properties of the hybrid composites. Most of the studies made on the flexural properties of hybrid composites use flat surfaced specimens. Therefore, it is important to know what is available about the flexural properties of corrugated surfaced plates too.

Finally, three point bending models are investigated to determine what the approach should be to this problem and how to design the model. The main concern will go to the boundary conditions.

2.1. Self-Reinforced Composites

Self-reinforced composites are a growing field of study. The traditional carbon or glass fibre-reinforced composites provide high stiffness and strength. Still, chemical differences between fibres and the polymeric matrix lead to a weak fibre-matrix interface contributes to low compressive strength, making them prone to damage initiation.

To achieve good fibre-matrix interface properties, Capiati and Porter [8] combined a polyethylene (PE) matrix with PE fibres, creating self-reinforced composites. These composite materials have some advantages, like low density, good recyclability, easy impregnation and excellent toughness [14].

Due to problems with service temperature, high creep sensitivity and high price [12, 10], the focus on self-reinforced composites switched to other polymers. A large potential was found in self-reinforced polypropylene. The main advantages, in comparison with self-reinforced polyethylene, are a higher service temperature and toughness, a wider processing window and the lower price [12, 10]. In fact, SRPP is the toughest SRC [10].

2.1.1. Drawing

To achieve these good properties, the polymer fibres have to be oriented. This can be done by solid state drawing, which takes place between the glass transition temperature, T_g and melting temperature, T_m. Before drawing, the polymer can be considered to be isotropic. In this state, the molecular chains are folded into lamellae that are highly oriented. The lamellae themselves can be densely packed creating spherulites, which are normally large and randomly oriented, causing the isotropic state of the polymer.

Normally, the polymer is passed through two rollers with different rotation speed. This process re-orients the molecular chains by stretching, rotating and breaking up crystal lamellae [15, 16]. As a result, the isotropic polymer becomes anisotropic.

The draw ratio, λ is a key parameter to characterise the oriented polymers. It is defined in Equation 2.1 as the ratio between the initial cross-sectional area, ϕ_0 of the tape over the final cross-sectional area, ϕ_f:

$$\lambda = \frac{\phi_0}{\phi_f},$$

(2.1)

2.1.1.1. Overdrawing

When a certain draw ratio is exceeded, a regime of overdrawing is reached. For polypropylene (PP), it is possible to observe this phenomenon by a change in appearance of the polymer from transparent to white. This whitening occurs due to the creation of voids and crazes inside the polymer [17].

Overdrawing is a similar process to necking, where the cross section decreases so that the density remains constant. In the case of the overdrawing regime, the cross section is maintained, meaning that the density has to be decreased. The microstructure of a drawn PP tape can be seen in Figure 2.1.
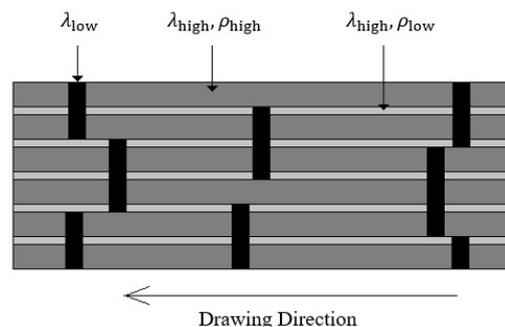
Figure 2.1. The microstructure of a drawn PP tape, containing regions with different draw ratio and density (adapted from [18]).

A biaxial stress state is formed in the high draw ratio regions. Due to the high orientation of the polymer, the transverse strength is reduced. This combination of biaxial stress state and low transverse strength creates regions with low density by creating voids and crazes. These regions decrease even more the transverse strength of the tape. Alcock et al. [18] confirmed this reduction in density by measuring the overall density of the tape as a function of the draw ratio. The evolution of density as function of the draw ratio can be observed in Figure 2.2.
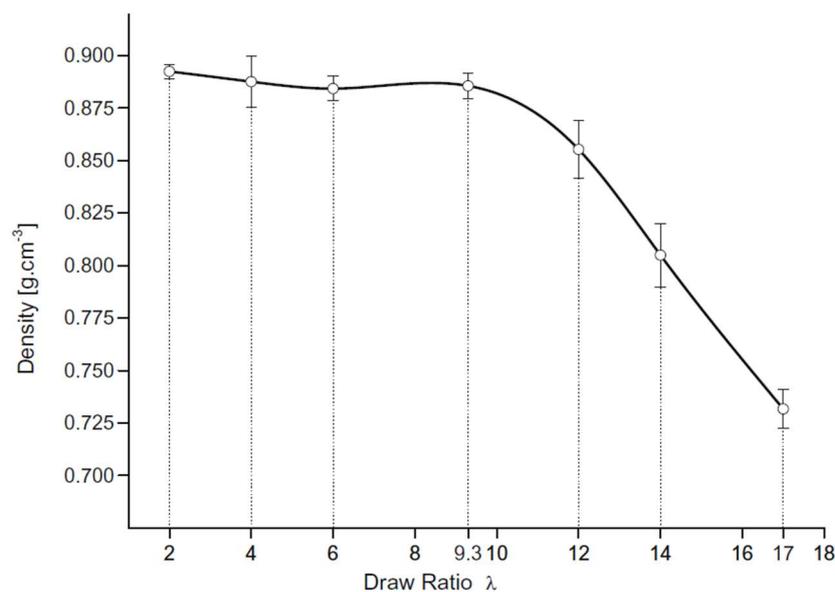
Figure 2.2. Evolution of the density of a PP tape with the draw ratio (adapted from [18]).

2.1.1.2.   Mechanical Properties

The mechanical properties of drawn polymers depend on the draw ratio, λ. The mechanical properties of an isotropic PP usually consist of a 1-1.5 GPa tensile modulus, a 25-33 MPa tensile strength and a 150-300 % failure strain. [19].

With the variation of the draw ratio, the mechanical properties can be tailored. Yamada et al. [20] proved that, even though the crystal orientation levels off at a draw ratio of 9, the tensile modulus keeps on increasing due to the increase of the orientation of tie molecules. The increase in tensile modulus with the draw ratio can be observed in Figure 2.3. The specific tensile modulus is the ratio between tensile modulus and density of the polymer.
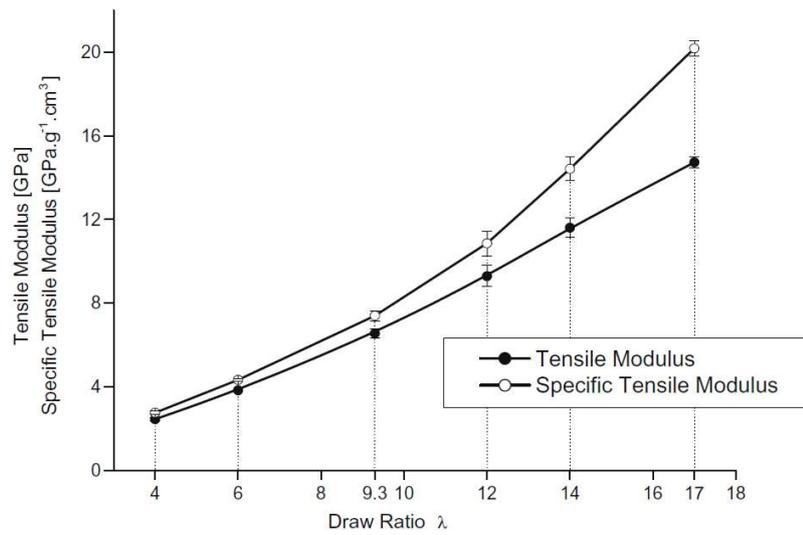
Figure 2.3. Evolution of the tensile modulus as a function of the draw ratio (adapted from [18]).

The tensile strength is known to be controlled by the orientation of the crystals [21]. As referred before, this orientation levels off for $\lambda = 9$. It is at that point that the tensile strength reaches a plateau, indicating that this property is indeed controlled by the orientation of the crystals. The failure strain tends to decrease as the draw ratio increases. If the tape was linear elastic (which is a reasonable approximation for $\lambda > 10$ [10]), the increase of the tensile modulus but stabilization of the tensile strength can explain the decrease in failure strain. The evolution of both the tensile strength and failure strain are shown in Figure 2.4. The specific tensile strength is the ratio between the property and the density.
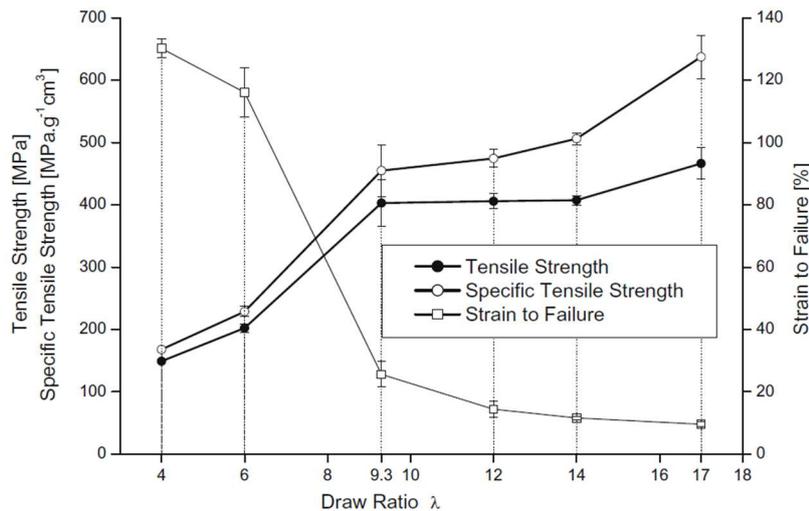
Figure 2.4. Evolution of the tensile strength and failure strain as a function of the draw ratio (adapted from [18]).

2.1.2. Production of SRPP

The two main processes for making SRPP have been commercially developed: CURV® and PURE®/Tegris®. The technical names for the processes are hot compaction and bi-component tape technology, respectively.

In the hot compaction process, heat and pressure are applied to mono-component oriented fibres or tapes. They are melted on the outside, while maintaining the oriented core. The bi-component tape technology starts off with a bi-component tape composed of a homopolymer core and a thin copolymer layer on the outside. When heat and pressure are applied, only the copolymer layer is melted, maintaining the core intact. The schematization of the processes is shown in Figure 2.5.
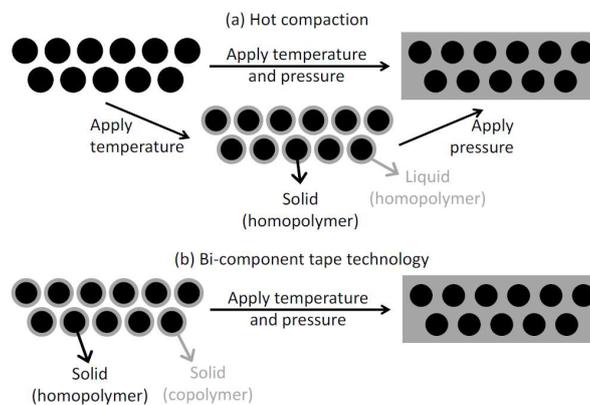
Figure 2.5. Comparison between hot compaction (a) and bi-component tape technology (b) processes (adapted from [14])

Both processes lead to high volume fractions of the tapes, in a range from 70 to 90 %. The way that this parameter is controlled is different though. While in bi-component tape technology, the tape volume fraction is controlled by the thickness of the copolymer layer, in hot compaction process, this variable is controlled by the process parameters [22, 23]. The importance of the process parameters is a lot more pronounced in hot compaction process, leading to a narrower processing window. A careful adjustment of parameters as temperature [24], pressure [10, 13, 25 – 29], dwell time [30 - 36] and cooling rate [37 - 40] has got to be achieved in order to melt only the outer layers of the polymer, and not the whole fibre in hot compaction process.

Hot compaction process was recently optimized by Swolfs [14] for general applications of SRPP. The optimal process conditions are 5 min at 188 ºC and 39 bar. After the dwell time, the composite is cooled down to 40 ºC in 5 min, leading to a cooling rate of about 30 ºC/min.

2.2. Hybrid Composite Materials

A hybrid composite contains at least two fibre types embedded in a matrix. After the invention of carbon fibres [41, 42], their high price was a big problem. So, the search on hybridization of composites became highly active. Combining two fibre types in a single composite serves the purpose of maintaining the advantages of both fibre types, while the disadvantages are alleviated. There can be three types of hybrid composites, accounting for the dispersion of both fibre types: interlayer, intralayer and intrayarn (See Figure 2.6).
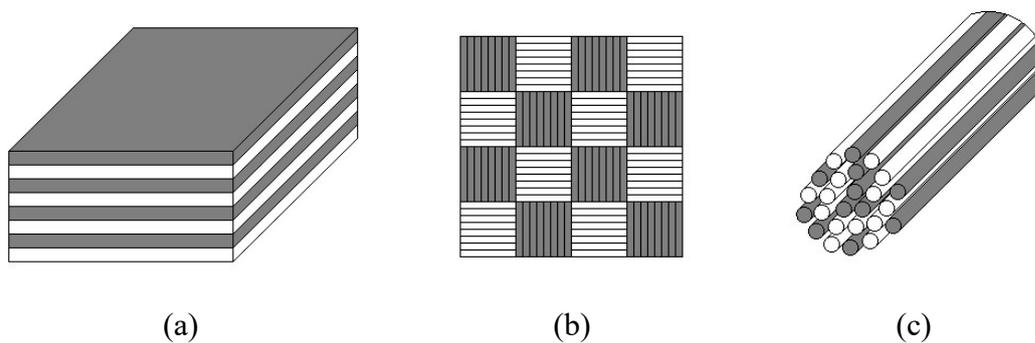
Figure 2.6. Schematic comparison between an interlayer (a), intralayer (b) and intrayarn (c) hybrid composite. (adapted from [14]).

Interlayer hybrid composites are generally the least dispersed type. The layers of each fibre type are simply placed on top of each other (Figure 2.6a). Intralayer hybrid composites usually have a medium dispersion, as both fibre types are present in each layer (Figure 2.6b). They can be, for example, woven together obtaining a woven sheet with both fibre types. Intrayarn hybrid composites can be the most dispersed type of these composites. Both fibre types are placed together in a single yarn, giving something of a random placement of the fibres (Figure 2.6c). Only interlayer hybrid composites are used in this study.

The two types of fibres are commonly referred to as low elongation (LE) and high elongation (HE) fibres. This terminology does not mean that the LE fibres have a low failure strain or the contrary for HE fibres. This designation only implies that the LE fibres present the lowest failure strain from both fibre types. Saying this, the designation still applies even if both fibres are considered brittle or ductile. In this study, the LE fibres are brittle while the HE fibres are ductile.

2.2.1. The Hybrid Effect

A lot of definitions have been given to the term "hybrid effect". One of them is reported by Hayashi [43] as the apparent enhancement of the failure strain of the LE fibres, in comparison with the failure strain of the same fibres in a non-hybrid composite. Another is the deviation from the linear rule of mixtures [44, 45]. By no means should the hybrid effect be described as the enhancement of the ultimate failure strain of the hybrid composite in comparison with the failure strain of a composite made from the LE fibres. The hybrid effect takes into account more mechanical properties than the failure strain.

Some theoretical hypothesis became available to explain this concept [46 - 49]: residual stresses, changes in the damage development leading to the final failure of the hybrid composite and dynamic stress concentrations. The concept is now well established but not yet thoroughly understood.

The first hypothesis is attributed to residual shrinkage stresses due to differences in thermal contraction of both fibre types. For example, in a hybrid composite with carbon and glass fibres, after the resin is cured, the glass fibres will shrink while the carbon fibres will maintain their length. Not being able to contract, the glass fibres will be subjected to tensile stresses and the carbon fibres to compressive stresses. When loaded in tension, the carbon fibres will fail for a higher strain since they have to overcome the compressive stresses first. This contributes for the hybrid effect but not fully explains it.

The second hypothesis is related to the way failure develops. Manders and Bader [50] explained that this problem can be dealt with in a statistical or fracture mechanics approach. It is easier to use the statistical approach and therefore, it has received more attention. In a composite, fibre strength is not a single, unique value, but it is rather a stochastic variable. If the fibres are intact, they all carry the same stress.

When the first fibre breaks, the matrix is loaded in shear and transfers stress to the broken fibre, which will recover the stress carrying capability after a certain distance is reached. The neighbour fibres will be subjected to stress concentrations and take over the additional load in a range between 5 % and 15 % [51 - 53] in the plane of the fibre break. The stress concentrations lead to a higher probability of failure of the neighbour fibres. As the strain increases, these are likely to break and develop clusters of fibre breaks. If the clusters grow enough, an unstable growth occurs, leading to the failure of the composite.

Hybrid composites can interfere with this failure development. For example, the different stiffness or diameter of the LE and HE fibres can be a factor [49]. Another factor is the possibility of the LE fibres to be bridged by the HE fibres [54, 55], which delays the growth of the clusters and can also increase the critical cluster size. Finally, if a hybrid composite is compared to a LE fibre composite with the same volume, then the volume of LE fibres is lower in a hybrid composite, reducing the probability of failure [56, 57].

The third hypothesis is attributed to dynamic stress concentrations. When a fibre breaks, the load on that fibre is locally relaxed and the fibre springs back. A stress wave, which travels along the fibres, is created, causing temporary stress concentration [58, 59]. Xing et al. [60] extended this concept to hybrid composites. These authors used a hybrid composite with one row of LE and one row of HE fibres. Their model demonstrated that two stress waves propagate when a fibre breaks. One of the waves propagates through the LE fibre row, while the other propagates through the HE fibre row, but always out-of-phase. This leads to lower stress concentrations in a hybrid composite, in comparison with a LE fibre composite. The lower stress concentrations can lead to a positive hybrid effect.

2.2.2.   Flexural Properties

In hybrid composites, the flexural properties change not only with the types of layers that are contained in the laminate but also with the sequence of the layers in the same laminate. Therefore, by changing the lay-up sequence, it is possible to tailor the flexural properties of the material. When a non-hybrid laminate is subjected to bending, the stress is null in the neutral plane and increases with the distance from this plane. The inner layers are subjected to a low stress and do not contribute much to the stiffness and strength of the composite. In contrast, the outer layers are the ones that contribute the most to the flexural properties, since they carry the most amount of stress in a laminate.

In a hybrid composite, the maximum stress may not occur in the outermost layers. Even for smaller strains in the inner layers, due to differences in stiffness, these can be carrying a higher stress. Advanced theories, like the classical laminates theory (CLT), should be used to predict the response of a hybrid composite in bending [61]. The stress distribution in hybrids and non-hybrids in shown in Figure 2.7.

(a)   (b)
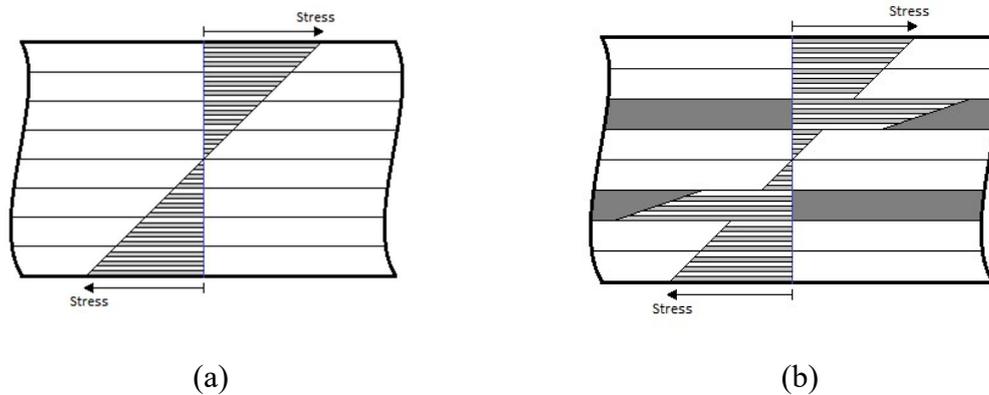
Figure 2.7. Stress Distribution in a (a) non-hybrid and in a (b) hybrid composite subjected to bending.

2.2.2.1.   Flexural Modulus

Hybrid effects in the flexural modulus are not likely to occur, since it can be perfectly predicted with CLT. The flexural modulus of a hybrid composite lies between the property of each non-hybrid.

Jawaid et al. [62] studied different stacking sequences using tri-layered natural fibre hybrids. They reported that using jute fibres (the most brittle) as the outside layers would increase the flexural modulus. The fact that flexural modulus is controlled by the properties of the outermost layers can justify that behaviour [63 - 66].

If more than 3 layers are used, the number of possible sequences is higher. Diharjo et al. [67] studied symmetrical stacking sequences with the goal of replacing glass fibre layers with carbon in the outermost layers. The study showed that an increase in carbon fibre volume fraction would improve the flexural modulus, like it is to be expected by the CLT predictions.

Swolfs [14] studied the effect of carbon fibre volume fraction in intralayer UD CFRPP/SRPP hybrids. He only focused on the flexural modulus, since the samples never fractured, given the high ductility of the SRPP. The flexural modulus increased slowly with the carbon fibre content until a CF V_f of 7 %. When the CF content was 11 %, the flexural modulus strongly increased.

2.2.2.2.   Flexural Strength

The flexural strength of a hybrid composite is not so easy to interpret, since it cannot be predicted with CLT. Dong et al. [68] studied carbon/glass intralayer hybrids,

obtaining flexural strengths 40 % and 9 % higher than the carbon and glass non-hybrids, respectively.

The work of Giancaspro et al. [69] showed that glass fibre composites failed in the tensile side, while the carbon fibre composites failed in the compressive side. The replacement of the outermost layers on the tensile side of glass fibre composites by carbon fibre layers was proved to increase the flexural strength. The same did not happen when they were added to the compressive side, where the failure mode changed from failure in the tensile side to crushing on the compressive side.

By replacing the 12.5 % of carbon fibres by silicon carbide fibres on the compressive side of carbon fibre composites, Davies et al. [70] demonstrated that the flexural strength was 22 % higher. It is suggested that the compressive strength of the silicon carbide fibres is higher than for carbon fibres.

An optimal amount of glass fibres exists to achieve the highest flexural strength possible [69, 71]. The highest flexural strength in a carbon/glass composite when 12.5 % of its volume is made of glass fibres, all in the compressive side [71]. In flat laminates, a symmetrical lay-up is not the optimal design for a composite loaded in bending.

Even though the focus was not on flexural strength, Swolfs [14] also reported buckling of the specimens on the compressive side. The buckling occurred due to the already existing crimp of the carbon fibre yarns in the fabric of the intralayer hybrid.

The investigation in natural fibre hybrids is also found in literature. The flexural strength of this type of composites is usually between the performances of each fibre type [62, 67, 72]. The application of a NaOH treatment to sisal fibres was proven to increase the flexural strength due to the improvement of the adhesion to the matrix [73].

2.3. Corrugated Composite Laminates

Corrugated structures have the capability of being very stiff in the longitudinal direction and flexible in the transverse direction (See Figure 2.9). This kind of structures is usually seen in boat docks but made out of steel. This study is directed to composite materials so there is no sense in reviewing the literature on corrugated steel structures. There are two kinds of approaches made in literature: experimental and analytical models. Both will be reported in this section.

2.3.1. Experimental

Shao et al. [74] studied the evolution of the apparent flexural rigidity, EI, when the span to depth ratio was varied. The corrugated structures used were not continuous, in a sense that they were constituted by symmetrical double Z cross section panels connected to each other, like shown in Figure 2.8. Still, the shape of the cross section is very similar to the one studied on this thesis. They proved that span to depth ratio has an effect on EI. An increase in span to depth ratio would decrease the influence of shear deformation to the deflection. Therefore, the flexural rigidity would increase asymptotically until a stable value.
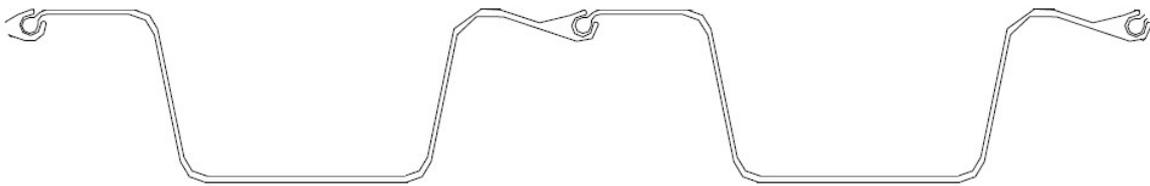
Figure 2.8. Linked Symmetrical double Z cross section panels (adapted from [74]).

Tamrakar and Lopez-Anido [75] also studied this kind of structures to evaluate the effect of the strain rate, using wood plastic composites. The results showed that EI increased along with the strain rate. More recently, Wang et al. [76] studied the effect of fibre volume fraction on the flexural properties of these sheet pile panels. They reported that the fibre volume fraction in the transverse direction, not only influences the failure modes of fibre reinforced plastics, but also the rigidity and load capacity.

The only continuous corrugated structure study found in literature was performed by Yokozeki et al. [77]. The corrugations were round and not trapezoidal, like shown in Figure 2.9. Tensile and flexural tests were executed in the longitudinal and transverse directions and the ultra-anisotropic of corrugated composite structures confirmed.
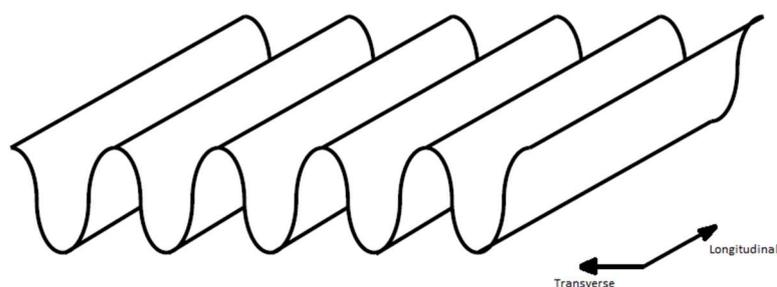
Figure 2.9. Continuous round corrugated structure studied by Yokozeki et al. (adapted from [77]).

2.3.2. Analytical Models

The classical laminate theory is a useful tool to predict the mechanical properties of laminated composites. Unfortunately, the applications where CLT can be used are limited, since only flat surfaces can be used. In the past few years, there have been some improvements and analytical models, based on CLT, were developed to predict the mechanical properties of corrugated surfaced composites.

One was presented by Samanta and Mukhopadhyay [78]. In their study, according to the geometry of the corrugated surface, the matrices used in CLT are corrected, in order to convert the corrugated surface into an orthotropic plate. The same approach was followed by Yokozeki et al. [77], who derived the longitudinal and transverse rigidities of the plate using the CLT matrix components and the geometry of the cross section.

The simplest analytical model was developed by Giroux and Shao [79]. In their study, a method to determine the apparent modulus was determined. This method divides the structure of the surface into flanges and webs. The layers in the corrugated surface would be like shown in Figure 2.10.
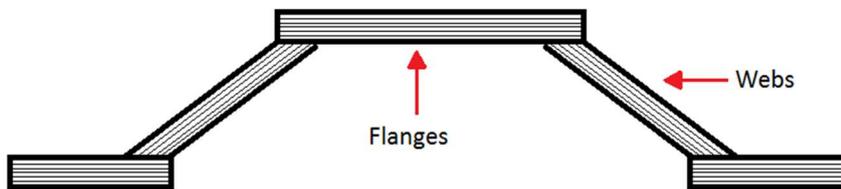
Figure 2.10. Giroux and Shao's analytical model shape approximation.

To determine EI, equations 2.2 and 2.3 are used [79]:

$$(EI)_{flange} = \frac{b_1}{3} \sum_{j=1}^{n} (E_x)_j (z_j^3 - z_{j-1}^3), \tag{2.2}$$

$$(EI)_{web} = \sum_{i=1}^{m} \frac{(E_x)_i (t_w)_i}{t_w} \left[\frac{1}{12} \frac{t_w}{\cos\theta} h_1^3 + \frac{t_w}{\cos\theta} h_1 \cdot d^2 \right], \tag{2.3}$$

Where b_1 is the width of the flanges, E is the young's modulus, z_j is the closest distance from the jth composite layer in the flange to the neutral axis, $(t_w)_i$ is the thickness of the ith composite layer in the web, t_w is the entire thickness of the web, θ is the angle between the web and the neutral axis, h_1 is the vertical height of the web and d is the distance from the centroid of the web to the neutral axis of the section.

The separation between flanges (a) and webs (b), along with the specific parameters, is illustrated in Figure 2.11.
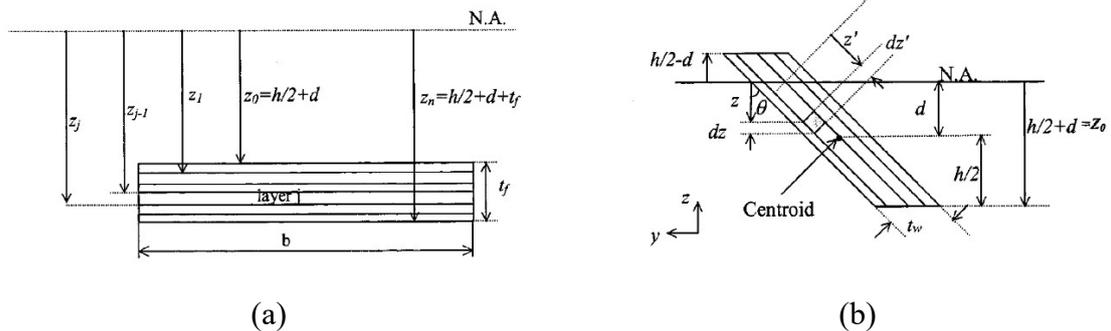
Figure 2.11. Example of a flange (a) and of a web (b) from Giroux and Shao's study (adapted from [79]).

2.4. Three Point Bending Modelling

Different approaches can be used to simulate a three point bending test but detailed information on those approaches is difficult to find. The most challenging part of the modelling is the boundary condition definition in the contact locations. It is important to understand that the movement of the sample in the support contact area is made along the perimeter of the rollers, like it is illustrated in Figure 2.12. A simple restriction of the movement in the thickness direction may be a good approximation but it is not the most correct one. For a correct model, the rollers should be designed and therefore, the contact between them as well.
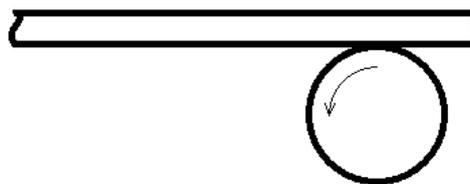
Figure 2.12. Movement of a sample around the roller during a flexural test.

In order to account for that possibility, approaches like using analytical rigid bodies for the supports [80], applying restriction to the mid-span section and displacement in the support contact zone [81], using rigid surfaces as the supports [82], applying sinusoidal forces in the support contact zones [83] or even forcing the rotation of the support roller, so that the contact is made always in the same nodes but in a different angle [84] are used. It was also found that a mesh refinement is necessary in the contact zones, for more accurate results [85].

2.5. Conclusions

This chapter is the basis for the following presentation of results, as the author attempts to approach the important subjects so that the reader can better understand the work developed. SRPP is an important SRC due to its high toughness and low price. To obtain a SRC, the polymers have to be oriented by drawing. The draw ratio has to be carefully studied, so that the optimal mechanical properties are achieved.

Two main processes are used to manufacture SRPP. The difference between both of them is in the process parameter window. To produce SRPP with hot compaction, the temperature, pressure, dwell time and cooling rate have to be considered. Swolfs [14] has performed an optimization of the process.

The hybridization of composites can be made by joining at least two fibre types in a matrix. The flexural properties of hybrid composites are dependent on the position and volume fraction of the LE fibres. The flexural modulus can be well predicted by the CLT but the flexural strength cannot. Replacing carbon fibre layers on the compressive side by glass fibre layers tends to improve the flexural strength of a hybrid composite. The same happens when glass fibre layers are replaced by carbon fibre layers in the tensile side of a glass fibre composite.

The study of corrugated structures is still limited. It was proven that the apparent modulus depends of the span to depth ratio and strain rate in a flexural test. The ultra-anisotropic nature of these structures was also demonstrated, being stiff in the longitudinal direction but flexible in the transverse direction. The use of analytical models, based on CLT, to predict the stiffness of corrugated composite laminates can be very useful.

Finally, the development of three point bending models is a challenging task because of the application of the boundary conditions. A great number of approaches are described in literature, but they can be difficult to implement. A mesh refinement in the supports and loading nose locations is necessary when contact models are involved.

3. EXPERIMENTAL

3.1. Materials

3.1.1. Self-Reinforced Polypropylene

The self-reinforced polypropylene used in this study was generously provided by Propex Fabrics GmbH. In its isotropic state, the melting temperature of the PP is 163 ºC.

The tapes that constitute the fabric have been drawn at a draw ratio between 10 and 15. The drawing conditions are confidential. The tapes have a rectangular cross section, with a thickness of around 50 µm, a width of 2.4 mm and an areal density of 110 tex. Prior to hot compaction, the tapes have a tensile strength, modulus and failure strain of 500 MPa, 10 GPa and 9 % respectively [86].

The weaves used have a twill 2-2 pattern (See Figure 3.1). The fabrics are produced on a pilot scale loom. Since the tapes have a high width to thickness ratio and there is overfeeding, they tend to fold along their length during the weaving process. Overfeeding is achieved by the excess of tapes fed in one direction or due to battening of the loom. The weaves provided by Propex Fabrics GmbH have an overfeeding of 150 %. During the section "3.4.4 Optical Microscopy", the folded tapes are visible in the cross section and will be pointed out. After production, each layer of the weave has a thickness of around 150 µm [14].
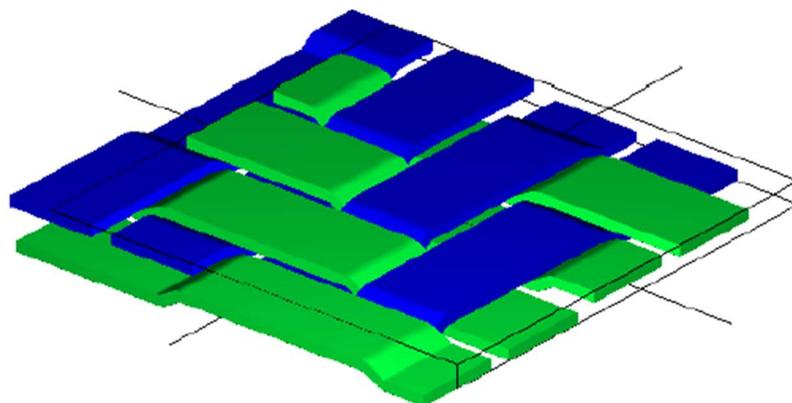
Figure 3.1. 3D Illustration of a twill 2-2 weave pattern without overfeeding (adapted from [14])

3.1.2. Unidirectional Carbon Fibre Reinforced Polypropylene

The unidirectional carbon fibre-reinforced polypropylene prepregs were kindly provided by Jonam Composites (United Kingdom). The prepregs contain T700 carbon fibres but the exact grade of the PP is unknown. Based on the production experience, the PP from the prepregs is different from the one in the SRPP fabrics, as it is more brittle and adhesive to the steel mould.

Prior to hot compaction, the prepregs have a thickness of 160 μm, a width of 100 mm and a carbon fibre volume fraction of 32 ± 1 % (Specifications of the manufacturer). Although they have an excellent impregnation, the prepregs have two drawbacks: the carbon fibres are bundled together and there are matrix-rich regions near the surface. Figure 3.2 shows microscopy images from their cross section [14].
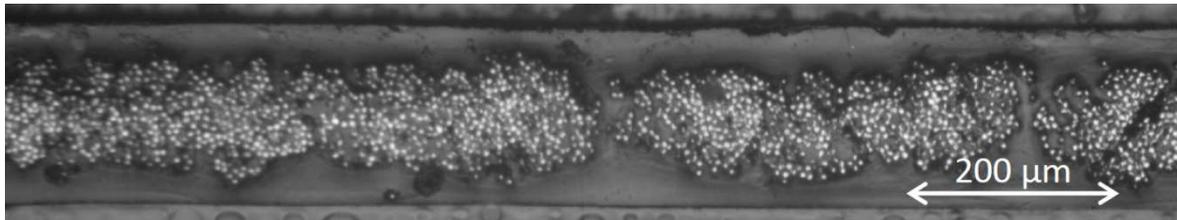
Figure 3.2. Microscopy Image from the prepregs cross section (adapted from [14]).

3.2. Production

3.2.1. Samples Produced

Before going into the stacking sequences and dimensions of the samples produced, it is important to introduce the cross section of the corrugated plates. Figure 3.3 shows the shape and dimensions of the cross section, in mm.
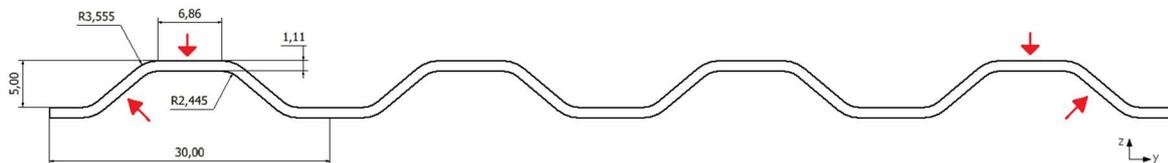
Figure 3.3. Corrugated surface cross section and dimensions.

The corrugated surface has a trapezoidal shape with round edges. The corrugations repeat themselves with a period of 30 mm and the nominal height is 6.11 mm. The length and width of the mould are equal to 310 mm. It is also important to define the three directions of the plate. The "*y*" and "*z*" axis defined in Figure 3.3 are the transverse

and normal directions, respectively. The longitudinal direction is normal to the cross section plane. The red arrows purpose will be presented in the section "3.2.1.2 Dimensions".

3.2.1.1. Stacking Sequences

A number of different stacking sequences were considered in this study. The mould is designed for a thickness of 1.11 mm, like shown in Figure 3.3. Since the thicknesses of the SRPP and UD CFRPP are 150 µm and 160 µm, respectively, the number of appropriate layers to use is 7. Using 7 layers and restraining the options to symmetrical lay-ups, the total number of possible stacking sequences is 16.

As referred in the section "3.1.2 Unidirectional Carbon Fibre Reinforced Polypropylene", the PP used in the prepregs is more adhesive to the mould than the one used in the SRPP fabric. There is also the technical difficulty of placing releasing agent over all the corrugated surface of the mould. Therefore, the production of plates where the outside layers are made out of UD CFRPP is problematic. The stacking sequences were restricted to the ones with SRPP layers as outside layers as a consequence. The lay-ups studied and their carbon fibre volume fraction are presented in Table 3.1. To determine the CF V_f of each lay-up, equation 3.1 can be used.

$$CF\ V_f = \frac{n_c \times t_c \times f}{n_c \times t_c + n_s \times t_s},$$

(3.1)

Where f is the carbon fibre volume fraction of the prepregs, n_c is the number of UD CFRPP layers, n_s is the number of SRPP layers, t_c is the thickness of the UD CFRPP layers and t_s is the thickness of the SRPP layers.

To understand the stacking sequence annotations, it is important to know that "S" and "C" stand for SRPP and UD CFRPP, respectively. The "*so*" outside the parenthesis means that the lay-up is symmetrical and contains an odd number of layers. An annotation with 4 letters is enough to describe the lay-up, where the fourth letter represents the middle layer.

Table 3.1. Stacking sequences produced and tested.

Stacking Sequence	CF V_f	Stacking Sequence	CF V_f
$(S/S/S/S)_{so}$	0%	$(S/S/C/C)_{so}$	14%
$(S/S/S/C)_{so}$	5%	$(S/C/S/C)_{so}$	14%
$(S/S/C/S)_{so}$	10%	$(S/C/C/S)_{so}$	19%
$(S/C/S/S)_{so}$	10%		

3.2.1.2. Dimensions

To measure the flexural properties of the corrugated hybrid composites, the size of the plates is not appropriate. To avoid shear deformation and torsion, the length and width of the samples has to be carefully considered [74].

A high span to depth ratio is required and so, the length should be the maximum possible, which is the size of the plate in the longitudinal direction. That way, the span length is only limited by the testing machine. The width should be high enough to avoid torsion of the cross sections, but not as long as it would exceed the dimension of the rollers. To that purpose, a width of 120 mm (4 corrugated cycles) is preferred.

The thickness varies with the number of SRPP and UD CFRPP layers. According to the specifications from the prepregs and Swolfs [14], the thickness should be between 1.05 and 1.09 mm. Unfortunately, during the production, the PP from the prepregs flowed out of the mould and made the hybrid plates thinner than expected.

With the exception of the (S/S/S/S)$_{so}$ lay-up plates, every plate showed voids in the UD CFRPP layers on one half of the plate. Those defected parts were not used for characterization. Therefore, each plate corresponds to only one sample. The plates were cut along the longitudinal directional with a steel guillotine. That method presented itself to be accurate enough while not damaging the samples too much.

The plates presented an accumulation of SRPP material on the borders of the plate. In order to be able to use the guillotine, those borders had to be cut first using a band saw. The damage induced by the cutting process is irrelevant, since the areas cut by this process are not subjected to any stress during the bending tests.

After cutting, the samples were measured. The length and width of the samples were measured with a ruler and the thickness with a micrometre. The thickness is not constant along the whole width, so a total of 4 points (See red arrows in Figure 3.3) were

measured in the mid-span location, where the load is applied. The nominal thickness of the sample is the average of the 4 thicknesses measured. The average thickness of the samples is presented on Table 3.2.

Table 3.2. Sample Dimensions.

Stacking Sequence	Thickness [mm]	Width [mm]
$(S/S/S/S)_{so}$	1.05 ± 0.10	11.93 ± 0.05
$(S/S/S/C)_{so}$	1.00 ± 0.30	11.86 ± 0.12
$(S/S/C/S)_{so}$	0.95 ± 0.01	11.92 ± 0.07
$(S/C/S/S)_{so}$	0.96 ± 0.02	11.96 ± 0.05
$(S/S/C/C)_{so}$	0.88 ± 0.02	11.96 ± 0.05
$(S/C/S/C)_{so}$	0.89 ± 0.02	11.96 ± 0.10
$(S/C/C/S)_{so}$	0.83 ± 0.03	12.00 ± 0.06

After observations under an optical microscope, it was confirmed that the thickness of the UD CFRPP layers is only 0.1 ± 0.02 mm. This thickness was measured using appropriate software (ImageJ) and was slightly inferior for $(S/C/S/C)_{so}$ and $(S/C/C/S)_{so}$ lay-ups.

3.2.2. Hot Compaction

The production of the plates was made using a Pinette Press Zenith 2. The heating rate of this press is 5 ºC/min. The procedure used for the production of the corrugated plates was adapted from Swolfs [14], with the compaction being made at 188 ºC and 39 bar for 5 min. The cooling rate of 30 ºC/min was not possible to achieve with this press. The equipment has another inconvenient, which is a less precise temperature control.

The interfacial temperature between mould and material should be uniform. Since the corrugated shape may induce temperature concentrations in certain parts of the mould, the usual procedure of pre-heating the press was not performed. Also, the high thickness of the mould would make it impossible to know the interfacial temperature between the mould and plate. Therefore, the mould was placed inside the press while it was still at a low temperature.

The press was then heated until 185 ºC, so that the top and bottom halves of it, which usually have different heating rate, could get to a homogenous temperature while not melting the SRPP tapes. When the 185 ºC were reached, the press was heated until 188 ºC and remained at that temperature for 5 minutes. The highest temperature in the press for each produced plate was recorded. The top and bottom average highest temperatures were 187.98 ± 0.45 ℃ and 189.18 ± 0.33 ℃, respectively.

After the dwell time had passed, the press was cooled down at an average rate of 4.86 ± 0.05 ℃/min until it reached 90 ºC. After that, there are no morphological modifications expected in the material, so and the mould was taken out of the press and the sample collected. In Figure 3.4, pictures of the corrugated surface sample mould (Figure 3.4a) and a non-hybrid plate (Figure 3.4b) can be seen. The production process for hybrids and non-hybrids was the same.
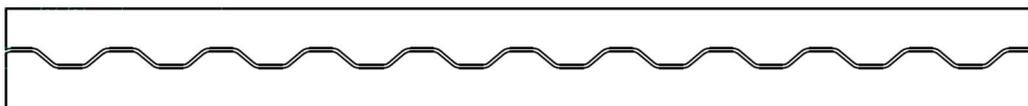
(a)

(b)

Figure 3.4. (a) Corrugated surface sample mould and (b) Non-hybrid SRPP plate

3.3. Test Methods

3.3.1.   Flexural Tests

The three point bending flexural tests were performed according to ASTM D7264/D7264M – 07 standard on an Instron 5567 equipped with a 1 kN load cell. The span

length used was 250 mm, which corresponds to a span to depth ratio of about 40, well within the range suggested in the standard. At least five specimens from each lay-up were tested. The loading nose displacement was set to a rate of 10 mm/min. The test was concluded after the force-displacement curve displayed a constant force since none of the samples fractured (See Figure 3..8)

The extracted data consisted of the force-displacement curve, from which the flexural properties were determined. The flexural properties extracted are presented in the section "3.4.1 Flexural Properties".

Figure 3..5. Set up of a flexural test.

3.3.2.   Depth Variation Analysis

The use of corrugated surfaces is known to improve the stiffness on the longitudinal direction [77]. With the application of a bending force, the shape of the cross section tends to change from corrugated to flat (See Figure 3..6). With that change, the specimen loses its ability to carry the load. It is possible that this geometrical deterioration has a big effect on the properties of the force-displacement curve.
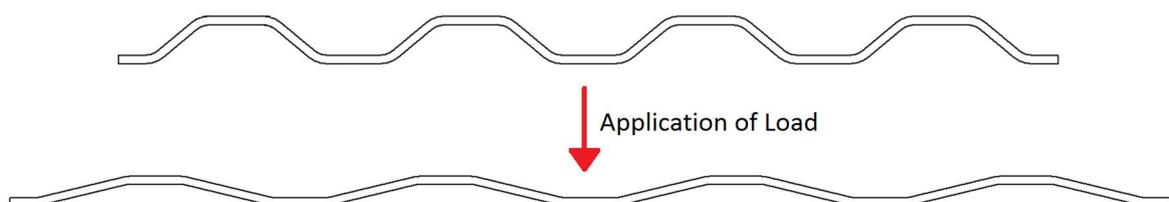
Figure 3.6. Deformation of the cross section with the application of load.

To determine the influence of the depth variation, flexural tests should be performed with flat samples, where no geometric deterioration can occur. The results should be compared to check if the failure strain is the same for the corrugated and flat surfaced samples, thus assessing the influence of the geometric deterioration.

At least one corrugated sample from each lay-up was filmed while being tested, using a camera. The camera was placed in a way so that the side of the sample appeared along with the loading nose, like presented in Figure 3..7. With the images taken and an appropriate software (like ImageJ), it is possible to measure the depth of the cross section during the test. The distance from the camera to the sample was kept constant, so that the distances measured in the images can be compared.

By measuring the thickness of the plate in the image, it is possible to determine the depth of the cross section.

(a)   (b)
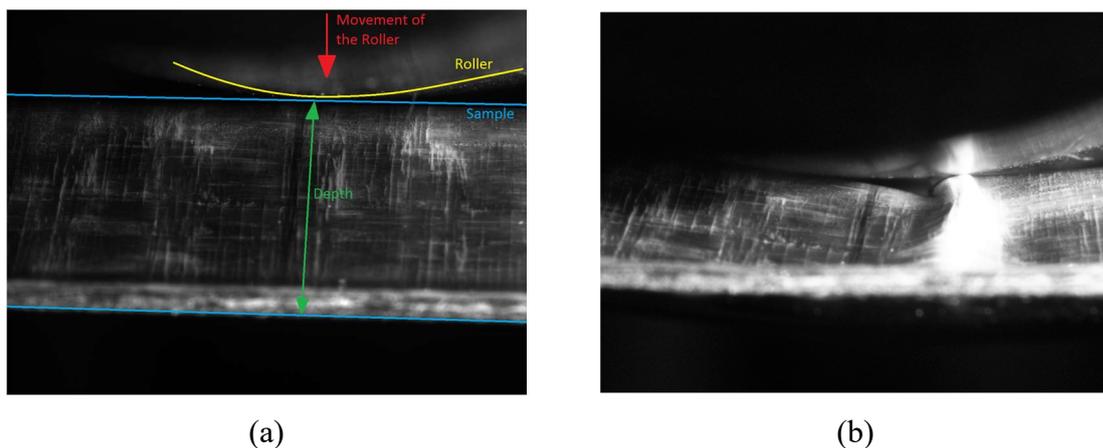
Figure 3..7. Image captured with camera during a flexural test preformed on a $(S/C/C/S)_{so}$ sample where (a) is the undamaged specimen with the indication of the main components and (b) is the damaged sample

3.3.3. Transmitted Light Imaging

The detection of damaged areas in SRPP is possible by shining light trough the non-hybrids, due to their semi-transparent nature. All the hybrids are opaque, making it impossible to do the same. Damaged and undamaged areas are possible to differentiate since light scatters on damaged surfaces. By placing the samples in front of a strong and constant lightbox, the samples were photographed before and after being tested.

3.3.4.   Interrupted Tests

Even with the images captured with a camera (See section "3.3.2 Depth Variation Analysis"), it is difficult to follow the damage evolution. After at least three samples from each lay-up were tested, the relevant points (See from Figure 3.17 to Figure 3.22) from the force-displacement curves were summarized and interrupted tests were performed.

To conduct these, the flexural tests were executed until the relevant points were reached. After they were achieved, the tests were interrupted and the samples analysed and photographed from the compressive and tensile side of the plate, using the transmitted light imaging technique. After characterization, the samples were further loaded until the next relevant point was reached.

For most of the stacking sequences, the relevant points were the maximum flexural load and the region of the force stabilization (See Figure 3.8). To assess the capacity of the damaged sample, a final test was conducted after the stabilization period is reached and the sample is already damaged.
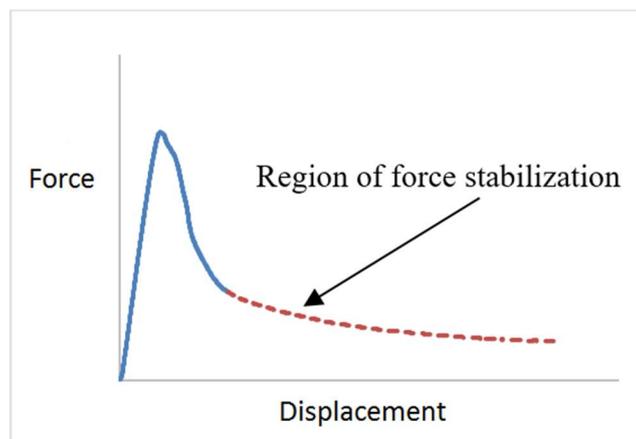
Figure 3.8. Region of force stabilization (dashed line).

To summarize, three tests were conducted: (1) until the maximum flexural load, (2) until the stabilization phase and (3) a final test. The tests were interrupted at additional points for the $(S/S/S/S)_{so}$ and $(S/C/S/C)_{so}$ lay-ups, which present other interesting points. The other interesting points are sudden load drops, which will be pointed out in the section "3.4.3 Interrupted Tests"

Not all lay-ups are reported in the section "3.4.3 Interrupted Tests". The $(S/S/C/S)_{so}$ and $(S/C/S/S)_{so}$ are not presented in the main text, but can be consulted in APPENDIX C. Each sub-section consists of the photographs at each stage of the interrupted

tests taken from the compressive (top images) and tensile (bottom images) side of the plate, along with the description of the damage evolution observed. The first set of images in each sub-section are from the undamaged samples. The blue marks in the samples were made by the author, prior to the tests, to determine the position of contact between the loading nose and the sample.

The area visualized in the images corresponds to the section of the plate illustrated in Figure 3.9.
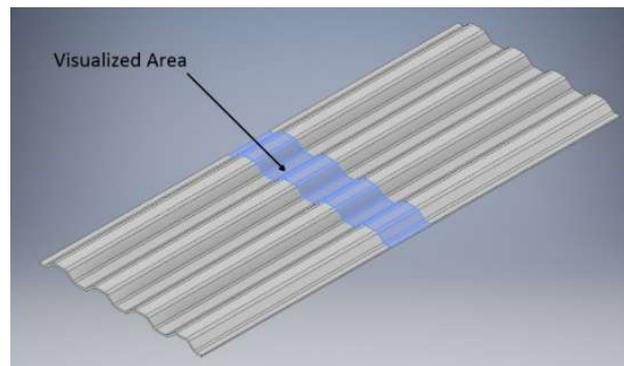
Figure 3.9. Visualized area between interrupted tests presented in the following sections. The compressive and tensile sides are the opposite faces of the same location.

3.3.5. Optical Microscopy

After being tested, the visibly damaged areas were cut from the sample and analysed under an optical microscope. This technique uses visible light and a system of lenses to magnify images of small samples. The images taken had a magnification of 4x, 10x or 50x. The magnification is detailed in each image.

The specimens were cut from the compressive and tensile side of the plate at the span middle location or from a location distant from the damaged areas, where no damage occurred. The undamaged specimens were cut so that a comparison could be made between damaged and undamaged specimens. The cut specimens location and plane of observation are presented in Figure 3.10. The terminology compression damage (CD) and tension damage (TD) specimen will be used in the sections "3.4.3 Interrupted Tests" and "3.4.4 Optical Microscopy".

<div align="center">(a)   (b)</div>
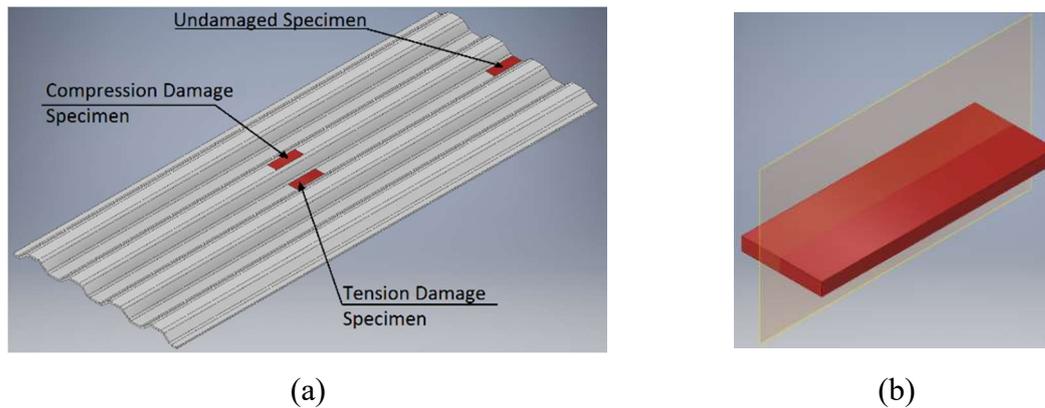
Figure 3.10. (a) Specimen cut location and (b) plane of observation in microscopy control

3.4. Results and Discussion

3.4.1.   Flexural Properties

ASTM D7264/D7264M – 07 is designed for specimens with rectangular cross sections. Since this is a special case, it was not possible to determine the stress-strain curves. The properties presented are determined from the force-displacement curves. Therefore, in this case, equivalent properties are studied. Those will be the stiffness (1), maximum flexural load (2), displacement at maximum flexural load (3) and energy absorption (4) (See Figure 3.11).

As shown before, the plates from the different lay-ups present variation in thickness. In an attempt to homogenise the data, the flexural properties were divided by the thickness of each sample, obtaining a "normalised" property. The width of the samples also has an effect on the force-displacement curve. The variation of this dimension with the lay-up is not significant though. Therefore, the force-displacement curves are only normalized by the thickness. Both simple and normalized properties are presented in the following sections.

Figure 3.11. Force-Displacement curve for the (S/S/S/S)$_{so}$ lay-up and identification of flexural properties.

3.4.1.1. Stiffness

The stiffness was measured in the constant slope zone of the force-displacement curve. To standardize that zone, the slope was measured between 1 and 3 mm of displacement. All curves present a constant slope in that location of the curve.

The stiffness increases with the carbon fibre V_f and with the distance from the UD CFRPP layers to the middle of the laminate. The increase with the carbon fibre V_f is higher than the one verified with the change of position of the UD CFRPP layers. That can be seen in Figure 3.12 that shows the variation of the stiffness with the lay-up. The carbon fibre content increases from bottom to the top. The third and fourth bar (10 % CF V_f), as the fifth and sixth (14 % CF V_f), have similar stiffness. It is more evident that the stiffness increase with the position of the UD CFRPP layers is lower when the normalized stiffness is considered.

The fact that the layers are generally further away from the neutral plane, in comparison with flat specimens, is the probable reason why the UD CFRPP layer position does not influence the stiffness. Only the CF V_f influences this property.

(a)   (b)
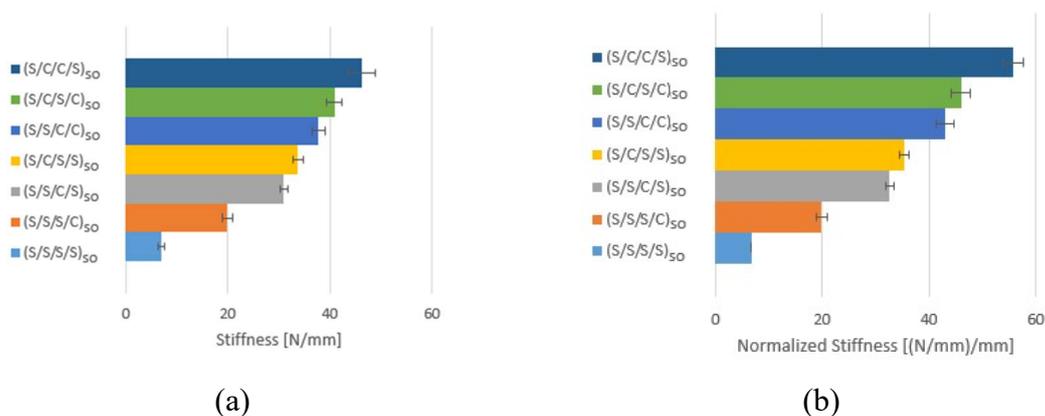
Figure 3.12. Stiffness comparison between stacking sequences (a) simple and (b) normalized

3.4.1.2. Maximum Flexural Load

Considering the normalized property, it seems that, generally, the increase in the CF V_f is accompanied by an increase in the maximum flexural load. The differences between lay-ups are smaller than for the stiffness.

Still, contrary to the stiffness, the $(S/S/C/C)_{so}$ lay-up presents a lower maximum flexural load than the $(S/C/S/C)_{so}$ lay-up which has the same carbon fibre content. In fact, the maximum flexural load from the $(S/S/C/C)_{so}$ lay-up (14 % CF V_f) is similar to the one from the 10 % CF V_f lay-ups. The same seems to happen to the $(S/C/C/S)_{so}$ lay-up (19 % CF V_f), in comparison with the $(S/C/S/C)_{so}$ lay-up (14 % CF V_f).

It is important to notice that these are the only stacking sequences that have UD CFRPP layers placed next to each other. The fibre break clusters growth can be therefore influenced by the thickness of the UD CFRPP layers. A thicker layer would be prone to damage propagation. The maximum flexural load comparison between lay-ups is presented in Figure 3.13.
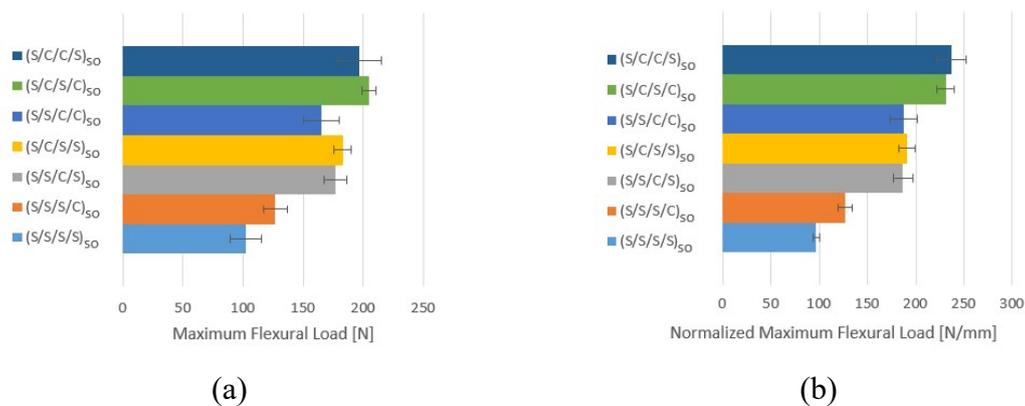
Figure 3.13. Maximum Flexural Load comparison between stacking sequences (a) simple and (b) normalized

3.4.1.3. Displacement at Maximum Flexural Load

The displacement at the maximum flexural load is the property that defines the capacity of the material to deform before failure. Since none of the samples actually fractured, the failure criterion is defined as the moment when the material does not support the maximum flexural load anymore.

The non-hybrid lay-up $(S/S/S/S)_{so}$ presents, by far, the highest displacement at the maximum flexural load. Adding UD CFRPP layers decreases this property quickly but it remains fairly constant after the CF V_f reaches 10 %. Once again, the two lay-ups with UD

CFRPP layers placed next to each other present the lowest displacement when the failure criterion is reached.

Either these two lay-ups fail earlier due to their high UD CFRPP layer thickness or the $(S/C/S/C)_{so}$ lay-up fails at a higher displacement, possibly due to a hybrid effect. More attention will be given to these three stacking sequences in the sections "3.4.3 Interrupted Tests" and "3.4.4 Optical Microscopy". The lay-up comparison of the displacement at the maximum flexural load is presented in Figure 3.14.
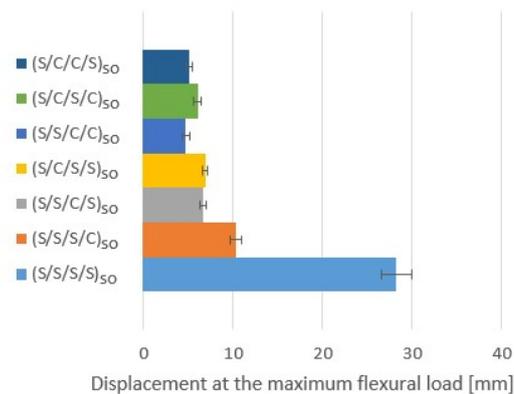
Figure 3.14. Displacement at Maximum Flexural Load comparison between stacking sequences.

3.4.1.4.   Energy Absorption until the Maximum Flexural Load

The toughness of a material is defined as the ability of a material to absorb energy before fracturing [87]. Since the samples never fracture when loaded in bending, the toughness in this case cannot be determined, but a similar property as the energy absorption until failure can. This property is the amount of energy that the material absorbs before failure, being the failure criterion the same as before.

SRPP is known for its high toughness [10] so, it is no surprise that the non-hybrid lay-up is the one with the highest energy absorption until failure. This property depends mostly on the previously presented properties of maximum flexural load and displacement at the maximum flexural load. The variation with the stacking sequence ends up being similar to the variation of the displacement at the maximum flexural load, because of the same reasons. The least energy absorbing lay-up is the $(S/S/C/C)_{so}$, given its low displacement at failure and not so high maximum flexural load supported.

One of the most interesting hybrid composite lay-ups is the $(S/C/S/C)_{so}$, that has a high maximum flexural load and reasonable displacement at the maximum flexural load.

This translates in a fairly good energy absorption until the failure point. The evolution of this property with the lay-up is presented in Figure 3.15.

A different failure criteria could be taken. For example, the point where the force reaches 50 % of the maximum flexural load. Details about that failure criteria and its influence on the energy absorption can be found in APPENDIX A .

(a)   (b)
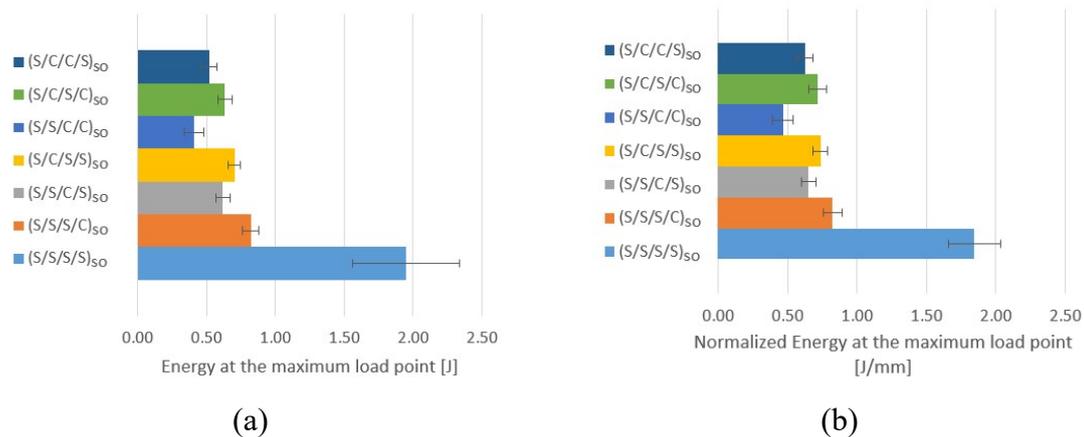
Figure 3.15. Energy Absorbed until the Maximum Flexural Load comparison between stacking sequences (a) simple and (b) normalized

3.4.2.   Depth Variation

The depth of the cross section tends to decrease during the test, as the corrugated profile tends to get more flat. This measurement can only be made until a certain moment in the test. The edge of the plate closer to the camera starts rotating along the longitudinal direction of the sample, blocking the view. Still, it is possible to get an idea on how the depth of the profile evolves during the test.

The graphics in Figure 3.16 show the evolution of the depth of the profile with the displacement of the loading nose. The depth variation and force-displacement curves are overlapped to see in which moments of the test the depth of the profile evolve faster or slower. The pattern is repeated for the other lay-ups and can be consulted in APPENDIX B.

In the beginning of the tests, the depth of the profile decreases slowly. After the maximum load is reached, the plate starts to get damaged and the depth of the cross section decreases at a higher rate. The damage of the material is therefore related to the flattening out of the plate, as the flattening is related to the loss of ability to carry load. After the material is damaged, the depth of the cross section starts to stabilize again.

(a)

(b)
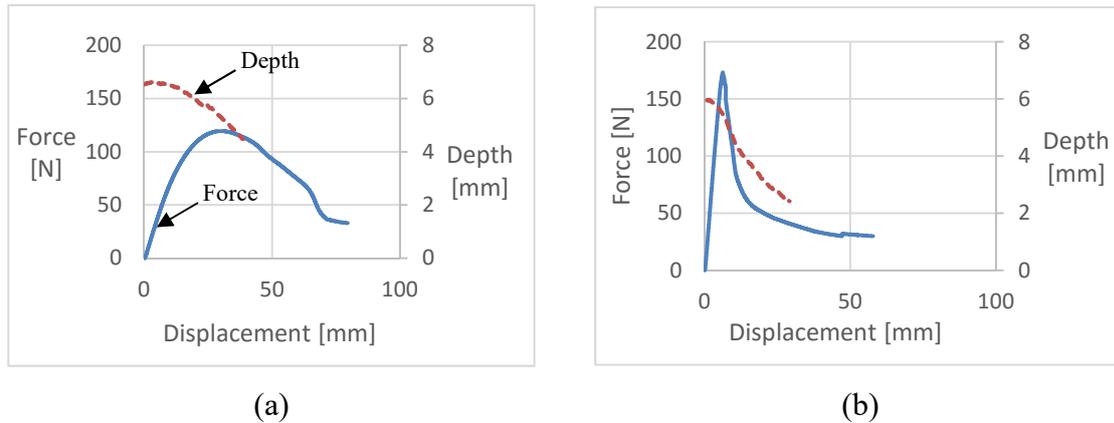
Figure 3.16. Evolution of the cross section depth with the displacement of the loading roller, overlapped with the force-displacement curve of the sample for the (a) (S/S/S/S)$_{so}$ and (b) (S/S/C/S)$_{so}$ lay-ups.

The fact that a UD composite is used can also explain why the flattening out occurs. This type of composites has a low transverse strength, facilitating the expansion on the same direction. Using a multidirectional carbon fibre composite would give more resistance in the transverse direction to the plate.

3.4.3.   Interrupted Tests

3.4.3.1.   (S/S/S/S)$_{so}$

After the sample is loaded until the maximum force is reached, no damage is yet visible with the transmitted light imaging technique (Figure 3.17b). For that phase of the curve, either the damage is not visible with this technique, or the material is still under the elastic (non-linear) domain and/or the geometric deterioration causes the curve to peak.

When the sample is submitted to the flexural test a second time, the curve peaks for the same force and displacement, reinforcing the idea that the material is still under the elastic domain (Figure 3.17g). This test was performed until a first load drop occurs and some damage starts appearing in the flat portions of the plate (Figure 3.17c). Only the flat portions that were under compression display signs of damage, showing that the SRPP is probably weaker under compression than under tension. Compression tests on SRPP have not been executed or found in literature.

The damage is still subtle but can be seen especially near the blue marks in the left and right side of the sample. The use of the transmitted light imaging technique makes the damaged areas darker, in relation to the rest of the sample. To identify the damaged areas

in the (S/S/S/S)$_{so}$ lay-up, it is recommended that the reader looks for darker areas. The contrary is verified for hybrids, since the damage presents itself as a whitening of the surface.

When the sample is loaded until the force stabilizes, damage in the curved parts of the sample appear (Figure 3.17d). The stress concentrations in these locations may induce the damage to occur preferentially in this curved parts of the sample. After the final test, the damaged areas in the plate grow, but no new damaged areas seem to appear (Figure 3.17e).

(a)

(b)

(c)

(d)

(e)

(f)

(g)

Figure 3.17. Interrupted test backlight images from the (S/S/S/S)$_{so}$ lay-up: (a) untested, (b) after max. load, (c) after the first load drop, (d) after the force stabilization and (e) after last test, (f) the relevant points and (g) interrupted tests curves.

3.4.3.2.   (S/S/S/C)$_{so}$

For this lay-up, it is important to notice that some production defects can be seen in the UD CFRPP layers. This defect consists of misalignments of the carbon fibres, as shown in Figure 3.18. It is present in all hybrid plates, even though it is only visible without using the optical microscopy technique for this lay-up.
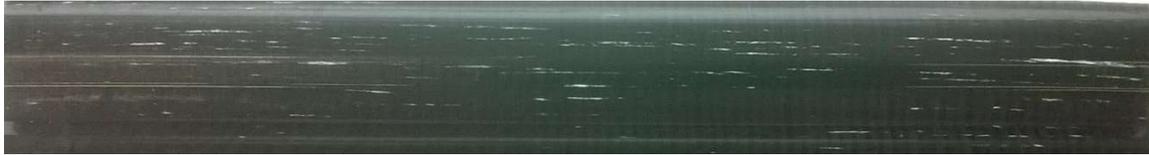
Figure 3.18. Backlight image of a (S/S/S/C)$_{so}$ sample showing the carbon fibres misalignments.

After the maximum load is achieved, damage is already visible. Some white lines appear in the CD (compression damage) specimen locations (Figure 3.19b). The white lines are distributed periodically in the longitudinal direction.

The plate is loaded again until the force-displacement curve reaches a stable condition. The number of white areas around the mid-span zone increases and it is now visible that they are centred on this place (Figure 3.19c). Some whiter areas also appear in the curved parts of the sample due to the presence of stress concentrations in those locations.

When the sample is loaded again, no new damage appears to be visible. Once again the damaged areas grow, at least in the CD specimen location on the right side of the sample (Figure 3.19d). The maximum flexural load achieved during the last test was much lower than the one obtained in previous tests (Figure 3.19f). The damage is only visible on the compressive side of the plate, reinforcing the idea that the material is weaker in compression.

Figure 3.19. Interrupted test backlight images from the (S/S/S/C)so lay-up: (a) untested, (b) after max. load, (c) after the force stabilization and (d) after last test, (e) the relevant points and (f) interrupted tests curves.

3.4.3.3. (S/S/C/C)so

After the first test, only small white areas appear in the CD specimen locations. After this test, they only show up localized in the mid-span zone, where the loading nose contacted the sample (Figure 3.20b).

The plate is then loaded again until the force decreases and stabilizes. In this stage, where the carbon fibres seem to have already broken, some very thin lines appear in the mid-span location (Figure 3.20c). Growing from this location, some less white areas appear, which seem to be signs of delamination.

After the last test is conducted, the only modifications noticeable are that, viewing from the compressive side, some small white areas appear on the TD (tensile damage) specimen location (Figure 3.20d). The thickness from the very thin lines, where the

carbon fibres are most likely to have fractured, slightly increases. The maximum load that occurs in this test is similar to the last force recorded in the previous test and happens for the same displacement (Figure 3.20f).
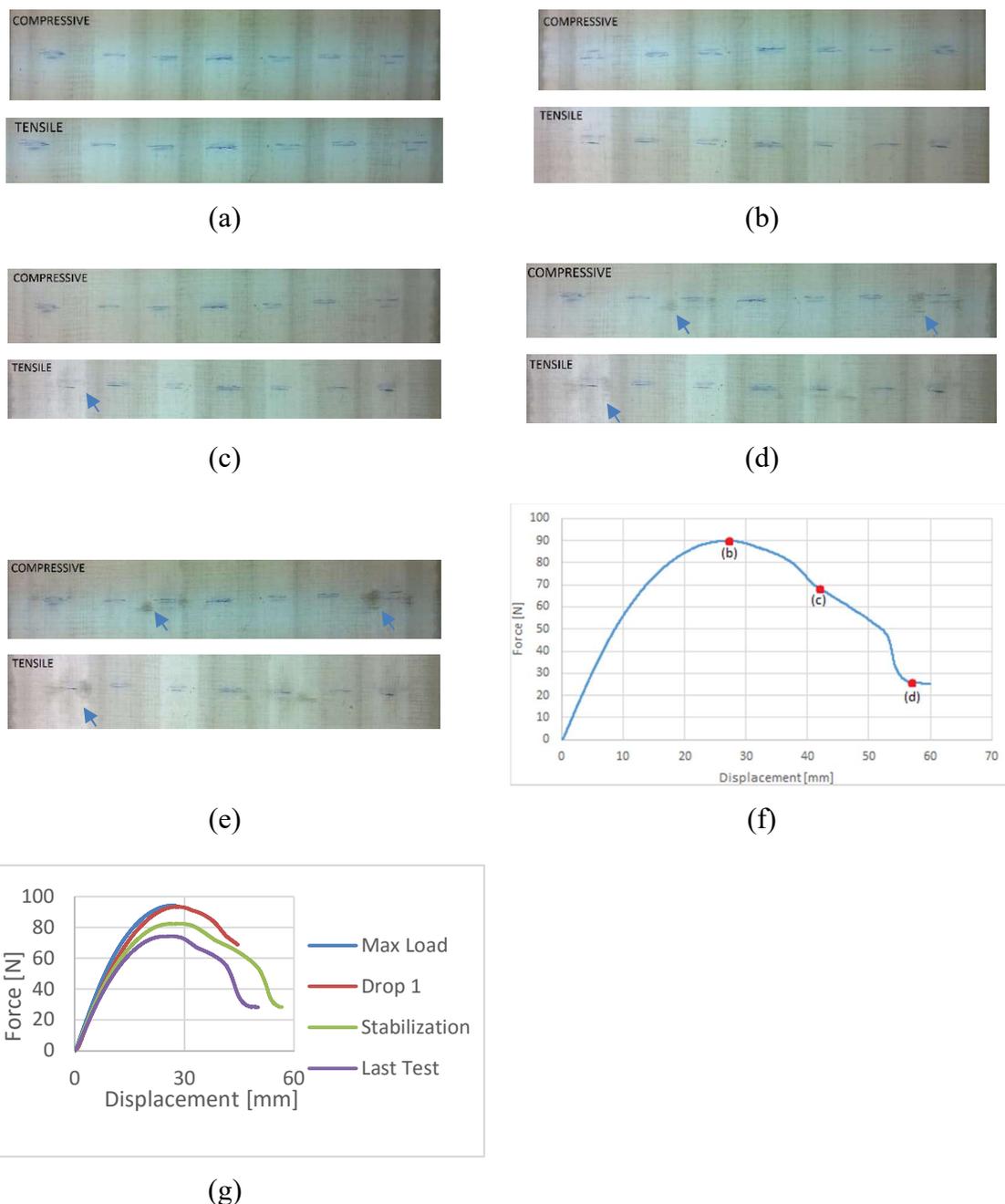

Figure 3.20. Interrupted test backlight images from the (S/S/C/C)so lay-up: (a) untested, (b) after max. load, (c) after the force stabilization and (d) after last test, (e) the relevant points and (f) interrupted tests curves.

3.4.3.4. (S/C/S/C)so

Before looking into the backlight images, it is important to notice the force-displacement curve for this lay-up (Figure 3.21g). After the curve reaches its peak, the load drops in stages, forming a ladder shaped curve. Before performing the interrupted tests, the hypothesis was that the shape derived from the fact that the UD CFRPP layers fractured one by one along the thickness. To verify that, the tests were interrupted at additional points.

The first test is interrupted when the maximum load is achieved. The only damaged area that appeared was the one visible on the left side of the sample, viewing from the compressive side, in a CD specimen location (Figure 3.21b). When the sample is tested again, two similar lines appear on the second and third flat portions, counting from left to right, that were under compression (Figure 3.21c). The third test is done again until the force

dropped. Finally, damage in the right CD specimen location is visible (Figure 3.21d). Still, the characteristics of this damaged area are different since it is less localized and also less white. The former hypothesis, about the UD CFRPP layers breaking in sequence, is thus rejected, since the ladder shape is due to damage occurring in the different CD specimen locations of the sample.

The fourth test is conducted until the force decreased and stabilized. The right CD specimen location is the one where most changes occur (Figure 3.21e). A more localized white line appears, showing the signs that the UD CFRPP layers fractured in that flat portion. Also, some delamination is still visible around it, which seems to be the same delamination visible before. In the other three CD specimen locations, a slight whitening of the curved parts of the sample start to appear.

Finally, a last test is performed. Once again, the maximum force achieved in this test was similar to the last force value recorded in the previous test and for the same displacement value (Figure 3.21h). After this test, damage is present now in the TD specimen locations. The major white lines seem to be the propagation of the lines on the compressive side (Figure 3.21f). Still, some other white areas, unrelated to previous damage, show up.

Like for the $(S/S/C/C)_{so}$ lay-up, damage appears in the TD specimen locations, but only being visible from the compressive side. A shift from the neutral plane is likely to happen, since the stress distribution is different after the damage occurs. Together with the flattening out of the sample, these two events can be the reason to the appearance of damage on these locations. Again, flexural tests on flat samples could be done to check for the shifting of the neutral plane.

(a)   (b)

(c)

(d)

(e)

(f)

(g)

(h)
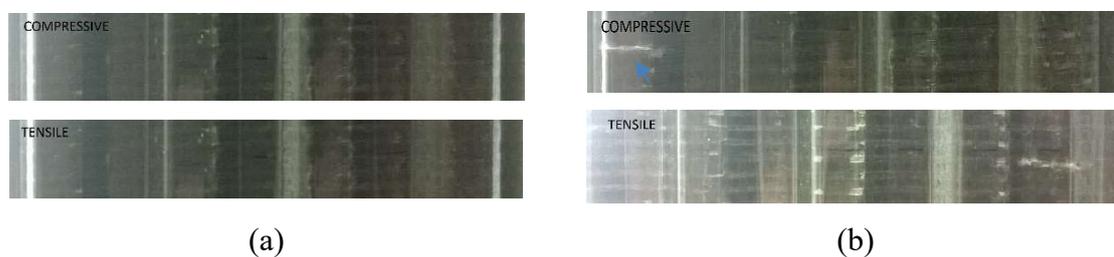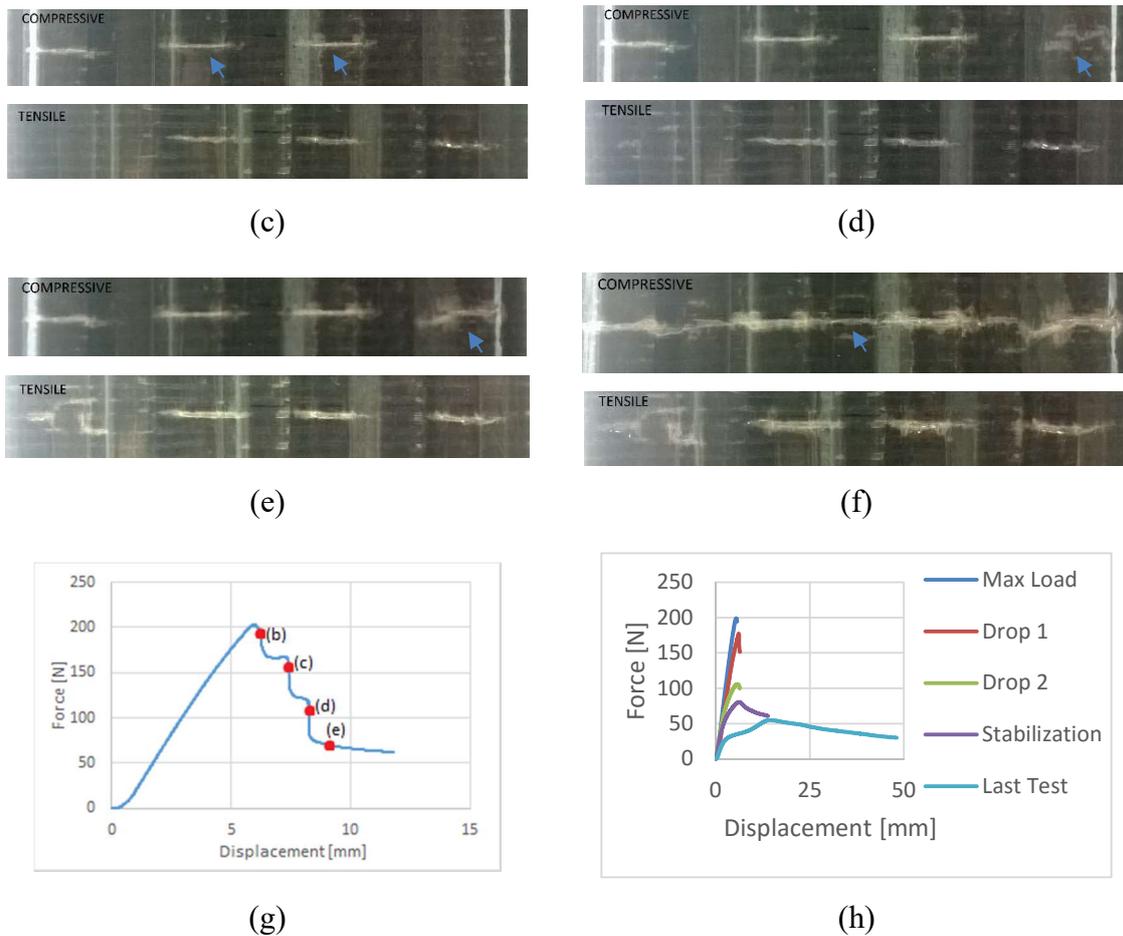
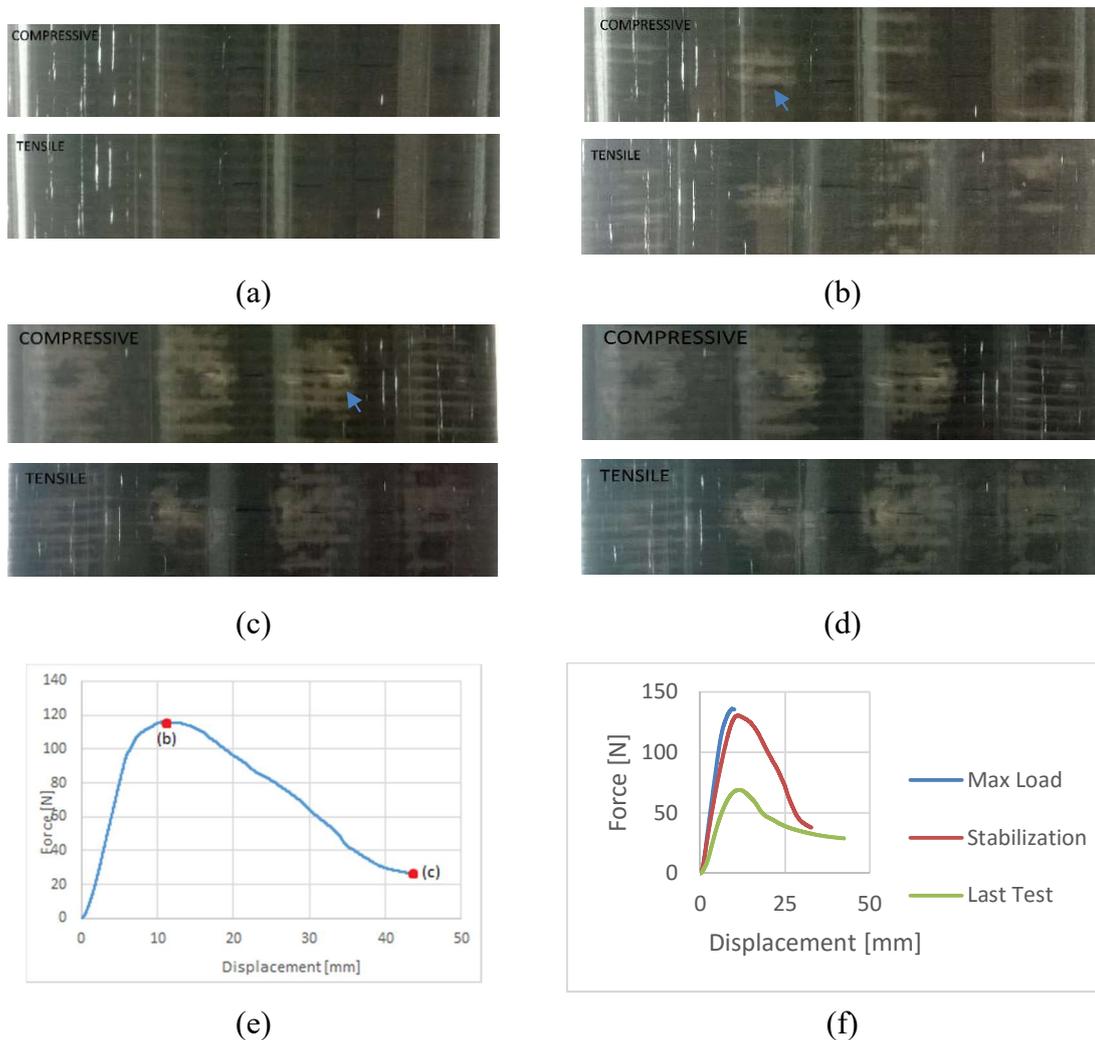**Figure 3.21.** Interrupted test backlight images from the (S/C/S/C)$_{so}$ lay-up: (a) untested, (b) after max, load, (c) after drop 1, (d) after drop 2, (e) after stabilization and (f) after the last test, (g) the relevant points and (h) the interrupted test curves.

3.4.3.5. (S/C/C/S)$_{so}$

The first test is conducted until the maximum load is reached. After this test, some damage appears on the two middle CD specimen locations (Figure 3.22b). From these two, the left one seems to present more damage, having also signs of delamination in the corner locations.

The second test was performed until the force decreased and stabilized. In the force dropping phase of the curve, a slightly pronounced ladder shape can be seen (Figure 3.22e). After this test, the localized damage can be seen in all four flat portions that were under compressive stress (Figure 3.22c). The previous damaged areas have also grown.

After the last test, the damage in the plate appears to have propagated to the TD specimen locations (Figure 3.22d). The delaminated area around the previously visible white

lines seems to have increased. Some new white areas have also appeared in the TD specimen locations.

(a)

(b)

(c)

(d)

(e)

(f)

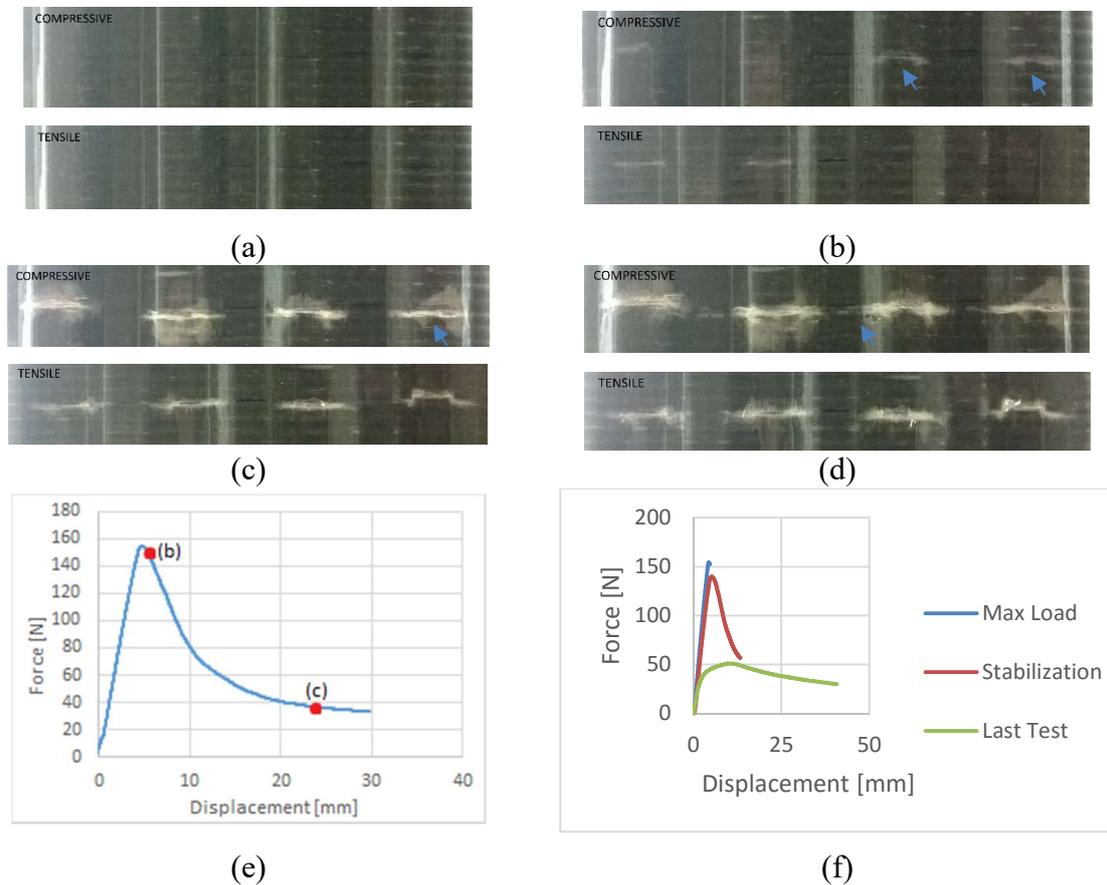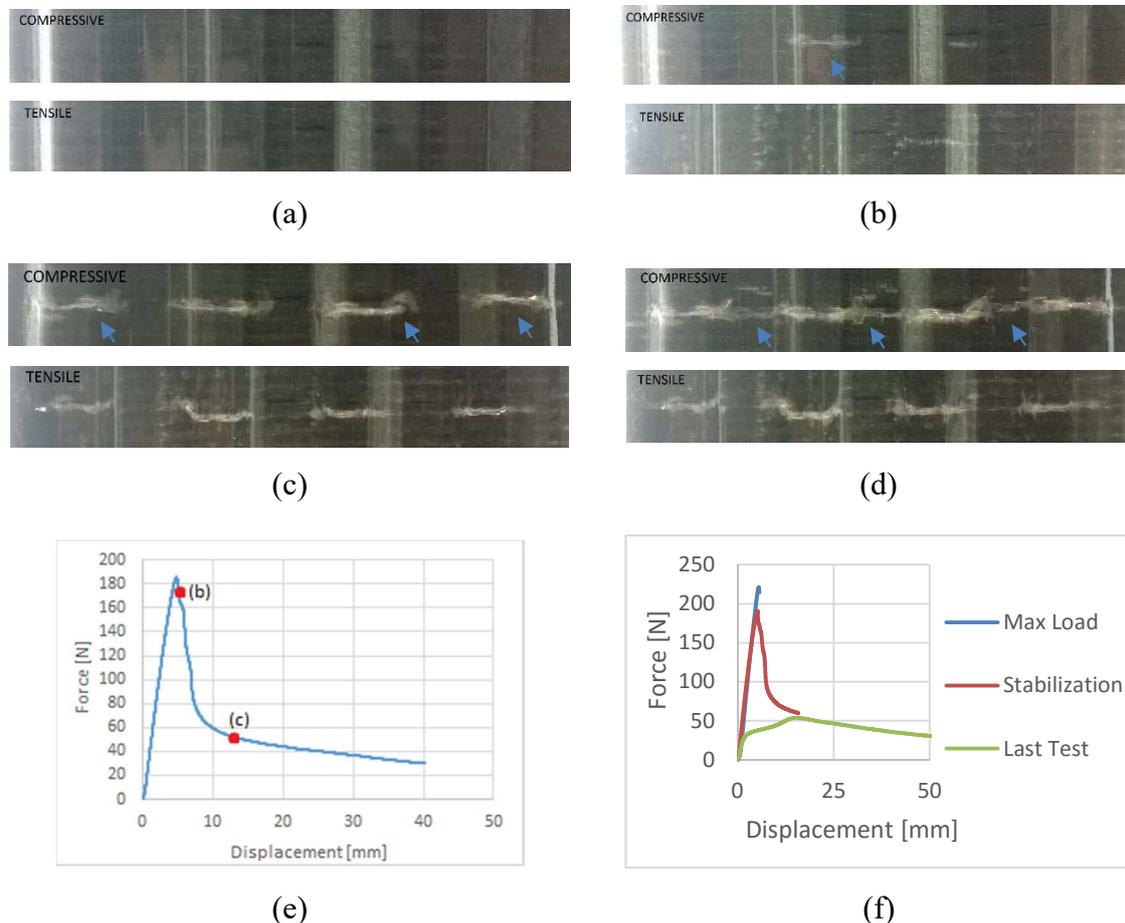**Figure 3.22.**Interrupted test backlight images from the (S/C/C/S)$_{so}$ lay-up: (a) untested, (b) after max. Load, (c) after stabilization and (d) after the last test, (e) the relevant points and (f) the interrupted tests curves.

3.4.4. Optical Microscopy

The previous section presented the evolution of damage with the state of deformation. Only the surface damage could be seen in most of the samples, since the transmitted light imaging technique is only effective for the non-hybrid lay-up.

With the use of the optical microscopy technique, damage can be seen through the thickness and not only on the surface. The disadvantage is that the images presented in this section are only from totally damaged specimens, not capturing the actual evolution of the damage. Still, a combination of both methods, interrupted tests and optical microscopy, are enough to understand the failure mechanisms in the corrugated hybrid composite plates.

Only the most relevant lay-ups will be presented in this section. The application of this technique to the (S/S/C/S)$_{so}$ and (S/C/S/S)$_{so}$ lay-ups is reported in APPENDIX D.

3.4.4.1. (S/S/S/S)$_{so}$

The visible damage in the non-hybrid lay-ups occurs mostly in the form of delamination. The location of the delamination can be between layers or even between tapes in the same layer. Figure 3.23a shows the case of a delamination that occurred between tapes from the same layer. Coincidentally, it is on the surface of a CD specimen, causing the complete detachment of the tape to the rest of the laminate.

Another form of damage, that can be visible on a TD specimen (Figure 3.23b), is similar to delamination, called longitudinal splitting. The rectangular shape of the left side of the void space makes the difference, showing that a longitudinal tape fractured. Notice that in the TD specimen, most of the damage is located near the compressive side of the sample. Even tough in the beginning of the test that specimen is completely under tension, one of the side of the specimen is closer to the neutral plane. The compressive side indicated is that side.

(a)

(b)
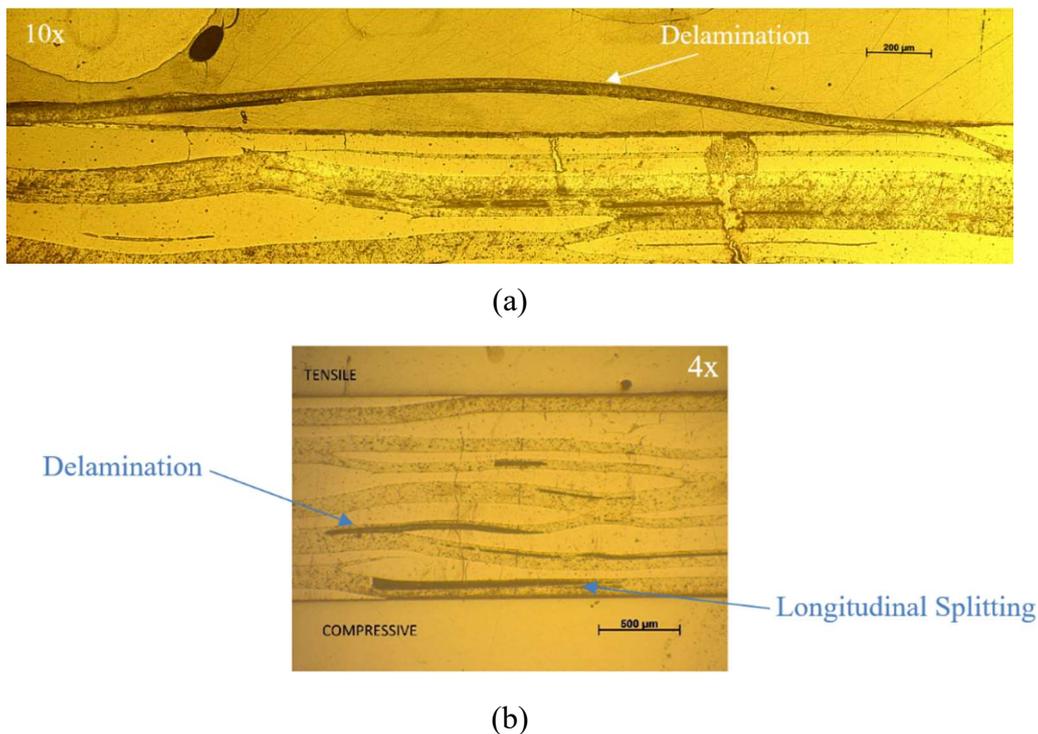
Figure 3.23. Optical Microscopy images from a (S/S/S/S)$_{so}$ lay-up CD specimen showing (a) delamination and a TD specimen showing (b) longitudinal splitting and delamination.

3.4.4.2. (S/S/S/C)$_{so}$

The samples from this lay-up showed a periodicity of white transverse lines around the mid-span location. Introducing a UD CFRPP layer to the plate, the possibility of delamination between SRPP and UD CFRPP layers introduces itself (Figure 3.24a). This

type of delamination presents different characteristics, since the distance in the normal direction of these is higher. SRPP damage is also present in these specimens, like in all other examined specimen.

The failure of these samples also occurs due to carbon fibre breaks (Figure 3.24b). When looking at the entire CD specimen, it is clearly visible that near the location of these breaks, the thickness of the UD CFRPP layer increased. It is like if these layers suffered of buckling.

Inspecting the TD specimens, the only visible damage is under the form of delamination and some signs of CF fractures. (Figure 3.24b) shows a portion of the TD specimen showing the carbon fibre breaks.

(a)

(b)

(c)
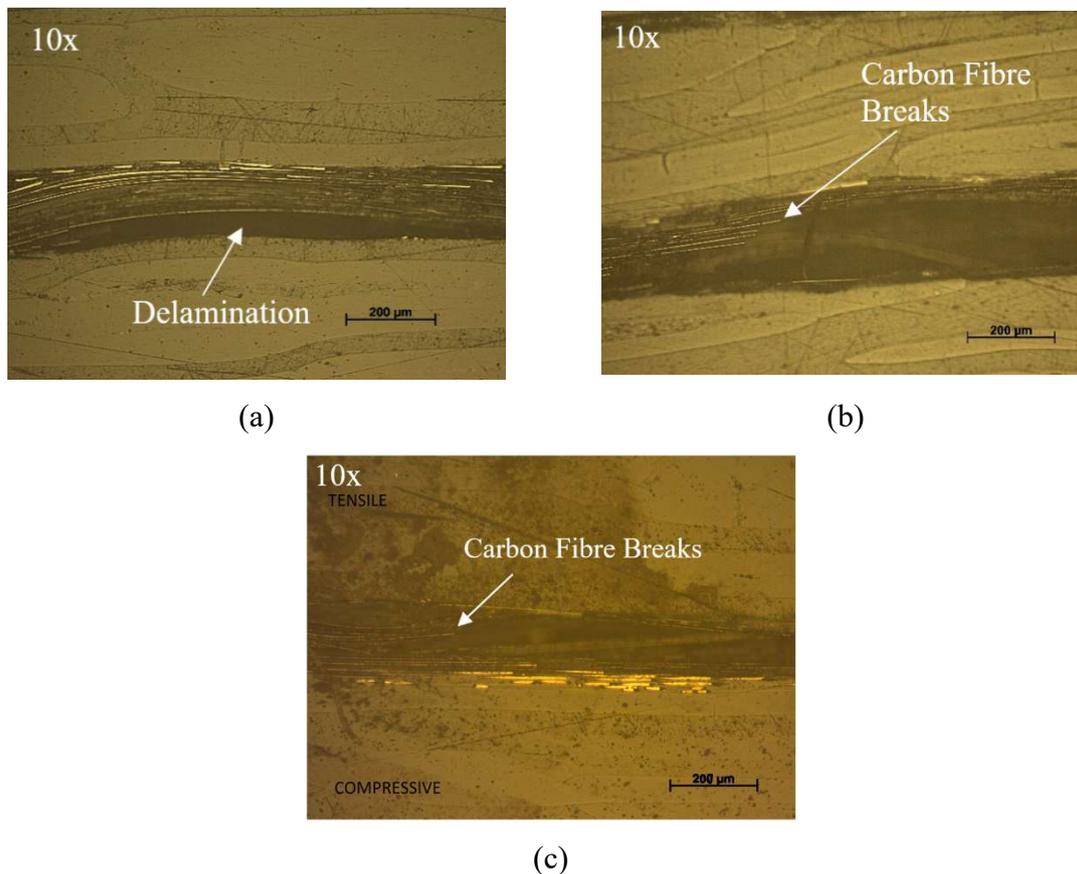
Figure 3.24. Optical Microscopy images from a (S/S/S/C)$_{so}$ lay-up CD specimen showing (a) delamination and (b) carbon fibre breaks and also from a TD specimen (c) showing carbon fibre breaks

3.4.4.3. (S/S/C/C)$_{so}$

This lay-up has three UD CFRPP layers placed next to each other. The most visible kind of damage present in the CD specimens is the carbon fibre breaks (Figure 3.25a). Next to these, the UD CFRPP layers show a large curvature, presenting evidence of local

buckling of the layers. The interesting observation is that only one of the UD CFRPP layers presents carbon fibre breaks, being the other two only curved.

Also visible, in a position adjacent to the curved layers, is delamination between the two types of layers (Figure 3.25b). On the surface of the specimen, transverse tape cracking is also visible, both on the top and bottom of the image. The tape on the top is clearly folded along its longitudinal direction, confirming the overfeeding of the tapes in the fabric.

Like it was seen in the section "3.4.3 Interrupted Tests", the TD specimen locations barely showed any signs of damage (Figure 3.25c). Analysing these specimens under the microscopy, it is confirmed that no visible damage is present.
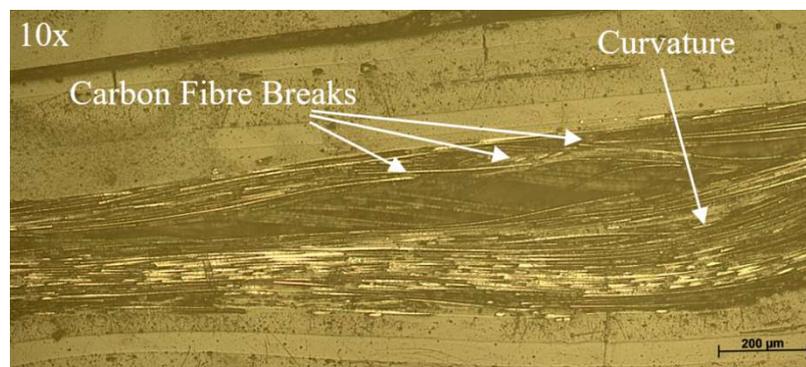
(a)
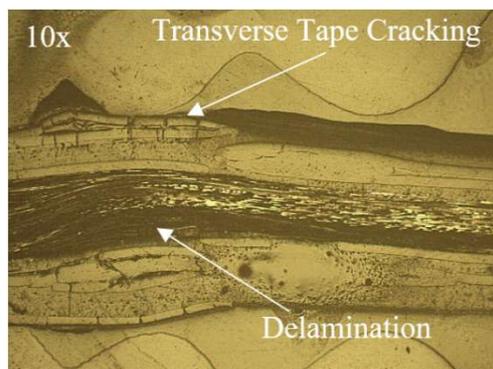
(b)
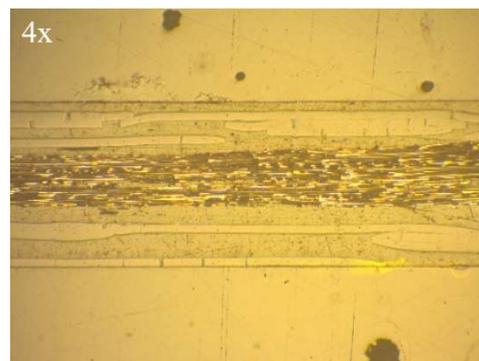
(c)

Figure 3.25. Optical Microscopy images from a $(S/S/C/C)_{so}$ lay-up CD specimen showing (a) carbon fibre breaks and (b) delamination and transverse-tape cracking and also from a TD specimen (c) with no visible damage.

3.4.4.4. $(S/C/S/C)_{so}$

All the UD CFRPP layers present carbon fibre breaks in the CD specimens from this lay-up (Figure 3.26a). Along with these, the buckling of the composite layers is visible,

being the radius of curvature very small in this case. Next to them, delamination between SRPP and UD CFRPP layers is also present in the CD specimen.

Considering just the SRPP damage, transverse tape cracking is shown in Figure 3.26b, close to a tape that seems to have suffered of longitudinal splitting.

Contrarily to the previous lay-up, the TD specimen from the (S/C/S/C)$_{so}$ lay-up shows some damage next to the compressive side of the specimen (bottom). This damage consists of carbon fibre breaks in the UD CFRPP layer closer to the compressive side of the plate. The delamination derived from the layers curvature (Figure 3.26c), reinforcing the idea that the damage present in the TD specimen is due to compression, even though this side of the plate was originally under tensile stress (See 3.4.3.4 (S/C/S/C)$_{so}$).
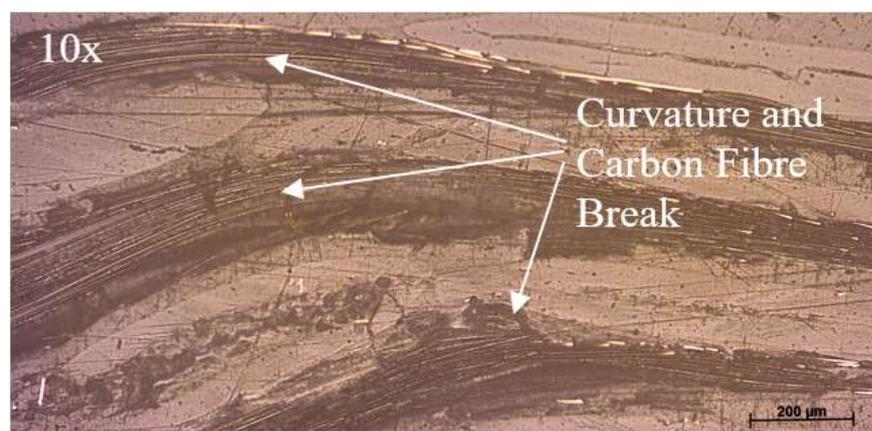
(a)
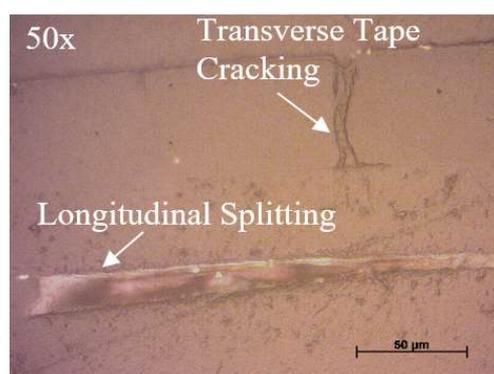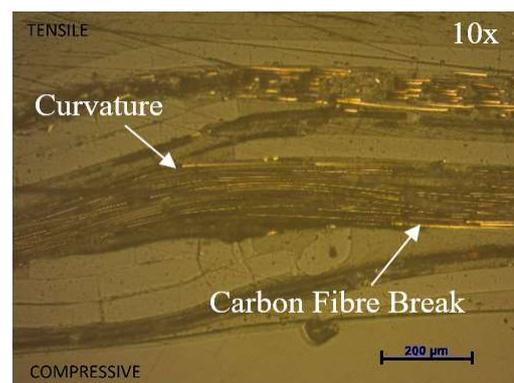
(a)   (b)

Figure 3.26. Optical Microscopy images from a (S/C/S/C)$_{so}$ lay-up CD specimen showing (a) carbon fibre breaks and (b) transverse and longitudinal tape cracking and also from a TD specimen showing (c) carbon fibre breaks and delamination.

3.4.4.5. (S/C/C/S)$_{so}$

This is the lay-up that has the highest carbon fibre V$_f$, having two sets of UD CFRPP layers placed together. Once again, carbon fibre breaks are found on the CD specimens (Figure 3.27a). Due to those fractures, the specimen suffered from buckling, causing the delamination between both types of layers. Transverse SRPP tape cracking can also be found next to them, this time on an inside layer. Longitudinal splitting is also present on this type of specimen (Figure 3.27b).

Looking into the TD specimens (Figure 3.27c), damage on UD CFRPP is only visible next to the compressive side of these. This damage consists mostly of carbon fibre breaks. Adjacent to these, a transversely cracked tape is also present.

(a)   (b)

(c)
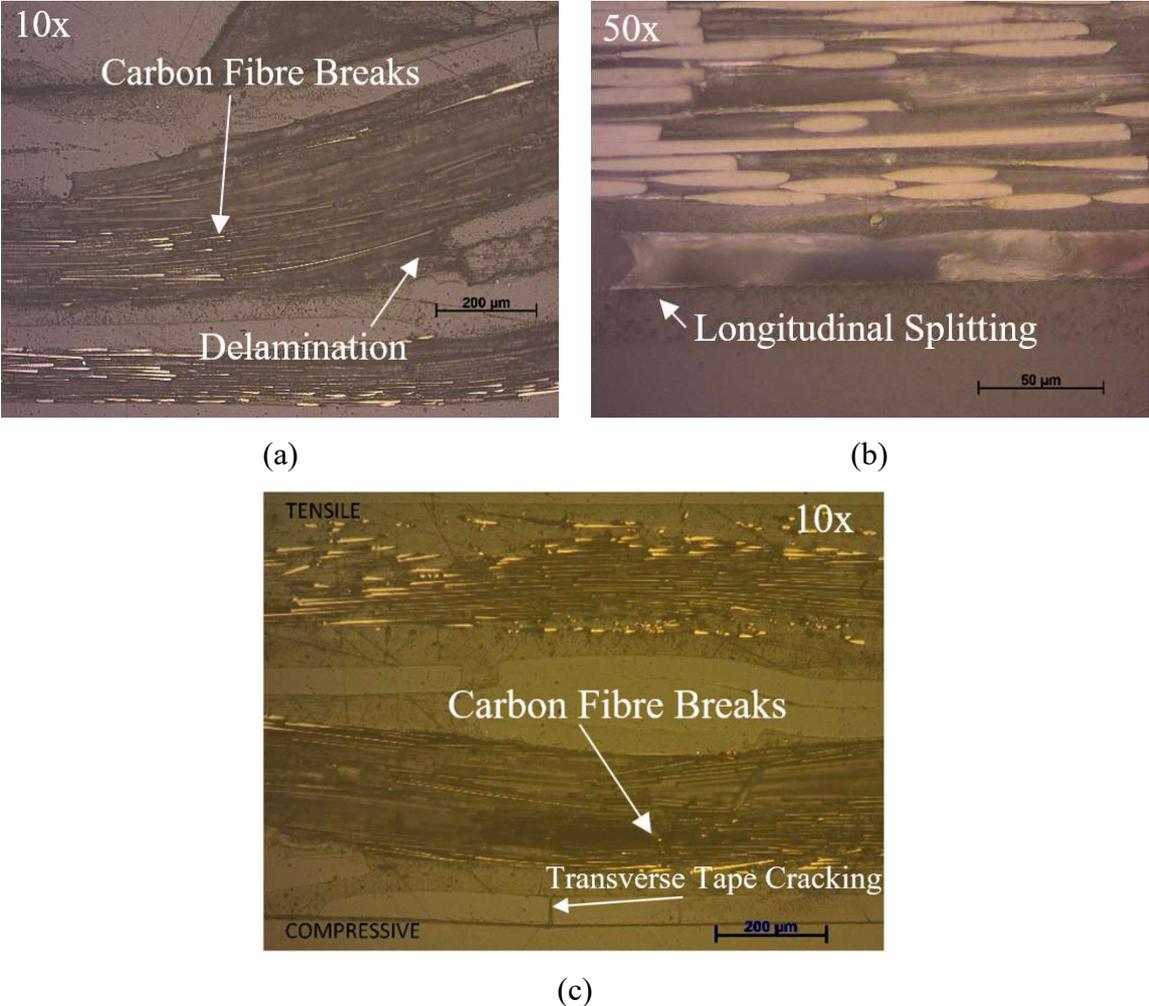
Figure 3.27. Optical Microscopy images from a (S/C/C/S)$_{so}$ lay-up CD specimen showing (a) carbon fibre breaks and delamination and (b) longitudinal splitting and also from a TD specimen showing (c) carbon fibre breaks

3.5. Conclusions

In this chapter, the experimental results were analysed and some conclusions can be drawn. The first, and most important one, is that the stiffness of the plates is not sensitive to the position of the carbon fibre layers. The stiffness increase due to the CF V_f is more significant than due to UD CFRPP layer position, given the higher distance of the layers to the neutral, in relation to the thickness.

The same happens with the maximum flexural load, although there are some exceptions, like the $(S/S/C/C)_{so}$ and $(S/C/C/S)_{so}$ lay-ups, where the maximum flexural load is lower. Those are, coincidentally, the only lay-ups that have UD CFRPP layers placed together. The thickness of the UD CFRPP is higher for these lay-ups, which has an influence on the damage propagation.

The displacement at the maximum flexural load and energy absorbed until the same point are much higher for the non-hybrid lay-up than for the hybrids. Both properties present a decreasing trend with the increase of CF V_f. The reasons that support this behaviour are the same that were listed for the other properties.

Moving to the interrupted tests results, both types of layers show evidences of a lower compression strength comparing to their own tensile strength, seeing that all the samples failed in compression. Even though they failed, none actually fractured due to the high ductility of the SRPP. In fact, after being unloaded, the plates almost returned to their original shape. The data from the interrupted tests shows that most of the load carrying capacity had been lost when a final test, performed when the samples are already damaged, was conducted.

The non-hybrid plates were observed with the transmitted light imaging technique, showing signs of damage under compression, which is accentuated near the curved parts of the plate. The damage in the rest of the plates was only observed with a naked eye. The $(S/S/S/C)_{so}$ stacking sequence is the only one where damage is distributed along the longitudinal direction. In all the other hybrid lay-up plates, the damage is much more concentrated around the mid-span location. After a certain amount of displacement of the loading nose was applied, damage also starts to be visible in the TD locations.

By analysing the specimens under the microscope, it was discovered that the failure mechanisms do not change with the lay-up. Most of the damage in SRPP is under the form of delamination, transverse tape cracking or longitudinal splitting. The UD CFRPP

failure consisted of carbon fibre fractures and buckling of the layers. Next to these, the specimen seem to have suffered of delamination between UD CFRPP and SRPP layers.

The TD specimens also present evidence of damage, but it is only found on the side closer to the neutral plane. The only hybrids that presented carbon fibre breaks on these specimens were the ones with UD CFRPP layers close to the surface. The CF breaks are found on the side closest to the neutral plane, being the other intact.

To find out more about the damage evolution of the corrugated plates, compression tests should be made on SRPP and UD CFRPP samples, to assess the compression properties of these materials. Also, flexural tests should be done on flat samples with the same lay-ups, so that it is easier to determine strains and stresses and to track the shifting of the neutral plane. The elimination of geometric deterioration would also be an advantage of these tests.

4. MODELLING

4.1. Materials Modelling

4.1.1.   Self-Reinforced Polypropylene

In order to obtain the properties of a single SRPP layer, the software *WiseTex* and *TexComp* were used. The first one was used to build the woven fabric and the second one to get the mechanical properties. The most important property to obtain was the tensile modulus in the longitudinal direction, since that is the direction solicited in the flexural test. The other properties are just an estimation made with the software packages, in order to assign orthotropic properties to the model. Using both software packages, the orthotropic properties on Table 4.1 were obtained.

Table 4.1. SRPP material model properties.

Unit Cell	10.6 x 10.6 x 0.15 mm		SRPP Material Model	
Areal Density	82.9 g/m2			
V_f	60 %			
Mechanical Properties				
$E_{xx} = E_{yy}$	3.04 GPa	Linear Density	110 tex	Weave
E_{zz}	1.44 GPa	Tape Dimensions NF	0.05 x 2.4 mm	
G_{xy}	0.72 GPa	Tape Dimensions F	0.1 x 1.2 mm	
$G_{xz} = G_{yz}$	0.49 GPa	Density	0.9 g/cm3	
v_{xy}	0.17	Spacing	2.66 mm	
$v_{xz} = v_{yz}$	0.26	Weave	Twill 2-2	

The tape properties and weave characteristics were obtained from the work of Tabatabaei et al. [88] and Swolfs [14], who optimized the SRPP production process. The same process was used in this study.

The dimensions of the unit cells of the SRPP woven fabric present a thickness of 0.15 mm. That is consistent with the thickness measured in the experimental part of this study and will be the thickness of each layer used in the model. The estimated tape volume fraction for SRPP after hot compaction is 60 %.

The elastic properties have been modelled, but the stress-strain curve of the SRPP consists of a bi-linear curve (See Figure 4.1). Knowing that a polymer can have a non-linear elastic behaviour, it was not studied yet the point in which the transition is made from the elastic to the plastic regime in this SRC. To do that, loading and unloading tests should be made and the damage evolution monitored.

To obtain the second part of the stress-strain curve, the software ABAQUS was used. Using the plastic regime, available on this software, the rest of the values for plastic strain and stress were introduced. This does not mean that the second part of the curve corresponds to the plastic regime. It is only the easiest way to assign a similar stress-strain curve to the material, in relation to the one measured by Swolfs [14]. Figure 4.1 shows the overlapping of both curves (model and experimental). Notice that no difference is visible between both curves.

A simple tensile test model was assembled to obtain this data. With a rectangular cross-sectioned part, one end of the specimen was fixed, while a displacement was applied to the other end. All the elements of the model are subjected to the same values of strain and stress.
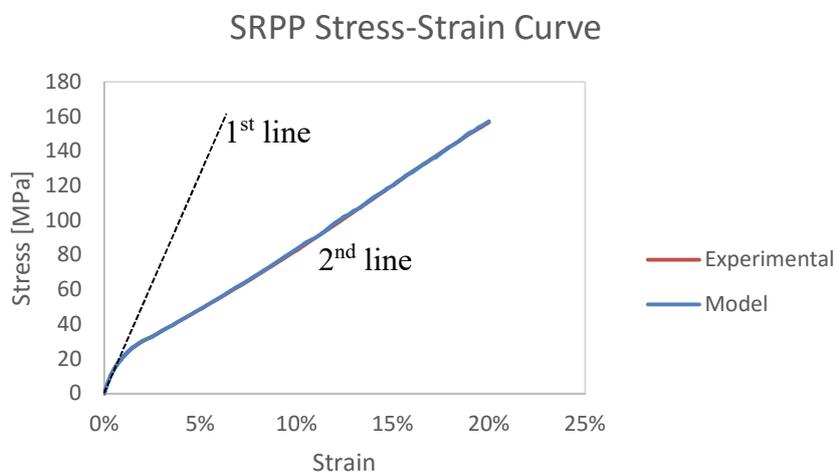
Figure 4.1. Modelled and Experimental Stress-Strain curve obtained for SRPP.

4.1.2. Unidirectional Carbon Fibre Reinforced Polypropylene

The UD CFRPP material is considered to be fully elastic until failure. The prepregs contain T700 carbon fibres, which properties are standardized [89]. To obtain the elastic properties from this material, Chamis's [90] formulae was used. The mechanical

properties of the UD CFRPP material are presented in table 4.2, as well as the input data Chamis' formulae.

Table 4.2. UD CFRPP material model properties.

Input Data					
			Carbon Fibre	PP Matrix	
Longitudinal Tensile Modulus [GPa]			230	1.5	
Transverse Tensile Modulus [GPa]			15	1.5	
Longitudinal Shear Modulus [GPa]			14.3	0.536	
Longitudinal Poisson Ratio			0.26	0.4	
UD CFRPP					
E_{11} [GPa]	74.62	G_{12} [GPa]	3.19	v_{12}	0.36
E_{22} [GPa]	3.06	G_{13} [GPa]	3.19	v_{12}	0.36
E_{33} [GPa]	3.06	G_{23} [GPa]	1.18	v_{23}	0.30

The tensile strength was determined using the rule of mixtures, being equal to 535 MPa. The prepregs used in the experimental work had a thickness of 0.16 mm. After the production, it was observed that the thickness decreased to 0.1 mm due to some PP flowing out of the mould. This experimentally observed thickness was only used to obtain the data presented in the section "4.3.2 Comparison with Experimental". The rest of the data was obtained using a model where the thickness of the UD CFRPP layers is 160 μm.

4.2. Model Characteristics

4.2.1. Cross Section

The model used to predict the flexural properties of a hybrid corrugated composite plate was developed using the software ABAQUS 6.14. The first step to create the model is to design the part. The cross section used in the model is slightly different than the one described in the section "3.2.1.2 Dimensions".

The only difference between the model and the experimental samples is the shape of the corners. While the samples produced by hot compaction have round corners, the model uses sharp edges, like it is shown in Figure 4.2. Using round corners in the model would increase the difficulty of the design and the simulation would take longer to execute. The disadvantage is that stress concentrations are added to the corner locations.

Figure 4.2. Cross section adaptation from the round corners (dashed line) to sharp edges.

The plate is divided by layers along its thickness. As referred before, the SRPP layers have a thickness of 150 μm, while the UD CFRPP layers have a thickness of 160 μm, unless it is said otherwise.

Since there are no technical difficulties that constrain the number of stacking sequences that can be studied, all the possible symmetric lay-ups with 7 layers are studied. Those contain two non-hybrid lay-ups (100 % SRPP and 100 % UD CFRPP) and 14 hybrid lay-ups. The carbon fibre V_f varies between 0 % and 32 %. The thickness of the plate, in the model, is varied between 1.05 and 1.12 mm, to accommodate the different lay-ups.

The width of the samples corresponds to 4 corrugated cycles, the same as explained in the section "3.2.1.2 Dimensions". In the model, the part is designed as only a quarter of the total sample, in order to reduce the simulation running time. The width of the model part consists of only 2 corrugation cycles, instead of 4.

The length of the part depends on the span length optimization, which is developed in the section "4.2.3 Span Length".

4.2.2. Boundary Conditions

Contrary to the boundary conditions described in the state of the art review for three point bending models, the model does not used any contact formulations between the rollers and the sample. The use of contact formulation would, once again, increase the simulation running time excessively and even introduce numerical divergences during the initial part of the test (while the contact nodes are settling).

The contact properties would influence the flexural properties obtained in the model. To avoid the numerical problems and study only the influence of the material properties on the flexural properties, a simple condition is used. The displacement in the support contact location is restricted in the normal direction. That assumption is valid for small displacements, since the movement along the roller is almost horizontal.

The displacement applied by the loading nose did not involve any contact either. In this case, a reference point was created. The transverse line representing the contact location between the samples and loading nose was constrained to the reference point. This way, the displacement that is applied to the reference point is mimicked by the constrained transverse line. The advantage is that the force and displacement can be directly obtained from the reference point data, which is the same data that is obtained in a flexural test.

Since only one quarter of the sample is modelled with ABAQUS, the symmetry boundary conditions have to be applied to the part. XSYM and YSYM boundary conditions are applied to the mid-span face and side face, respectively. (See Figure 4.3)
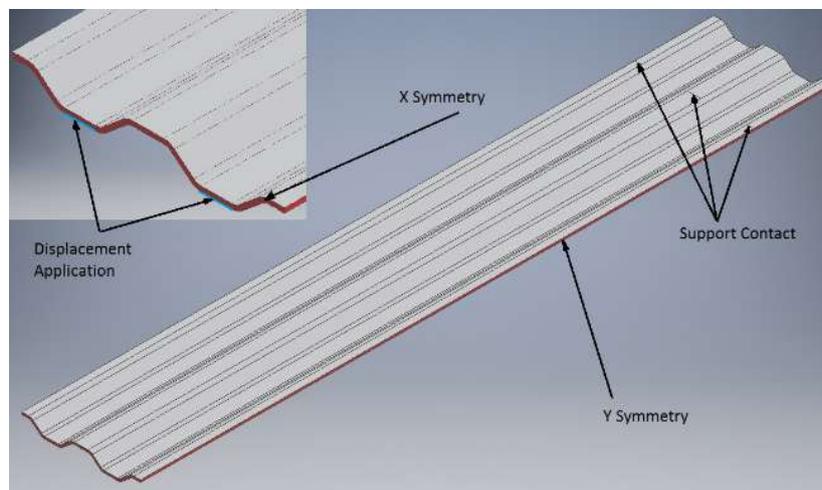
Figure 4.3. Boundary Conditions applied to the model part.

4.2.3. Span Length

The apparent flexural rigidity of a corrugated surface composite varies with the span to depth ratio [74]. An important task in the model development is the determination of the optimal span length. That way, the model does not use an excessive number of elements and only a small error is committed.

To do this optimization, the real mechanical properties have to be known first, in order to determine the error that is being committed. The first step is to use the classical laminate theory to determine the flexural modulus. The software packages ESA Comp or Autodesk Simulation Composite can be used for this purpose. Both software packages can only be used to determine the flexural modulus of flat surfaced composites. The optimization task will, therefore, be done with flat surfaces, in which it is possible to determine stresses

and strains directly from the force and displacement data. Equations 4.1 and 4.2 can be used to determine the stress and strain, respectively [91].

$$\sigma = \frac{3PL}{2b_2 {h_2}^2},$$ (4.1)

$$\varepsilon = \frac{6\delta h_2}{L^2},$$ (4.2)

Where σ is the stress at the outer surface, P is the applied force, L is the support span length, b_2 is the width of the cross section, h_2 is the height of the cross section, ε is the strain at the outer surface and δ is the mid-span displacement.

Knowing the CLT prediction values, the span to depth ratio was varied. Using a constant mesh size, the span to depth ratios used were 8, 16, 32, 40, 60, 100 and 140. The standard [91] followed in the experimental work recommends a span to depth ratio of 32. Still, a higher value will further reduce the shear deformation influence on the flexural modulus. In Figure 4.4, the evolution of the flexural modulus with the span to depth ratio can be observed. To obtain an average error under 3%, the span to depth ratio of 100 can be used.
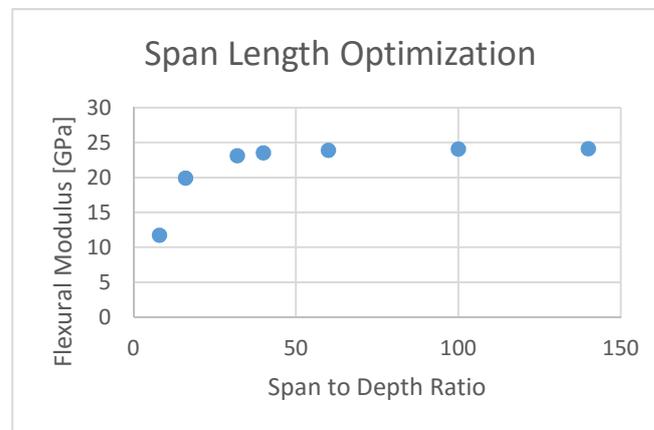
Figure 4.4. Flexural Modulus evolution with the span to depth ratio for a constant mesh size.

The depth of the corrugated profile varies between 6.05 and 6.12 mm. So, the span length used in the model is between 605 and 612 mm. The total length of the sample should be around 120 % of the span length, making this dimension around 730 mm. Since only one quarter of the sample is modelled, the length of the part is 365 mm.

4.2.4. Mesh Size

Having determined the optimal span to depth ratio, the mesh size is the other factor that influences any measured property in a numerical model. An increase in the number of elements is known to decrease the error committed with a model. The problem is that it increases drastically the simulation running time. Once again, an optimization has to be made, this time to the mesh size.

The method used is the same, comparing the values obtained with Finite Element Analysis (FEA) to the ones determined with CLT. It was discovered that using two elements per layer is the best way to obtain flexural modulus values closer to CLT predictions. Reducing the size in the longitudinal and transverse direction would barely have an effect.

The model uses C3D8R elements, an 8-node brick with reduced integration and hourglass control. The number of elements along the thickness is 14, i.e., two elements per layer. A mesh size of 1 mm was used in the longitudinal and transverse direction. The error was reduced to 1 % using this mesh characteristics.

4.3. Results and Discussion

4.3.1. Stiffness

When a simulation is executed with the model, the direct outputs are the force and displacement measured in the reference point. It is equivalent to the output from an experimental three point bending flexural test. Just like in the experimental tests, this is a special case that makes it difficult to determine stresses and strains. The only property studied in depth is the stiffness.

The study of this property will go into a further extent than the other mechanical properties, due to the reasons explained in the section "4.3.2 Comparison with Experimental".

The stiffness is studied across the variation of stacking sequence, which implicates the variation of CF V_f and UD CFRPP layer position. A higher detail is given to the UD CFRPP layer position variation. Finally, the stiffness is compared between flat and corrugated surfaced hybrid composites.

4.3.1.1. Stacking Sequences

As it was observed in the experimental work, the stiffness barely variates with the position of the UD CFRPP layers. The factor that contributes the most for the variation of this property is the CF V_f. The bar colour in Figure 4.5 represents a specific CF V_f, in a way that bars with the same colour are assigned to lay-ups that contain the same number of UD CFRPP layers.
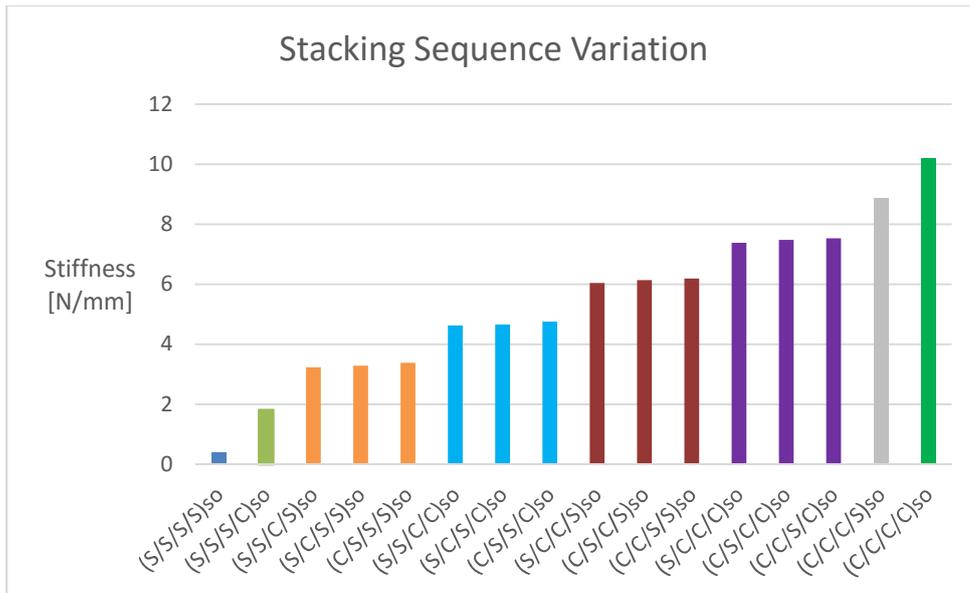
Figure 4.5. Stiffness Variation with the stacking sequence. The colours represent a different carbon fibre content.

4.3.1.2. Evolution with UD CFRPP Layer Position

For every CF V_f, by changing the stacking sequence, the average distance from the UD CFRPP layers to the middle of the laminate varies. That distance is illustrated in Figure 4.6 and it is a good indicator of the stiffness variation.

Figure 4.6. UD CFRPP average layer distance illustration.

As the UD CFRPP average layer distance increases, so does the stiffness of the plate. This is a slight variation in comparison with the change with the carbon fibre V_f, but exists. The evolution is the same for every group of stacking sequences with the same CF content. As the evolution is very similar, Figure 4.7 only shows the variation for one group. The figure shows two graphics, one without magnification, showing that the variation is very small, and another with magnification, so that the variations are visible.

<div align="center">(a)   (b)</div>
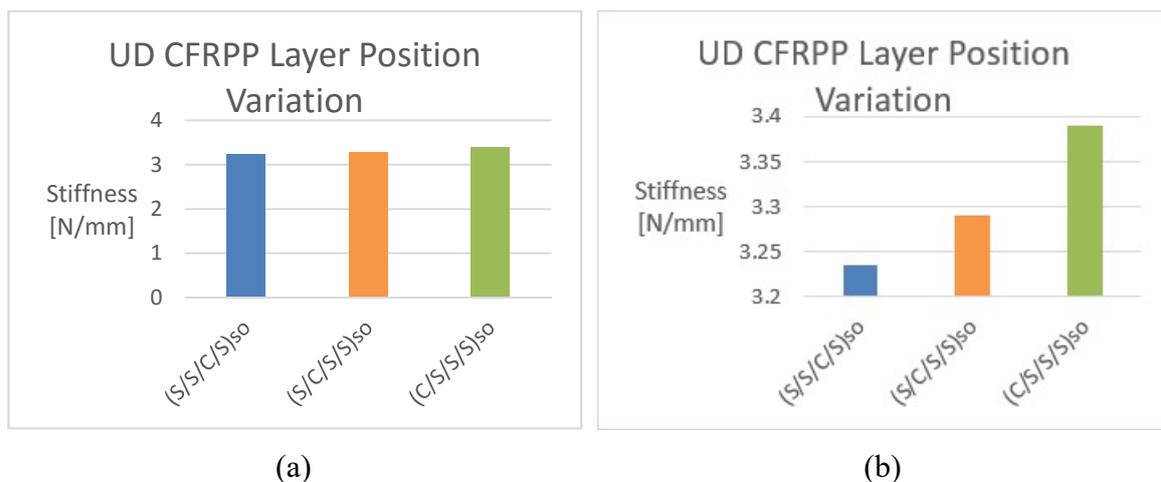
Figure 4.7. Stiffness variation with the UD CFRPP layer position (a) without and (b) with magnification

4.3.1.3.   Comparison between Flat and Corrugated Surfaces

Using the data from the simulations to optimize the span length and mesh size, it is possible to compare the stiffness between flat and corrugated surfaced samples. The span to depth ratio is not proportional to the stiffness, so no direct comparison can be made since the span to depth ratio used was the same.

Like it was presented in a previous section "2.2.2.1 Flexural Modulus", the stiffness of the flat surfaced composites is highly dependent on the position of the carbon fibre layers. In Figure 4.8b, it is possible to see that, for a group with the same CF V_f (same bar colour), the stiffness variation with the lay-up is much higher than the variation with the carbon fibre V_f. In fact, by replacing the middle layer in a flat sample, only a small increase in stiffness is verified. The same action done with a corrugated sample, produces a much higher variation. That is due to the fact that the middle layer contains the neutral plane when in a flat sample. In a corrugated sample, the neutral plane only coincides with the material in certain locations.

(a)

(b)
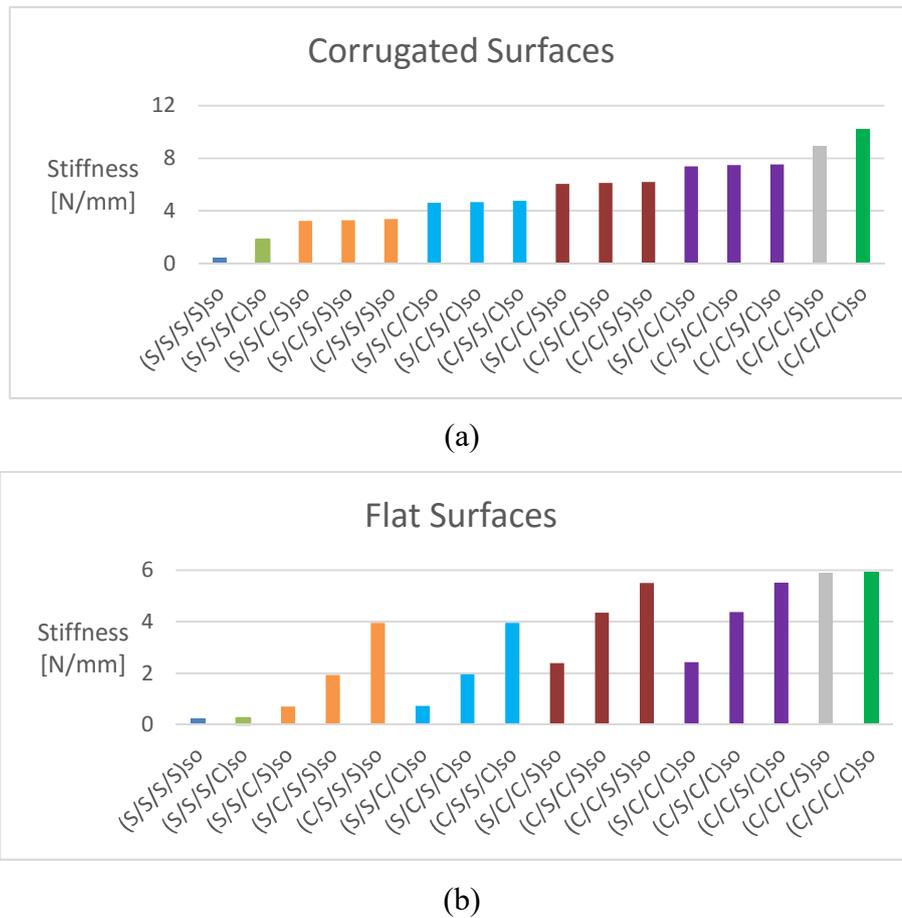
Figure 4.8. Stiffness variation in (a) corrugated and (b) flat surfaced composites

4.3.2. Comparison with Experimental

The remainder of this chapter is dedicated to a comparison between the model and the experimental results. This model is a preliminary work and can be improved. This section establishes the baseline for a future development of the model. The span length used in the model now is the same as it was used in the experimental three point bending tests, equal to 250 mm.

The mechanical properties are presented as a method of comparison, verifying the differences and similarities. The depth variation is also compared and is a vital parameter to be improved.

4.3.2.1. Stiffness

The stiffness is the parameter that can be better predicted by the model. Using a UD CFRPP layer thickness of 160 μm, as specified in the material properties, the model

stiffness is always higher than the one measured experimentally, confirming that the draining of PP during production affected the mechanical properties of the plates.

When the thickness of the UD CFRPP layers is altered to 100 µm, as was measured experimentally, the stiffness data from the model becomes very similar to the experimental results. Note that the material properties in the model were not changed, thus verifying that the CF V_f has not increased. The carbon fibres must have flowed in the transverse direction along with the PP. If they had not, the stiffness would still be higher.

Figure 4.9 shows the comparison of results between the model and experimental tests. The model results are divided according to the thickness of the UD CFRPP layers. "Model 160 µm" refers to a layer thickness of 160 µm, while "Model 100 µm" corresponds to a layer thickness of 100 µm.
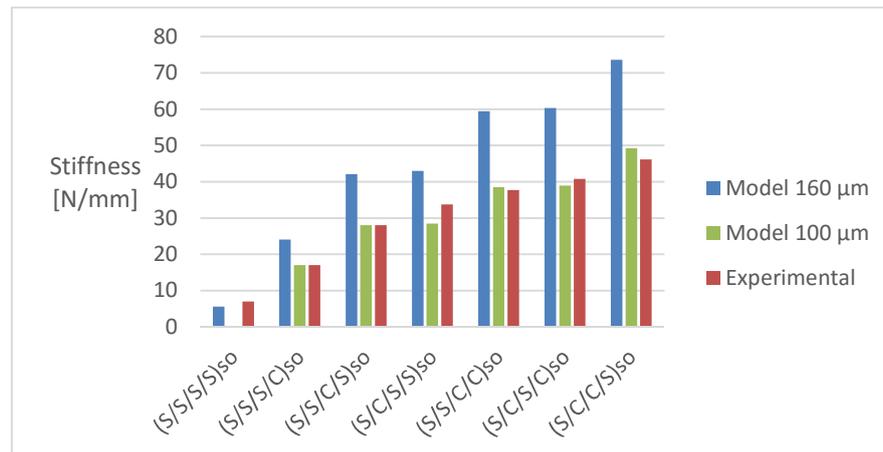
Figure 4.9. Stiffness comparison between the model and experimental tests.

4.3.2.2. Maximum Flexural Load

The tensile properties of each material were applied to the respective layers in the model. In the experimental chapter, it is visible that the plates always failed in compression. That introduces the idea that both materials are weaker in compression than in tension.

Assigning tensile stress-strain curves to both materials generates very different force-displacement curves than the ones obtained experimentally. Even though the thickness of the UD CFRPP layer influences the maximum flexural load, the values from model and experimental tests are still much higher in the model than measured experimentally. The property is presented for the model, again with both UD CFRPP layer thicknesses, and for the experimental tests in Figure 4.10.

The compressive properties should be measured experimentally. Since the compressive properties cannot be assigned to the material, it behaves equally when under tension and compression. This is obviously inaccurate but maintains the model coherent. Other factors can still be influencing the maximum flexural load values.
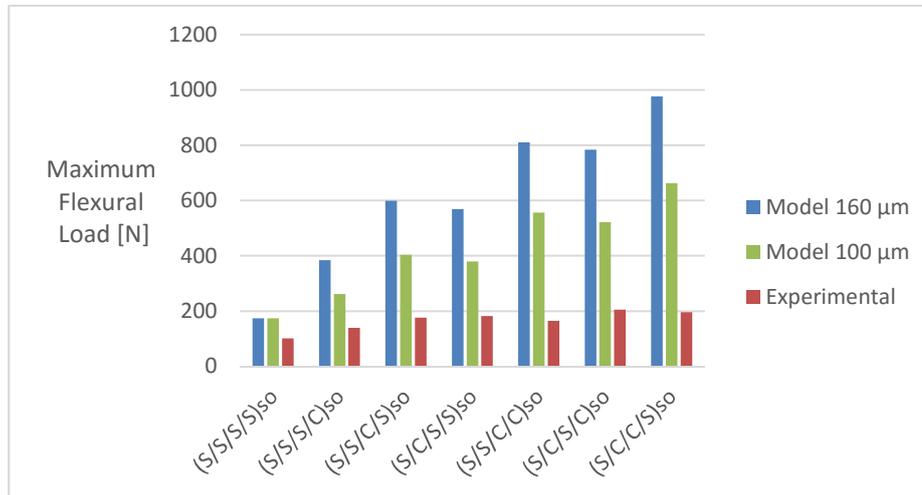
Figure 4.10. Maximum Flexural Load comparison between the model and experimental tests.

4.3.2.3.   Displacement at Maximum Flexural Load

The displacement at maximum flexural load is a measure of the failure strain. The highest difference between model and experimental results occurs for the non-hybrid lay-up. In this case, the value from the model is deceiving, as the load continued to increase until the end of the simulation, while in the experimental tests, the peak is achieved before the end. The tensile failure displacement for the $(S/S/S/S)_{so}$ lay-up would be even higher if the final displacement of the simulation was enough to provoke the failure of the material.

At least, from this results, it can be concluded that, when the sample failed experimentally, the SRPP was still far from a tensile failure. The comparison between model and experimental results is made in Figure 4.11.

For all the hybrid lay-ups, the displacement predicted by the model is higher than the one measured experimentally. The value is not altered by a change in the UD CFRPP layer thickness. Once again, other factors than the compressive failure of the materials can have an effect on the failure of the plate, reducing the displacement at the maximum flexural load.
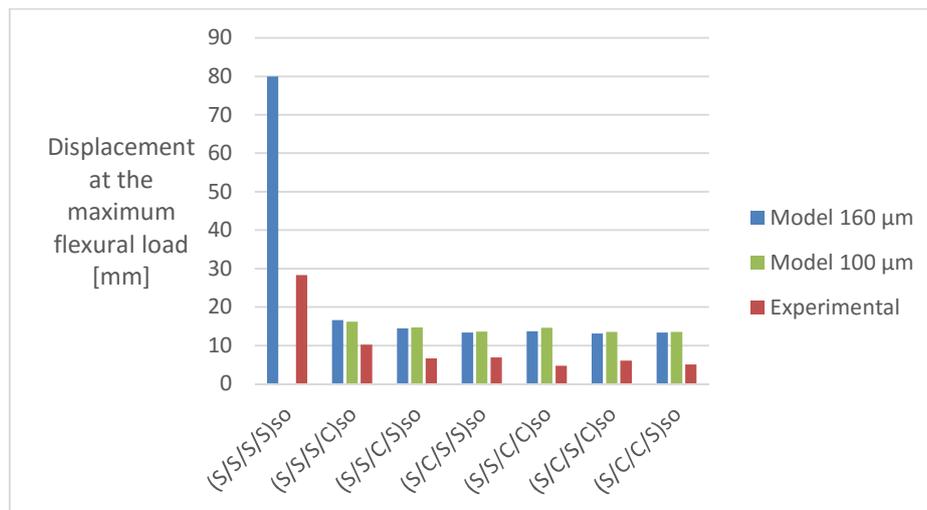
Figure 4.11. Displacement at maximum flexural load comparison between the model and experimental tests.

4.3.2.4. Depth Variation

Finally, it is also possible to check the profile depth reduction. The geometric deterioration can be a very important factor in the failure of the plate. A decrease in the depth of the profile results in a reduced load carrying capacity of the sample, anticipating the failure.

Figure 4.12 shows that there is barely any change in the cross section depth during the simulation. The result is that the sample keeps its corrugated profile during the test and the failure of the plate can only occur due to a material failure. The geometric deterioration has no effect in the failure of the sample, in the model.

This is, perhaps, the most important improvement to be made in the model. A review on the boundary conditions should be made to check if the plate expands in the transverse direction. The application of the round corners could be another step to improve the model.

The curves shown only represent the variation of the depth until the maximum load point is reached. After that, there is no sense in comparing, since the model does not capture that part of the failure development. By capturing the compressive yielding of the SRPP, the flattening out of the plate can be predicted better. That could also be an improvement to make in the model.
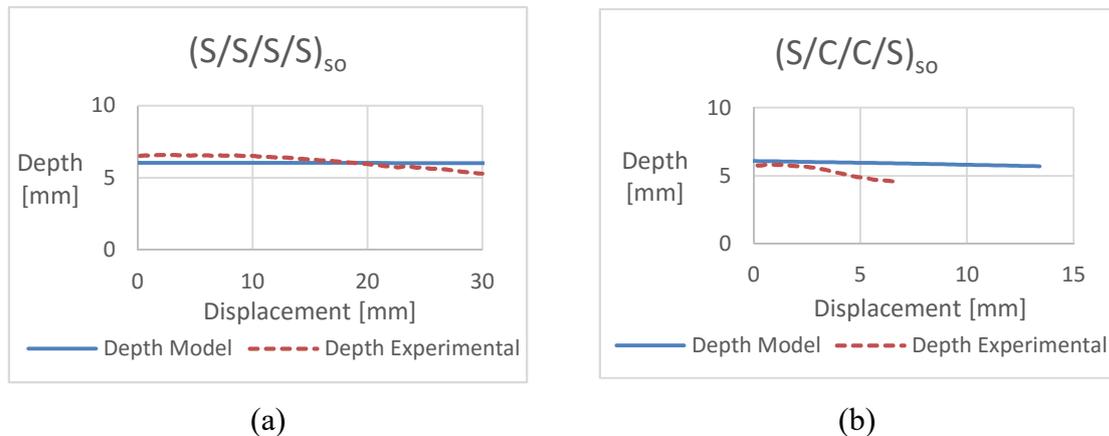
Figure 4.12. Depth variation measured experimentally and in the model for the (a) non-hybrid and (b) (S/C/C/S)$_{so}$ lay-ups.

4.4. Conclusions

In this chapter, the development of a baseline for a three point bending test model on a corrugated hybrid composite plate was explored. The stiffness was analysed and compared between stacking sequences and UD CFRPP layer position. A comparison was also made between the stiffness of corrugated and flat samples.

It was verified that the stiffness almost does not vary with the UD CFRPP layer position. The variation is only made the CF V_f. The evolution with the CF fibre layer position is very small but it can be concluded that the stiffness increases when the UD CFRPP layers are placed further away from the thickness middle position. The variation of stiffness in flat surfaced samples is much higher with the lay-up than with the carbon fibre content.

A second part of the chapter was dedicated to the comparison between model and experimental results. The biggest conclusion that can be made from this section is that the model is still very limited in its predictions. The only property where the prediction is fairly good is the stiffness. Still, the UD CFRPP layer thickness has to be adjusted if the PP from the prepregs flows out of the mould during production.

For the rest of the properties, it is clear that a different compressive and tensile behaviour should be assigned to both materials, since they are weaker in compression. Also, the depth variation is an important factor to determine the failure of the plate and it is not considered by the model. The addiction of round corners and a review of the boundary conditions can be made to improve the model.

There are other factors that were not explored in this chapter but can also be improved. So far, the model was only used to predict the behaviour until the maximum flexural load point. The majority of the damage observed experimentally happened after this point. The failure modes included delamination and transverse tape cracking. The first failure mode can be predicted by the model using cohesive elements, something that was not done in the model presented. To accommodate the prediction of the second failure mode, some elements should be allowed to split in the transverse direction, in order to capture the cracking of the tapes in the transverse direction.

Summing up, the model developed is only viable to study the elastic properties of the plate. To study the failure evolution, the model has to be further developed.

5. CONCLUSIONS

The flexural properties of corrugated hybrid composite plates were studied in this thesis, both experimentally and numerically. The hybrid composite consisted of polypropylene tapes and carbon fibres distributed by layers on a polypropylene matrix.

The results showed that the stiffness of the plates along their longitudinal direction does not depend on the stacking sequence, but only on the carbon fibre content. That is due to the high distance from the layers to the neutral plane, in relation to the thickness of the plate.

The maximum flexural load also showed a trend of increase with the CF V_f. The difference is that, for the lay-ups that contained UD CFRPP layers placed next to each other, the value of this property was lower in relation to other stacking sequences. The increased thickness of the UD CFRPP layers must have an effect on that. The same differences happened with the displacement and energy absorbed at the maximum flexural load. These properties exhibited a decreasing tendency with an increasing number of UD CFRPP layers.

One important factor, which most likely contributes for load carrying capacity of the plates, is the cross section depth variation. In all the cases, the depth of the profile decreased as the plate was loaded. This translates in a flattening out of the sample, reducing its load carrying capacity, since a corrugated structure is stiffer than a flat one [77].

The damage of the plates always started on the compressive side, enhancing the idea that both SRPP and UD CFRPP are weaker in compression than in tension. Compression tests on SRPP should be made to verify its compressive properties. The compressive properties of the carbon fibre material can be easily determined with a rule of mixtures.

After a certain amount of deformation is applied to the plate, damage starts to be visible on the tensile side of the plate, but only when it is observed from the compressive side. A shifting of the neutral plane and the cross section depth variation can have an effect on the appearance of this damage.

The microscopy images showed that the failure modes did not change with the stacking sequence. Most of this damage is presented on the form of delamination between

SRPP layers and between SRPP and UD CFRPP layers. It was verified that carbon fibre fractures occurred, accompanied by a curvature of the damaged layers around the transverse direction. Transverse tape cracking and longitudinal splitting were also verified on the SRPP layers. The same failure types were observed on the tension damage specimens, although these specimens only seemed to show damage closer to the compressive side. The TD specimens from the $(S/S/C/C)_{so}$ lay-up did not show any signs of damage.

To advance the experimental study of this type of structures, other lay-up plates can be produced. Even though it is problematic, it should not be impossible to produce plates with UD CFRPP layer at the surface. An interesting plate to study could be the one with a $(C/S/S/S)_{so}$ lay-up. With the UD CFRPP layers at the surface, being the rest of the plate made of SRPP, the maximum stress would occur for the outermost layer. Also, it would complete the set of lay-ups with 10 % CF V_f.

As referred in the conclusions of the experimental chapter, flexural tests could be made on flat specimens, with the same lay-ups as studied in this thesis. With this kind of specimens, the stress-strain curves should be possible to predict with Equations 3.1 and 3.2 (stress and strain determination). By eliminating the geometric deterioration of the structure, the yielding points would be material and not geometry dependent for sure.

Also, with the SRPP being an all-polymer composite, the elastic behaviour is not necessarily linear. Loading and unloading tensile tests can be helpful to determine the transition between elastic and plastic behaviour of the SRPP. That way, when loaded in bending, the transition between elastic and plastic regime could be also assessed.

A numerical model was developed using the software ABAQUS. A higher attention was given to the elastic properties, since these are the only ones that can be fairly well predicted. It was verified that this property increased with the CF V_f, but not with the position of the UD CFRPP layers. The variation with those layers position is slight but the stiffness still increased with the average distance from the UD CFRPP layers to the thickness middle position. Comparing with flat surfaced samples, the corrugated plates were stiffer. The variation of stiffness with the CF fibre layer position in flat samples is much more pronounced than with the carbon fibre content.

Comparing with the experimental results, when the expected thickness of the UD CFRPP layers was used, the stiffness results from the model were higher than the ones

measured experimentally. That occurred due to the flow of PP from the UD CFRPP prepregs to the outside of the mould, changing the thickness of this type of layers to 100 μm. When the thickness of these layers is altered in the model, the stiffness predicted by the model corresponds reasonably to the one measured in the flexural tests.

The other properties are not predicted well when the tensile properties are assigned to the material models. In fact, both the maximum flexural load and the displacement at this point are much higher in the model than measured experimentally. That can be attributed to the fact that the material model behaves equally in tension and compression. In reality, it was confirmed that the material is weaker in compression. The study of the compressive properties should be made and these assigned to the model. The material should behave according to a compressive or tensile stress-strain curve, depending on the element in question.

Still, other factors, not accounted for, can have an effect on the failure of the plates. The most important one is the depth variation of the cross section that is not verified in the model, but has an important contribution for the degradation of the load carrying capacity. A review of the boundary conditions and the design of round corners on the part should improve the model.

Further improvements are also possible, like the introduction of cohesive elements to account for the delamination, a major failure mode. Some elements should also be allowed to split, thus making possible the prediction of the transverse tape cracking.

With the stiffness being non-dependent of the UD CFRPP layer position, it may be possible to determine the stiffness of a corrugated plate in the longitudinal direction using a simple formulae. That would consist of a set of equations containing the geometrical properties of the plate and the mechanical properties of the composite materials. A future work in this area could go by the determination of that formulae.

Summing up, the future work to be developed is:

- Compression tests on SRPP and UD CFRPP;
- Flexural tests on flat specimens with the same lay-ups;
- Loading and unloading tests on SRPP to determine transition between elastic and plastic domain;

- Review on the boundary conditions of the model and design of round corners;
- Introduction of cohesive elements to simulate delamination;
- Development of a formulae to determine the stiffness of a corrugated plate as a function of the plate geometry and the carbon fibre volume fraction.

BIBLIOGRAPHY

[1]   "History of the composites industry", in http://www.acmanet.org/composites /history-of-composites. Accessed in July 30, 2016.

[2]   "History of the composites industry", in http://www.acmanet.org/the-industry/history. Accessed in July 30, 2016.

[3]   "About Triton Boats", in http://www.tritonboats.com/about.aspx. Accessed in August 25, 2016.

[4]   Bogoeva-Gaceva, G., Mäder, E. and Queck, H. (2000). "Properties of glass fiber polypropylene composites produced from split-warp-knit textile preforms." *Journal of Thermoplastic Composite Materials*, 13, 363-377.

[5]   Jespersen, S. T., Wakeman, M. D., Michaud, V., Cramer, D and Månson, J. –A. E. (2008). "Film stacking impregnation model for a novel net shape thermoplastic composite preforming process." *Composites Science and Technology*, 68, 1822-1830.

[6]   Kobayashi, S. and Tanaka, A. (2012). "Resin impregnation behavior in processing of unidirectional carbon fiber reinforced thermoplastic composites." *Advanced Composite Materials*, 21, 91-102.

[7]   Alcock, B , Cabrera, N. O., Barkoula, N. M., Loos, J. and Peijs, T. (2007a). "Interfacial properties of highly oriented coextruded polypropylene tapes for the creation of recyclable all-polypropylene composites." *Journal of Applied Polymer Science*, 104, 118-129.

[8]   Capiati, N. J. and Porter, R. S. (1975). "The concept of one polymer composites modelled with high density polyethylene." *Journal of Materials Science*, 10, 1671-1677.

[9]   Jones, R. S. and Riley, D. E. (2002). "A new self-reinforced polypropylene composite." *Proceedings of the 2nd Annual Conference of Society of Plastics Engineers, Automotive and Composites Division*, Michigan, USA.

[10]   Ward, I. M. and Hine, P. J. (2004). "The science and technology of hot compaction." *Polymer*, 45, 1413-1427.

[11]   "Material properties for PP-based composites", in www.matweb.com. Accessed in March 15, 2016

[12]   Alcock, B and Peijs, T. (2013). "Technology and development of self-reinforced polymer composites." In: Abe, A., Kausch, H. H., Moller, M., Pasch, H. editors. *Polymer composites – polyolefin fractionation – polymeric peptidomimetics - collagens*, 251, 1-76.

[13]   Karger-Kocsis, J and Bárány, T. (2014). "Single-polymer composites (SPCs): Status and future trends." *Composites Science and Technology*, 24, 77-94.

[14]   Swolfs, Y. (2015). "Hybridization of self-reinforced composites: modelling and verifying a novel hybrid concept." *Dissertation presented in partial fulfillment of the requirements for the degree of Doctor in Engineering Science*, Department of Materials Engineering, KU Leuven, Leuven.

[15]   Kmetty, A., Bárány, T. and Karger-Kocsis, J. (2010). "Self-reinforced polymeric materials: a review." *Progress in Polymer Science*, 35, 1288-1310.

[16]   Peterlin, A. (1971). "Molecular model of drawing polyethylene and polypropylene." *Journal of Material Science*, 6, 490-508.

[17]   Pae, K. D., Chu, H. –C., Lee, J. K. and Kim, J. –H. (2000). "Healing of stress-whitening in polyethylene and polypropylene at or below room temperature." *Polymer Engineering and Science*, 40, 1783-1795.

[18]   Alcock, B , Cabrera, N. O., Barkoula, N. M. and Peijs, T. (2009). "The effect of processing conditions on the mechanical properties and thermal stability of highly oriented PP tapes." *European Polymer Journal*, 45, 2878-2894.

[19]   "Polypropylene (PP)", in http://www.bpf.co.uk/plastipedia/polymers/pp.aspx. Accessed in July 15, 2016

[20]   Yamada, K., Kamezawa, M. and Takayanagi, M. (1981). "Relationship between orientation of amorphous chains and modulus in highly oriented polypropylene." *Journal of Applied Polymer Science*, 26, 49-60.

[21]   Flood, J. E. and Nulf, S. A. (1990). "How molecular weight distribution and drawing temperature affect polypropylene physical properties and morphology." *Polymer Engineering & Science*, 30, 1504-1512.

[22]   El Maaty, M. I. A., Bassett, D. C. and Olley, R. H. (1996). "The hot compaction of polypropylene fibres." *Journal of Materials Science*, 31, 1157-1163.

[23]   Ward, I. M. and Hine, P. J. (1997). "Novel composites by hot compaction of fibers." *Polymer Engineering and Science*, 37, 1809-1814.

[24]   Alcock, B , Cabrera, N. O., Barkoula, N. M., Spoelstra, A., Loos, J. and Peijs, T. (2007b). "The mechanical properties of woven tape all-polypropylene composites." *Composites Part A: Applied Science and Manufacturing*, 38, 147-161.

[25]   Barkoula, N. M., Peijs, T., Schimanski, T. and Loos, J. (2005). "Processing of single polymer composites using the concept of constrained fibers." *Polymer Composites*, 25, 114-120.

[26]   Bastiaansen, C. W. M. and Lemstra, P. J. (1989). "Melting behavior of gelspun/drawn polyofins." *Makromolekulare Chemie Macromolecular Symposia*, 29, 73-84.

[27]   Hine, P. J. and Ward, I. M. (2006). "Hot compaction of woven nylon 6,6 multifilaments." *Journal of Applied Polymer Science*, 101, 991-997.

[28]   Loos, J., Schimanski, T., Hofman, J., Peijs, T. and Lemstra, P. J. (2001). "Morphological investigations of polypropylene single-fibre reinforced polypropylene model composites." *Polymer*, 42, 3827-3834.

[29] Rein, D. M., Vaykhansky, L., Khalfin, R. L. and Cohen, Y. (2002). "Controlling the properties of single-polymer composites by surface melting of the reinforcing fibers." *Polymers for Advanced Technologies*, 13, 1046-1054.

[30] Alcock, B , Cabrera, N. O., Barkoula, N. M., Loos, J. and Peijs, T. (2006). "The mechanical properties of unidirectional all-polypropylene composites." *Composites Part A: Applied Science and Manufacturing*, 37, 716-726.

[31] Bárány, T., Izer, A. and Karger-Kocsis, J. (2009). "Impact resistance of all-polypropylene composites composed of alpha and beta modifications." *Polymer Testing*, 28, 176-182.

[32] Dasdemir, M., Maze, B., Anantharamaiah, N. and Pordeyhimi, B. (2011). "Formulation of novel thermoplastic composites using bicomponent nonwovens as a percursor." *Journal of Materials Science*, 46, 3269-3281.

[33] Fabich, B., Taketa, I., Gorbatikh, L., Lomov, S.V., Janetzko, S., Gries, T. et al. (2010). "Toughness improvement in hybrid composites of carbon fibre reinforced polypropylene and self-reinforced polypropylene." *Lancaster: Destech Publications, Inc*.

[34] Foster, R. J., Bonner, M. J. and Ward, I. M. (2011). "The use of nano and micron-sized particles to enhance the interlayer adhesion in self-reinforced, single-polymer composites." *Composites Science and Technology*, 71, 461-465.

[35] Hine, P. J., Broome, V. and Ward, I. M. (2005). "The incorporation of carbon nanofibres to enhance the properties of self-reinforced, single-polymer composites." *Polymer*, 46, 10936-10944.

[36] Hine, P. J., Unwin, A. P. and Ward, I. M. (2011). "The use of interleaved films for optimising the properties of hot compacted polyethylene single polymer composites." *Polymer*, 52, 2891-2898.

[37] Amer, M. S. and Ganapathiraju, S. (2001). "Effects of processing parameters on axial stiffness of self-reinforced polyethilene composites." *Journal of Applied Polymer Science*, 81, 1136-1141.

[38] Hine, P. J. and Ward, I. M. (2004). "Hot compaction of woven poly(ethylene terephthalate) multifilaments." *Journal of Applied Polymer Science*, 91, 2223-2233.

[39] Hine, P. J., Olley, R. and Ward, I. M. (2008). "The use of interleaved films for optimising the production and properties of hot compacted self-reinforced polymer composites." *Composites Science and Technology*, 68, 1413-1421.

[40] Jordan, N. D., Bassett, D. C., Olley, R. H., Hine, P. J. and Ward, I. M. (2003). "The hot compaction behaviour of woven oriented polypropylene fibres and tapes. II. Morphology of cloths before and after compaction." *Polymer*, 44, 1133-1143.

[41] Shindo, A. (1964). "On the carbonization of polyacrylonitrile fiber." *Carbon*, 1, 391-392.

[42] Tang, M. M. and Bacon, R. (1964). "Carbonization of cellulose fibers – 1. Low temperature pyrolysis." *Carbon*, 2, 211-220.

[43] Hayashi, T. (1972). "On the improvement of mechanical properties of composites by hybrid composition." *Proceedings of the 8th International Reinforced Plastic Conference*, 149-152.

[44] Marom, G., Fischer, S., Tuler, F. R. and Wagner, H. D. (1978). "Hybrid effects in composites: conditions for positive or negative effects versus rule-of-mixtures behavior." *Journal of Materials Science*, 13, 1419-1426.

[45] Summerscales, J. and Short, D. (1978). "Carbon fiber and glass fiber hybrid reinforced plastics." *Composites*, 9, 157-166.

[46] Fukuda, H. and Chou, T. W. (1983). "Stress concentrations in a hybrid composite sheet." *Journal of Applied Mechanics – Transactions of ASME*, 50, 845-848.

[47] Harlow, D. G. (1983). "Statistical properties of hybrid composites. I. Recursion analysis." *Proceedings of the Royal Society of London Series A: Mathematical, Physical and Engineering Sciences*, 389, 67-100.

[48] Zeng, Q. D., Fan, F. Q. and Zhang, Y. Y. (1993). "A random critical-core theory of microdamage in interply hybrid composites 1. First failure strain and hybrid effect." *Composites Science and Technology*, 49, 341-348.

[49] Zweben, C. (1977). "Tensile strength of hybrid composites." *Journal of Materials Science*, 12, 1325-1337.

[50] Manders, P. W. and Bader, M. G. (1981). "The strength of hybrid glass/carbon fibre composites." *Journal of Materials Science*, 16, 2233-2245.

[51] Behzadi, S., Curtis, P. T. and Jones, F. R. (2009). "Improving the prediction of tensile failure in unidirectional fibre composites by introducing matrix shear yielding." *Composites Science and Technology*, 69, 2421-2427.

[52] Hedgepeth, J. M. and Van Dyke, P. (1967). "Local stress concentrations in imperfect filamentary composite materials." *Journal of Composite Materials*, 1, 294-309.

[53] Nedele, M. R. and Wisnom, M. R. (1994). "Stress concentration factors around a broken fibre in unidirectional carbon fibre-reinforced epoxy." *Composite*, 25, 549-557.

[54] Kretsis, G. (1987). "A review of the tensile, compressive, flexural and shear properties of hybrid fibre-reinforced plastics." *Composites*, 18, 13-23.

[55] Phillips, L. N. (1976). "On the usefulness of glass-fibre-carbon hybrids." *British Plastics Federation Congress*, Brighton, United Kingdom.

[56] Curtin, W. A. (2000). "Dimensionality and size effects on the strength of fiber-reinforced composites." *Composites Science and Technology*, 60, 543-551.

[57] Wisnom, M. R., Khan, B. and Hallett, S. R. (2008). "Size effects in unnotched tensile strength of unidirectional and quasi-isotropic carbon/epoxy composites." *Composite Structures*, 84, 21-28.

[58] Hedgepeth, J. M. (1961). "Stress concentrations in filamentary structures." *NASA Technical Note D-882*, 1-36.

[59] Ji, X., Liu, X. R. and Chou, T. W. (1985). "Dynamic stress concentration factors in unidirectional composites." *Journal of Composite Materials*, 19, 269-275.

[60] Xing, J., Hsiao, G. C. and Chou, T. W. (1981). "A dynamic explanation of the hybrid effect." *Journal of Composite Materials*, 15, 443-461.

[61] Dong, C. and Davies, I. J. (2012a). "Flexural properties of hybrid composites reinforced by S-2 glass and T700S carbon fibers." *Composites Part B: Engineering*, 43, 573-581.

[62] Jawaid, M., Khalil, H. P. S. A and Bakar, A. A. (2011). "Woven hybrid composites: tensile and flexural properties of oil palm-woven jute fibers based epoxy composites." *Materials Science and Engineering: A*, 528, 5190-5195.

[63] Ary Subagia, I. D. G., Kim, Y., Tijing, L. D., Kim, C. S. and Shon, H. K. (2014). "Effect of stacking sequence on the flexural properties of hybrid composites reinforced with carbon and basalt fibers." *Composites Part B: Engineering*, 58, 251-258.

[64] Gowda, T. M., Naidu, A. C. B. and Chhaya, R. (2009). "Some mechanical properties of untreated jute fabric-reinforced polyester composites." *Composites Part A: Applied Science and Manufacturing*, 30, 227-284.

[65] Park, R. and Jang, J. (1999). "Performance improvement of carbon fiber polyethilene fiber hybrid composites." *Journal of Material Science*, 34, 2903-2910.

[66] Prabhakaran, R. T. D., Toftegaard, H., Markussen, C. M. and Madsen, B. (2014). "Experimental and theoretical assessment of flexural properties of hybrid natural fiber composites." *Acta Mechanica*, 225, 2775-2782.

[67] Diharjo, K., Priyanto, A.,.Purwanto, N. S., Suharty, N.S., Jihad, B. H., Nasiri, S. J. A., Widianto, D. and Suyitno (2013). "Study of flexural strength on hybrid composite glass/carbon-bisphenon for developing car body of eletrical vehicle." *Joint International Conference on Rural Information & Communication Technology and Electric-Vehicle Technology.*

[68] Dong, C., Duong, J. and Davies, I. J. (2012b). "Flexural properties of S-2 glass and TR30S carbon fiber-reinforced epoxy hybrid composites." *Polymer Composites*, 33, 773-781.

[69] Giancaspro, J. W. (2010). "Flexural response of inorganic hybrid composites with E-glass and carbon fibers." *Journal of Engineering Materials and Technology*, 132, 021005 (8 pp.).

[70] Davies, I. J. and Hamada, H. (2001). "Flexural properties of a hybrid polymer matrix composite containing carbon and silicon carbide fibres." *Advanced Composite Materials*, 10, 77-96.

[71] Dong, C. and Davies, I. J. (2012c). "Optimal design for the flexural behaviour of glass and carbon fibre reinforced polymer hybrid composites." *Materials & Design*, 37, 450-457.

[72] Ary Subagia, I. D. G. and Kim, Y. (2013). "A study on flexural properties of carbon-basalt/epoxy hybrid composites." *Journal of Mechanical Science and Technology*, 27, 987-992.

[73] Khanam, P. N., Khalil, H. P. S. A., Jawaid, M., Reddy, G. R., Narayana, C. S. and Naidu, S. V. (2010). "Sisal/carbon fiber reingorced hybrid composites: tensile, flexural and chemical resistance properties." *Journal Polymer Environment*, 18, 727-733.

[74] Shao, Y., Giroux, C. and Bdeir, Z. (2002). "Determination of EI for pultruded GFRP sheet pile panels." *3rd International Conference on Composites in Infrastructure*, 1-10.

[75] Tamrakar, S. and Lopez-Anido, R. A. (2010). "Effect of strain rate on flexural properties of wood plastic composite sheet pile." *Forest Products Journal*, 60, 465-472.

[76] Wang, J., Liu, W., Liang, R., GangaRao, H and Wan, L. (2015). "Analytical and experimental study on flexural behavior of pultruded fibre reinforced polymer sheet piles." *Journal of Composite Materials*, 49, 3836-3850.

[77] Yokozeki, T., Takeda, S., Ogasawara, T and Ishikawa, T. (2006). "Mechanical properties of corrugated composites for candidate materials of flexible wing structures." *Composites Part A: Applied Science and Manufacturing*, 37, 1578-1586.

[78] Samanta, A. and Mukhopadhyay, M. (1999). "Finite element static and dynamic analyses of folded plates." *Engineering Structures*, 21, 277-287.

[79] Giroux, C. and Shao, Y. (2003). "Flexural and shear rigidity of composite sheet piles." *Journal of Composites for Construction*, 7, 348-355.

[80] Tangwongwan, W. and Carmai, J. (2011). "Finite element modelling of titanium foam behavior for dental application." *Proceedings of the World Congress of Engineering*, Vol III, 4-9.

[81] Niemeyer, F. and Simon, U. (2015). "Computational methods in material science – Lab 1." Accessed in March 24, 2016, in the Web site of ULM University, in: https://www.uni-ulm.de/fileadmin/website_uni_ulm/uzwr/lehre-seminare /AdvMat-FEM/WiSe-2015-16/FE-Lab-1.pdf

[82] Ullah, H., Harland, A. R., Lucas, T. Price, D. and Silberschmidt, V. V. (2012). "Finite element modelling of bending of CFRP laminates: multiple delaminations." *Computational Materials Science*, 52, 147-156.

[83] Meng, M., Le, H. R., Rizvi, M. J. and Grove, S. M. (2014). "3D FEA modelling of laminated composites in bending and their failure mechanisms." *Composite Structures*, 119, 693-708.

[84] Baere, I. (2005). "Design of a three- and four-point bending for fatigue testing of fiber-reinforced thermoplastics." Accessed in March 25, 2016, in the Web site of Ghent University, in: http://users.ugent.be/~ivdbaere/doc/paper2005.pdf.

[85] Rager, A., Williams, J. G. and Ivankovic, A. (2005). "Numerical analysis of the three point bend impact test for polymers." *International Journal of Fracture*, 135, 199-215.

[86] Swolfs, Y., Van Den Fonteyne, W., Baets, J and Verpoest, I. (2014). "Failure behaviour of self-reinforced polypropylene at and below room temperature." *Composites Part A: Applied Science and Manufacturing*, 65, 100-107.

[87] "T700S Data Sheet", in http://www.toraycfa.com/pdfs/T700SDataSheet.pdf. Accessed in June 20, 2016

[88] Tabatabaei, S. A., Swolfs, Y., Wu, H. and Lomov, S.V. (2015). "Full-field strain measurements and meso-FE modelling of hybrid carbon/self-reinforced polypropylene." *Composite Structures*, 132, 864-873.

[89] "Toughness", in https://en.wikipedia.org/wiki/Toughness. Accessed in August 10, 2016

[90] Chamis, C. C. (1983). "Simplified composite micromechanics equations for hygral, thermal and mechanical properties." *NASA Technical Memoradum 88320, Houston, United States: NASA*.

[91] ASTM D 7264/D 7264M – 07 (2007). "Standard test method for flexural properties of polymer matrix composite materials." ASTM International, 100 Barr Harbor Drive, PO Box C700, West Conshohocken, PA 19428-2959, United States.

APPENDIX A - A DIFFERENT FAILURE CRITERIA

The failure criterion presented in "3.4 Results and Discussion" consisted in the moment where the plate could no longer support the maximum flexural load. With that criterion, a property similar to the toughness was defined. That property was the energy absorbed until the maximum flexural load point.

However, a different failure criterion can be used to define this property. If it is considered that the plate only fails after the force reaches 50 % of the maximum flexural load, the energy absorbed until that point does not only depend on the maximum flexural load and displacement at this point. It also depends on the way the force-displacement curve evolves after the maximum flexural load is achieved. This property can be determined by the area under the force-displacement curve until the failure criterion is reached, like it is illustrated on Figure A.1.
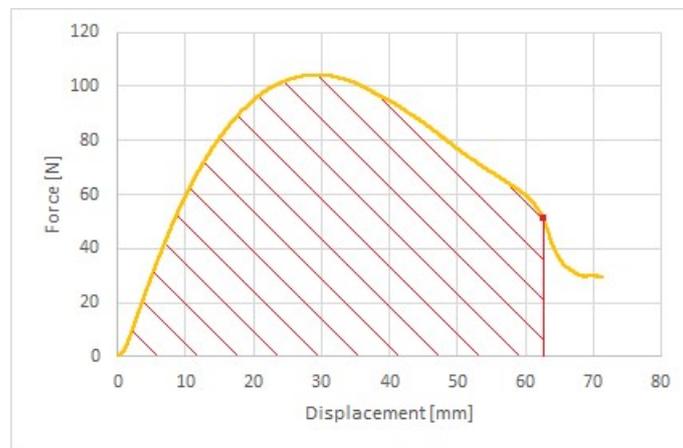

Figure A.1. 50 % of Maximum Flexural Load Failure Criteria.

This energy can also be determined with the normalized curves. The normalized force-displacement curves are obtained by dividing the force by the nominal thickness of the plate. Once again, the most energy absorbing lay-up is the $(S/S/S/S)_{so}$. Comparing to the charts presented in Figure 3.15, the energy absorbed still decreases with the increase of the carbon fibre content. In this case, the reduction of the energy absorbed seems to follow an rational function, with the exception of the $(S/S/C/S)_{so}$ lay-up, which presents a low energy absorption.

In fact, it is the two lay-ups on the top of the chart that have a faster load drop after the maximum is reached, making this property lower in comparison with the other stacking sequences. The plates with just one UD CFRPP layer also presents an increased energy absorption due to a slower load drop. The energy absorption until the force reaches 50 % of the maximum flexural load is presented in Figure A.2.
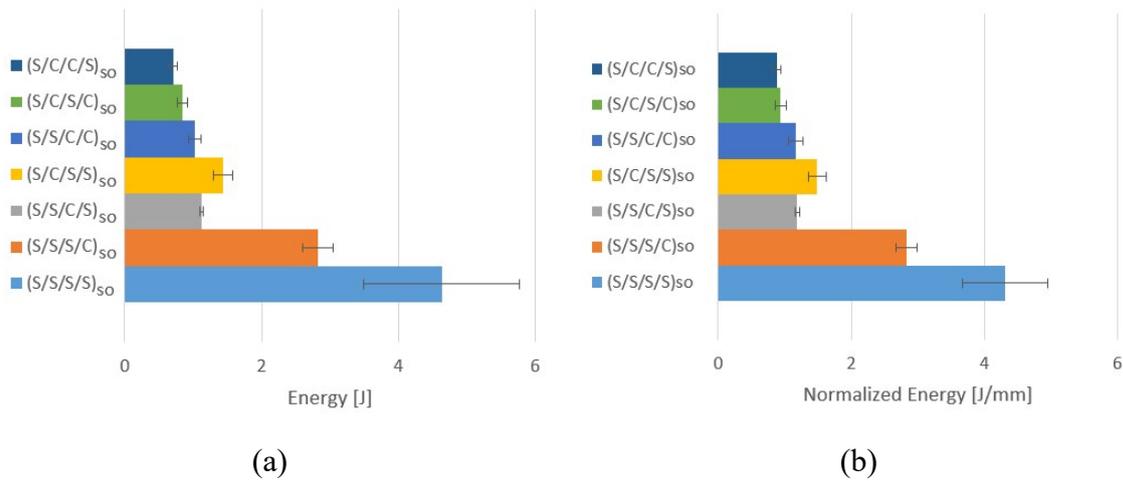

(a)   (b)

Figure A.2. Energy absorption until the force reaches 50 % of the maximum flexural load for the normal (a) and normalized (b) force-displacement curves.
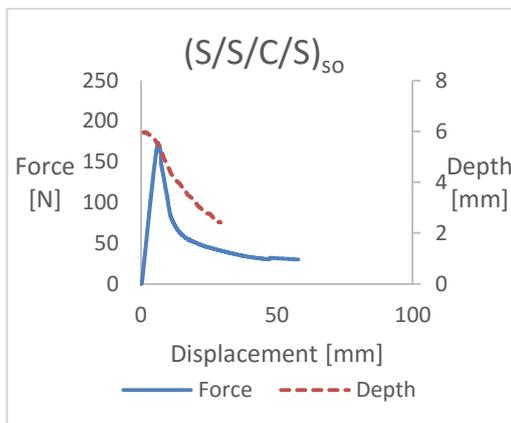
APPENDIX B - DEPTH VARIATION

In the main text, only two graphics were shown for the depth variation as a function of the loading nose displacement. In Figure B.1 all the graphics are presented. The behaviour and explanation are accessible in the aforementioned section.
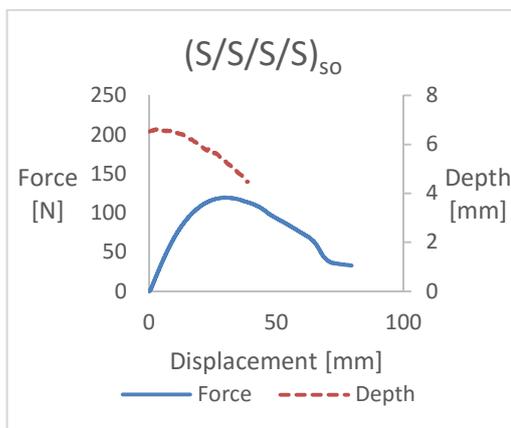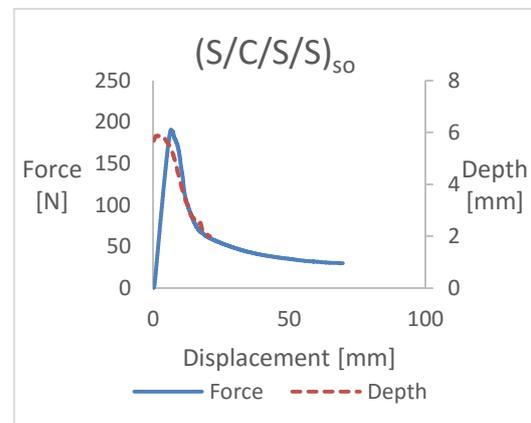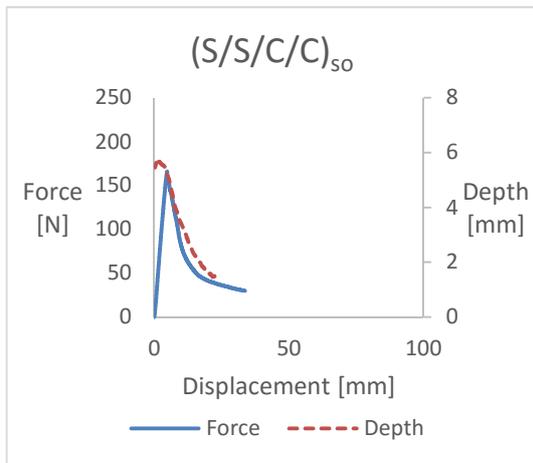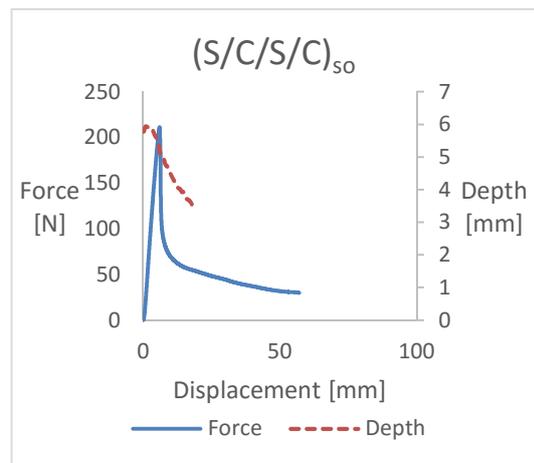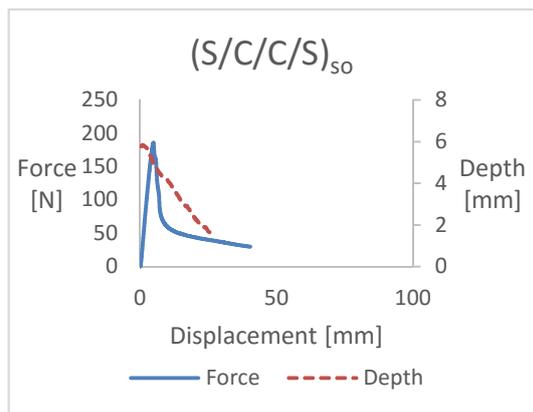

(a)
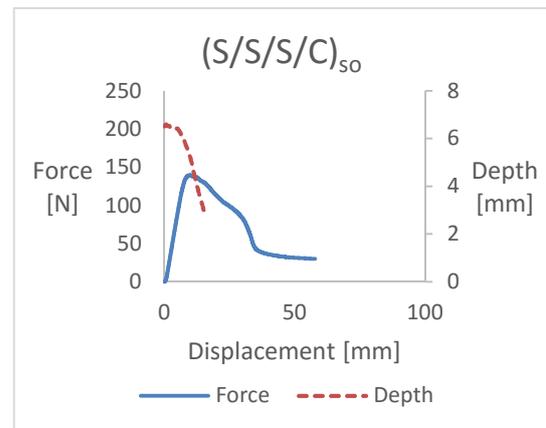
(b)

(c)

(d)

(e)

(f)

(g)

Figure B.1. Depth variation measured experimentally for all the different stacking sequences.

APPENDIX C - INTERRUPTED TESTS

In the mechanical property analysis made from the experimental data, it was concluded that the most interesting lay-ups to be studied in depth did not include the $(S/S/C/S)_{so}$ and $(S/C/S/S)_{so}$ stacking sequences. It was decided that, both in the interrupted tests or the optical microscopy sections, these lay-ups would not be analysed. These two final appendices are made to present the damage evolution of the two stacking sequences left.

The interrupted tests were performed to see how the visible damage on the surface evolved along the force-displacement curve. Before performing them, the relevant points in which to stop the flexural tests were studied from the results of previous samples with the same lay-up. The majority of the curves, in which these two lay-ups are inserted, had only two relevant points: the maximum flexural load and the stabilization phase. A final test was conducted to check the behaviour of the material after it was already damaged.

$(S/S/C/S)_{so}$

When the plate is loaded until the maximum flexural load point, two white areas appear in the left CD specimen locations (Figure C.1b). The other CD specimen locations also present some damage but it is not so pronounced and it is not even visible from the tensile side (bottom images). Only one of the white lines reaches the inclined portions of the plate.

The second test was conducted until the force stabilizes (Figure C.1c). The white areas are still localized in the mid-span zone and are now evident for all the four CD specimen locations. All of these white areas show a much localized whiter line (possibly where the carbon fibres fractured). Around them, some darker areas that seem to be delaminated areas, appear.

After the last test, the damaged areas had grown along the transverse direction, even to the TD specimen locations (top images). This damage is only visible when the plate is seen from the compressive side, but not from the tensile side, like it can be observed in Figure C.1d.
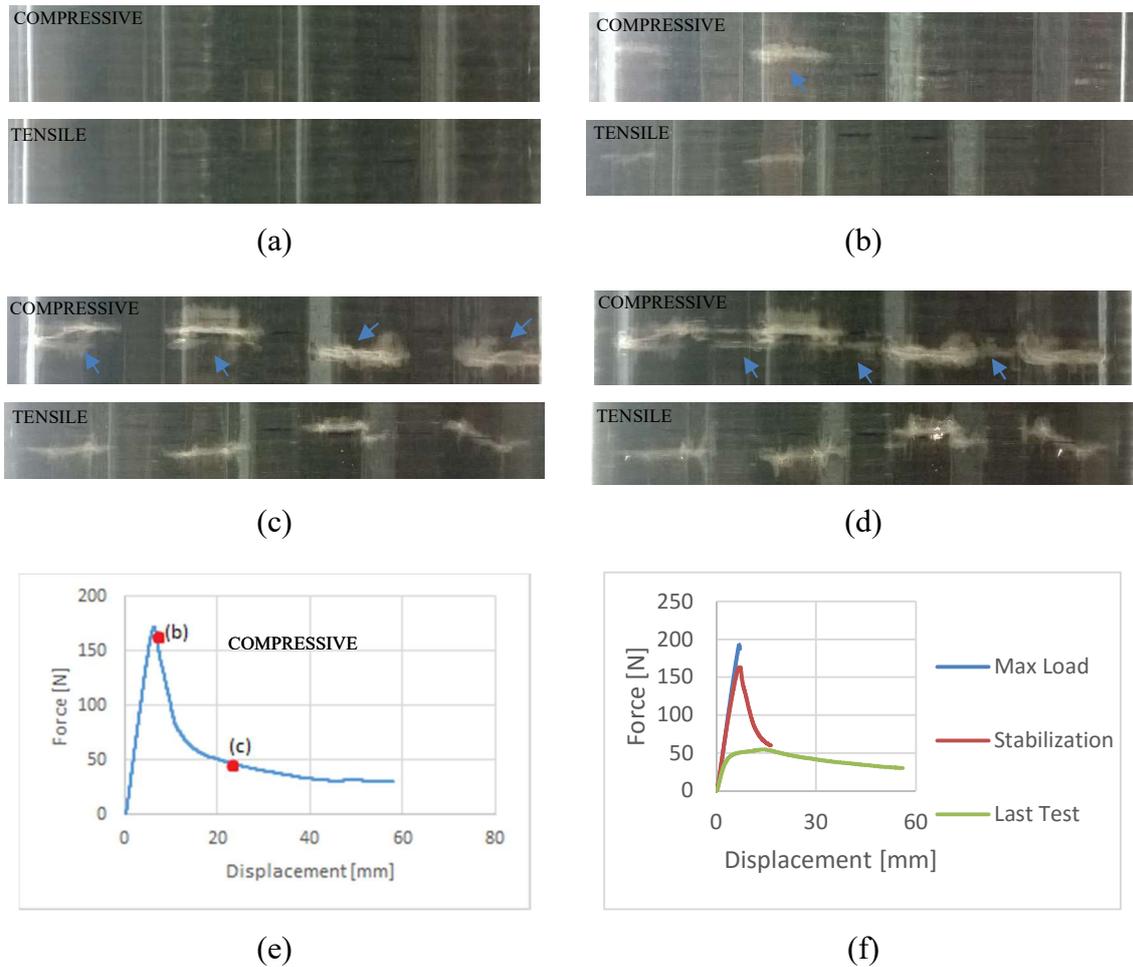
Figure C.1. Interrupted test backlight images from the (S/S/C/S)$_{so}$ lay-up: (a) untested, (b) after max. Load, (c) after stabilization and (d) after the last test, (e) the relevant points and (f) the interrupted test curves.

(S/C/S/S)$_{so}$

After the first test, that was conducted until the maximum load was achieved, white lines appear in the CD specimen location (Figure C.2b). The most pronounced damage is present on the second location from the left. One of the damaged areas (left side) shows a more distributed character that the other three, which are more localized.

The second test is conducted until the force-displacement curve stabilizes. The number of white lines increases and seems to spread in the longitudinal direction like in the (S/S/S/C)$_{so}$ lay-up, but is still more localized (Figure C.2c). In the left and middle of the image, some damage starts to appear in the TD specimen location. That damage is then amplified with the last test.

After the last test, damaged areas appear in the TD specimen location (Figure C.2d). Some of the white areas don't seem to be a propagation of the previous damage. The

size of the white areas increases in the longitudinal direction of the plate, indicating the progression of delamination.
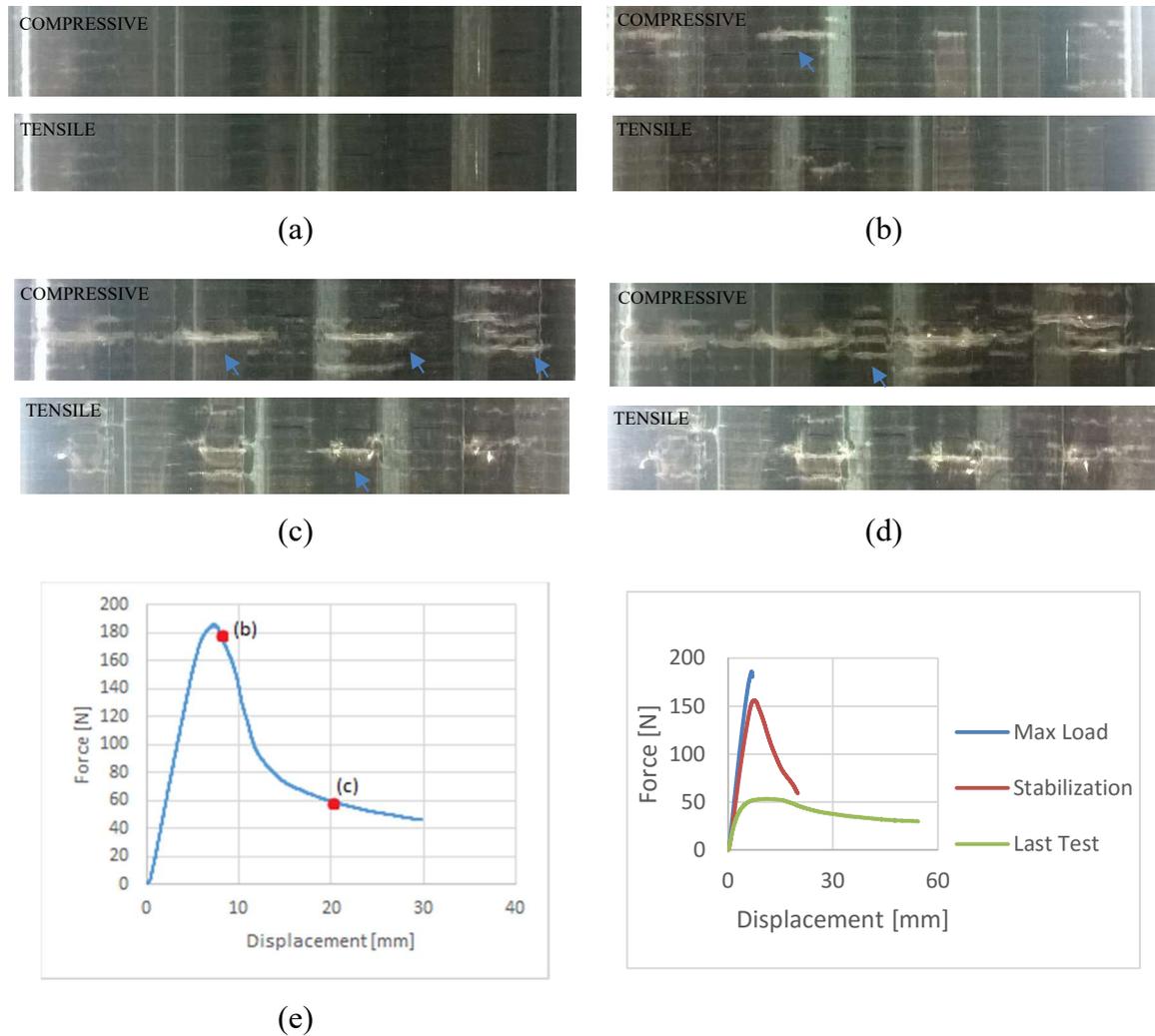

(a)

(b)

(c)

(d)

(e)

Figure C.2. Interrupted test backlight images from the (S/C/S/S)$_{so}$ lay-up: (a) untested, (b) after max. Load, (c) after stabilization and (d) after the last test, (e) the relevant points and (f) the interrupted test curves.

APPENDIX D - OPTICAL MICROSCOPY

After the flexural tests, some specimens were cut from the tested samples. The location from which the specimens were cut and the plane of observation during the optical microscopy analysis are presented in the section "3.3.5 Optical Microscopy". This technique allowed the author to identify the failure modes in each stacking sequence.

(S/S/C/S)$_{so}$

This lay-up has two UD CFRPP layers in the middle, separated by only one SRPP layer. The most visible damage that can be seen in the CD specimens is a large delamination (Figure D.1a). This delamination is the result of a folded tape that seems to have opened. Next to this delamination, the usual carbon fibre breaks are visible, along with the curvature of the fibres, showing the signs of buckling. In the top UD CFRPP layer (Figure D.1a), some delamination between the UD CFRPP and SRPP layers is also visible. Less visible is a tape that has transversely cracked.

Looking at the TD specimen (Figure D.1b), the only sign of damage that can be seen is delamination between a UD CFRPP and a SRPP layer closer to the compressive side of the specimen. The other carbon fibre layer seems to be undamaged but the middle SRPP layer shows transverse tape cracking. No carbon fibres seem to have fractured during the flexural tests on the TD specimen location.

(a)　　　　　　　　　　　　(b)

Figure D.1. Optical Microscopy images from a (S/S/C/S)$_{so}$ CD specimen showing (a) carbon fibre breaks and delamination and (b) delamination and transverse-tape cracking from a TD specimen.

(S/C/S/S)$_{so}$

This stacking sequence shows the most pronounced damage in both its CD and TD specimens. On Figure D.2a (CD specimen), a clear carbon fibre break is visible on the right side of the image. This fracture is mostly visible due to the sudden change of direction of the UD CFRPP layer. Next to it, a damaged folded tape is visible. The tape has opened and cracked transversely. Above the UD CFRPP layer, interlayer SRPP delamination is also visible.

The TD specimen (Figure D.2b) shows the most damage from all the TD specimens of all stacking sequences. That can occur because of the higher proximity of the UD CFRPP layer to the compressive side. It is possible to see that the carbon fibres have fractured and the layer changed direction, leading to a delamination between the UD CFRPP and SRPP layers. Another type of damage visible is the void space above the carbon fibre layer. It seems that part of a SRPP tape has been removed from the specimen. This can be evidence of a longitudinal splitting, like shown in other lay-ups.
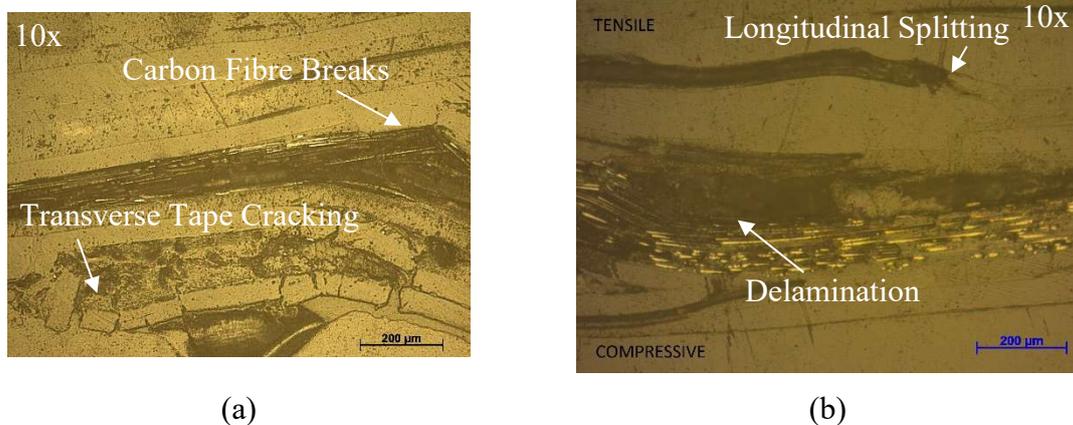

(a)   (b)

Figure D.2. Optical Microscopy images from a (S/C/S/S)$_{so}$ CD specimen showing (a) carbon fibre breaks and delamination and (b) delamination and transverse-tape cracking from a TD specimen.